TRANSIENT EXCITATION OF AN ELASTIC HALF-SPACE BY A POINT LOAD TRAVELING ON THE SURFACE

Thesis by

David Charles Gakenheimer

In Partial Fulfillment of the Requirements

For the Degree of

Doctor of Philosophy

California Institute of Technology

Pasadena, California

1969

(Submitted July 1, 1968)

ACKNOWLEDGMENTS

The author would like to thank his thesis advisor, Professor J. Miklowitz, for his guidance and encouragement throughout the course of this research.

The financial support from the National Aeronautics and Space Administration of a three-year NASA traineeship is also gratefully acknowledged.

ABSTRACT

The propagation of transient waves in an elastic half-space excited by a traveling normal point load is investigated. The load is suddenly applied and then it moves rectilinearly at a constant speed along the free surface. The displacements are computed for all points of the half-space as well as for all load speeds.

The disturbance is analyzed by using multi-integral transforms and an inversion scheme based on the well-known Cagniard technique. This reduces the displacements to single integral and algebraic contributions, each of which is identified as the disturbance behind a specific wave front. The same solution is valid for all load speeds, even though the wave front geometry varies greatly, depending on the speed of the load relative to the body wave speeds. Moreover, the surface displacements are obtained from the interior ones, but only after the Rayleigh waves are computed by a separate calculation. Then, by taking advantage of the form of the exact solution, wave front expansions and Rayleigh wave approximations are computed for all load speeds.

Several other analytical results are obtained for restricted values of the load speed. In particular, when it exceeds both of the body wave speeds the steady-state displacement field is separated from the transient one and reduced to algebraic form. Also, for the limit case of zero load speed a new representation of the interior displacements for Lamb's point load problem is displayed in terms of single integrals.

TABLE OF CONTENTS

LIST OF FIGURES

NOMENCLATURE†

Latin Symbols

(x,y,z)	cartesian coordinates, see Fig. 2
c	load speed
t	time parameter
$\underline{u}$	displacement vector
(u_x,u_y,u_z)	cartesian components of the displacement vector
c_d	dilatational body wave speed
c_s	equivoluminal body wave speed
$\underline{x}$	position vector
p	Laplace transform variable
$i = \sqrt{-1}$	
(u_{xd},u_{yd},u_{zd})	dilatational contributions to (u_x,u_y,u_z)
(u_{xs},u_{ys},u_{zs})	equivoluminal contributions to (u_x,u_y,u_z)
r	cylindrical coordinate, see Fig. 2
q,w	integration variables
K_{xd},K_{yd},K_{zd} K_{xs},K_{ys},K_{zs}	see equation (2.3-5)
$R(q,w)$	Rayleigh function, see equation (2.3-6)
m_d,m_s	see equation (2.3-7)
$\ell = \frac{c_d}{c_s}$	ratio of the body wave speeds

† This list of nomenclature includes only those symbols whose definition is assumed throughout the text. It is separated into sections which include Latin symbols, Greek symbols, and subscripts and superscripts. Within each section the symbols are presented in the order that they appear in the text.

c_R	Rayleigh wave speed
$q_d(\pm)$	q-transformation, see equation (2.4-4)
t_{wd}	pseudo-arrival time, see equation (2.4-4a)
C	contour in the q-plane
t_L	see equation (2.4-6)
n	radial coordinate, see Fig. 2
w_o	special value of the integration variable w; in subsection 2.4.1, see (2.4-6); in subsection 2.4.2, see (2.4-39)
A_{zd}, B_{zd}	contributions to u_{zd}
$\hat{K}_{zd}(q,w,\theta)$	see equation (2.4-10a)
$q_d = q_d(+)$	see equation (2.4-4) for $q_d(+)$
T_d	see equation (2.4-14a)
t_d	arrival time, see equation (2.4-14a)
$H(\sim)$	Heaviside function, see equation (2.4-16)
$w_d(\pm)$	w-transformation, see equation (2.4-19)
$w_d = w_d(+)$	
t_{dc}	arrival time, see equation (2.4-19a)
$\mathbb{C}$	contour in the w-plane
$\hat{K}_{zd}(w,\theta)$	see equation (2.4-20a)
P	precedes an improper integral to imply a Cauchy principal value
$q_s(\pm)$	q-transform, see equation (2.4-36)
t_{ws}	pseudo-arrival time, see equation (2.4-36a)
w_1	special value of the integration variable w, see text above equation (2.4-37)
q_{sd}	q-transformation, see equation (2.4-37)

t_{wsd}	pseudo-arrival time, see equation (2.4-37a)
A_{zs}, B_{zs}	contribution to u_{zs}
$q_s = q_s(+)$	see equation (2.4-36) for $q_s(+)$
$\hat{K}_{zs}(q,w,\theta)$	see equation (2.4-43a)
T_s	see equation (2.4-44a)
t_s	arrival time, see equation (2.4-44a)
$w_s(\pm)$	w-transformation, see equation (2.4-46)
$w_s = w_s(+)$	
t_{sc}	arrival time, see equation (2.4-46a)
$\hat{K}_{zs}(w,\theta)$	see equation (2.4-47a)
D_{zs}	contribution to u_{zs}
w_{sd}	w-transformation, see equation (2.4-52)
t_{sdc}	arrival time, see equation (2.4-52a)
T_{sd}	see equation (2.4-59a)
t_{sd}	arrival time, see equation (2.4-59a)
t_B	see equation (2.4-59a)
t_E	see text below equation (2.4-62)
t^o_{sdc}	see text below equation (2.4-77)
u^j_z, (j=1,...,7)	contributions to u_z for the interior of the half-space
w_{od}, w_{os}	see equation (2.4-82a)
a_d, a_s b_d, b_s a_{sd}, b_{sd}	see equation (2.4-98)
(u^j_x, u^j_y), (j=1,...,7)	contributions to (u_x, u_y) for the interior of the half-space
sgn (~)	see equation (2.5-8)

U_z^j, (j=1,...,4)	contributions to u_z for the surface of the half-space
$\underline{X}$	position vector in the surface plane of the half-space
$G(t^2, w^2)$	see equation (2.6-3)
t_R	Rayleigh wave arrival time, see equation (2.6-5)
$G(k^2)$	see equation (2.6-7)
t_{Rc}	Rayleigh wave arrival time, see equation (2.6-12)
(U_x^j, U_y^j), (j=1,...,5)	contributions to (u_x, u_y) for the surface of the half-space
(u_r, u_θ)	cylindrical components of the displacement vector
u_r^j, (j=1,...,4)	contributions to u_r for the interior of the half-space
K_{rd}^o, K_{zd}^o K_{rs}^o, K_{zs}^o	see equation (2.7-5)
U_r^j, (j = 1,...,3)	contribution to u_r for the surface of the half-space
M_{dc}, M_{sc}, M_{sdc}	see equation (3.1-16a)

Greek Symbols

λ, μ	Lamé constants
$\delta(\sim)$	Dirac delta function
θ	cylindrical coordinate, see Fig. 2
$\gamma = \frac{c_d}{c}$	ratio of the dilatational body wave speed to the load speed
$\gamma_R = \frac{c_d}{c_R}$	ratio of the dilatational body wave speed to the Rayleigh wave speed

ρ	spherical coordinate, see Fig. 2
α_d	see equation (2.4-19a)
ξ	coordinate, see Fig. 2
α_s	see equation (2.4-46a)
ϕ_c	see text below equation (2.4-46a)
α_{sd}	see equation (2.4-52a)

Subscripts and Superscripts

$(\underline{\quad})$	vector function
$(\overline{\quad})$	Laplace transformed function
$(\quad)_d$	a function related to the dilatational contribution
$(\quad)_s$	a function related to the equivoluminal contribution
$(\quad)_c$	a function which depends on the load speed
$\hat{(\quad)}$	a function which is part of another function

Chapter 1

INTRODUCTION

The problem treated in this investigation is that of a suddenly applied, normal point load which then travels rectilinearly at a constant speed on the surface of a homogeneous, isotropic, linearly elastic half-space. The objective is to find and analyze the waves that are generated by such a disturbance.

Although this problem has been considered in recent years by many authors, only two contributions towards a transient solution can be cited. First Payton [1][1] computed the transient surface displacements by using an elastodynamic reciprocal theorem. Then Lansing [2] rederived some of Payton's results by employing a Duhamel superposition integral. In order to effect their techniques, both of these authors drew on the simple form of Pekeris' [3] surface solution for Lamb's point load problem. This fact makes it difficult to use either of these techniques to analyze the disturbance in the interior of the half-space. Therefore it was appropriate to pursue the interior phase of the problem here. The remaining contributions to this problem include the steady-state results given by Mandel and Avramesco [4], Papadopoulos [5], Grimes [6], Eason [7], and Lansing [2]. The most complete of these is Lansing's work where integral expressions for the displacements are obtained for all points of the half-space and for all load speeds.

---

[1]Numbers in brackets designate references in the bibliography.

The continuing interest in the traveling point load problem is due, in part, to its physical applicability. For example, a vehicle like a truck exerts forces on the surface of the earth which are concentrated and that move. The ground motions excited by such a vehicle can be represented, with some qualifications, by the motions caused by a point load traveling on the surface of an elastic half-space. Moreover, the shock waves produced by a supersonic aircraft or a nuclear blast exert forces on the surface of the earth which move and whose effects might be estimated by superposing solutions of the traveling load problem considered here.

Of further interest is the fact that a point load moving on the surface of a half-space generates a non-axisymmetric disturbance. Very few wave propagation problems of this type have been solved and no general solution techniques are available. Other than the moving load cases discussed above, only Chao's [8] work need be mentioned to review all of the existing techniques. Chao computed the displacements due to a tangential surface point load by first separating out the angular dependence and then using procedures designed for an axisymmetric disturbance. However, in general such a separation of variables is not possible and his method has limited use. On the other hand, the technique developed here to analyze the moving load problem is more general and it should contribute guidelines for analyzing other non-axisymmetric half-space problems.

In Chapter 2 a formal solution to the moving load problem is obtained by using the Laplace and double Fourier transforms. This brings an inverse transform statement of the displacements to a triple integral form. By a sequence of real transformations and contour integrations this formula is replaced with one that allows the Laplace transform to be inverted by inspection. In this way each displacement is reduced to a sum of single integrals and algebraic terms. The basic ideas in this scheme of inversion are due to Cagniard [9]. However, the computations are greatly simplified by using a transformation introduced by DeHoop [10] for problems in acoustics and later used by Mitra [11] for an elastic half-space problem.

This inversion scheme is complicated by the fact that each displacement is a function of five parameters: three space coordinates, time, and the load speed. Nevertheless, an exact solution is computed which is valid for all interior points of the half-space. The same expression is also valid for all load speeds, even though the wave front geometry varies greatly depending on the speed of the load relative to the body wave speeds. The surface solution is obtained from the interior one, but only after the Rayleigh waves have been assessed by a separate calculation.

Each contribution to the displacements is identified as the disturbance behind a specific wave front. In particular, the integrals represent a system of waves which emanate from the initial position of the load as if they were generated by a stationary point source.

The algebraic terms represent disturbances that trail behind the load and whose wave geometry depends on the speed of the load. This form of the solution is advantageous for evaluating the displacements near the wave fronts. These wave front expansions are given in Chapter 3 along with some other analytical results pertaining to the Rayleigh waves and the steady-state displacement field.

Additional results are given in Chapters 2 and 3 for the limit case of zero load speed, for then the moving load problem passes to that one of a half-space excited by a surface point load with step time dependence. This problem, which is frequently referred to as Lamb's problem, has been treated thoroughly for the free surface by Pekeris [3], but the analysis for the interior of the half-space is not nearly as complete. It should be noted that Eason [12] has worked on the interior displacements using transforms. His results are in the form of single integrals, but they do not readily display the system of wave fronts associated with a concentrated surface load. In addition, Knopoff and Gilbert [13] have developed a technique for computing the first motions behind these wave fronts from a formal transform solution of the problem. However, as pointed out by Aggarwal and Ablow [14], this technique is not successful in detecting the logarithmic discontinuity at the equivoluminal wave front. In this work a new representation of the interior displacements for Lamb's problem is obtained in terms of single integrals, each of which is identified as the disturbance

behind a specific wave front. Then wave front expansions are computed which include the logarithmic singularity. Further contributions to Lamb's problem have been made by Lamb [15], Lang [16, 17], and Craggs [18]; but these publications have no bearing on the investigation given here.

CHAPTER 2

STATEMENT OF THE PROBLEM AND SOLUTION

2.1. STATEMENT OF THE PROBLEM

The subject half-space problem is depicted in Fig. 1 based on a cartesian coordinate system (x,y,z). The plane surface of the half-space is $z = 0$, with $z > 0$ forming the interior. A concentrated, normal load of unit magnitude travels on the surface along the positive x-axis at a constant speed c. The load acquires its velocity instantaneously at the origin of the coordinates at time $t = 0$.

The half-space is a homogeneous, isotropic medium governed by the equations of the linear theory of elasticity. The equations of motion for the case of vanishing body forces are

$$\mu\nabla^2\underline{u} + (\lambda+\mu)\nabla\nabla\cdot\underline{u} = \nu\frac{\partial^2\underline{u}}{\partial t^2}, \qquad (2.1\text{-}1)$$

where $\underline{u}$ represents the displacement vector (underlined characters represent vectors) with the cartesian components (u_x,u_y,u_z); λ and μ are the Lamé constants; ν is the material density; and ∇ is the del-operator. It has been shown (see, for example, Sternberg [19]) that every solution of (2.1-1) admits the representation

$$\underline{u} = \nabla\phi + \nabla\times\underline{\psi}, \qquad (2.1\text{-}2)$$

where ϕ and $\underline{\psi}$, known as the Lamé potentials, satisfy the wave equations

$$\nabla^2\phi = \frac{1}{c_d^2}\frac{\partial^2\phi}{\partial t^2} \quad , \qquad \nabla^2\underline{\psi} = \frac{1}{c_s^2}\frac{\partial^2\underline{\psi}}{\partial t^2} \tag{2.1-3}$$

and the divergence condition

$$\nabla \cdot \underline{\psi} = 0 \ . \tag{2.1-4}$$

c_d and c_s are the dilatational and equivoluminal body wave speeds respectively. They are defined by

$$c_d = \left(\frac{\lambda + 2\mu}{\nu}\right)^{\frac{1}{2}} \quad , \qquad c_s = \left(\frac{\mu}{\nu}\right)^{\frac{1}{2}} \ . \tag{2.1-5}$$

The appropriate stress (τ_{ij}) relation for this medium is

$$\tau_{ij} = \lambda\nabla \cdot \underline{u}\delta_{ij} + \mu(u_{i,j} + u_{j,i}) \ , \tag{2.1-6}$$

where δ_{ij} is the Kronecker delta.

The boundary conditions at $z = 0$ take the form

$$\left.\begin{aligned} \tau_{zz}(x,y,0,t) &= -\delta(y)\,\delta(x - ct) \\ \tau_{xz}(x,y,0,t) &= \tau_{yz}(x,y,0,t) = 0 \end{aligned}\right\} \ , \tag{2.1-7}$$

where $\delta(\sim)$ is the Dirac delta function and to represent quiescence at $t = 0$ the initial conditions appear as

$$\left.\begin{aligned} \phi(x,y,z,0) &= \frac{\partial\phi(x,y,z,0)}{\partial t} = 0 \\ \underline{\psi}(x,y,z,0) &= \frac{\partial\underline{\psi}(x,y,z,0)}{\partial t} = 0 \ . \end{aligned}\right\} \tag{2.1-8}$$

The potentials ϕ and $\underline{\psi}$, and the space derivatives of the potentials,

are required to vanish at infinity ($|\underline{x}| \to \infty$, $\underline{x}$ is the position vector, $z \geq 0$ for the half-space), i.e.,

$$\lim_{|\underline{x}|\to\infty} [\phi(x,y,z,t), \underline{\psi}, \text{ etc.}] = 0 \quad . \tag{2.1-9}$$

2.2. FORMAL SOLUTION

In view of the initial and boundary conditions appropriate transforms for the solution of (2.1-3) are given by the Laplace and double Fourier transform pairs

$$\bar{f}(p) = \int_0^\infty f(t)e^{-pt}\,dt\,, \qquad f(t) = \frac{1}{2\pi i}\int_{Br_1} \bar{f}(p)e^{pt}\,dp$$

$$\tilde{f}(k,v) = \int_{-\infty}^{\infty}\int f(x,y)e^{-i(kx+vy)}\,dx\,dy, \quad f(x,y) = \frac{1}{(2\pi)^2}\int_{-\infty}^{\infty}\int \tilde{f}(k,v)e^{i(kx+vy)}\,dk\,dv \tag{2.2-1}$$

(see Sneddon [20] for corresponding transform theorems), where p is the Laplace transform parameter, Br_1 is the well-known Bromwich contour in the right half of the p-plane, and k,v are real Fourier transform parameters. By applying these transforms in sequence to (2.1-3) in conjunction with the initial conditions (2.1-8) and the boundedness conditions (2.1-9), the ordinary differential equations

$$\frac{\partial^2\tilde{\bar{\phi}}}{\partial z^2} = \eta_d^2\tilde{\bar{\phi}}\,, \quad \frac{\partial^2\tilde{\bar{\psi}}_j}{\partial z^2} = \eta_s^2\tilde{\bar{\psi}}_j\,, \quad (j = x,y,z) \tag{2.2-2}$$

arise, whose solutions which are bounded for large z are

$$\left.\begin{aligned} \tilde{\phi} &= Ae^{-\eta_d z} \qquad \text{for } \operatorname{Re}\eta_d > 0 \\ \tilde{\psi}_j &= B_j e^{-\eta_s z} \qquad \text{for } \operatorname{Re}\eta_s > 0 \end{aligned}\right\} \tag{2.2-3}$$

(Re denoting the real part), where

$$\left.\begin{aligned} \eta_d &= (k^2 + v^2 + k_d^2)^{\frac{1}{2}}, \quad k_d = \frac{p}{c_d} \\ \eta_s &= (k^2 + v^2 + k_s^2)^{\frac{1}{2}}, \quad k_s = \frac{p}{c_s} \end{aligned}\right\} \tag{2.2-4}$$

and A, B_j are four constants to be determined. Satisfying the divergence condition (2.1-4) and the three boundary conditions (2.1-7) produces the following four equations for A, B_j:

$$\left.\begin{aligned} &(\frac{\lambda}{2\mu}k_d^2 + \eta_d^2)A + iv\eta_s B_x - ik\eta_s B_y = \frac{-1}{2\mu(ick+p)} \\ &2ik\eta_d A - kvB_x + (k^2+\eta_s^2)B_y + iv\eta_s B_z = 0 \\ &-2iv\eta_d A + (v^2+\eta_s^2)B_x - kvB_y + ik\eta_s B_z = 0 \\ &ikB_x + ivB_y - \eta_s B_z = 0 \ . \end{aligned}\right\} \tag{2.2-5}$$

The solution of this system of equations and (2.2-3) yield

$$\left.\begin{aligned} \tilde{\phi} &= \frac{-[k_s^2 + 2(k^2+v^2)]}{\mu(ick+p)T(k,v,p)} e^{-\eta_d z}, \quad \tilde{\psi}_z = 0 \\ \tilde{\psi}_x &= \frac{-2iv\eta_d e^{-\eta_s z}}{\mu(ick+p)T(k,v,p)}, \quad \tilde{\psi}_y = \frac{2ik\eta_d e^{-\eta_s z}}{\mu(ick+p)T(k,v,p)} \end{aligned}\right\}, \tag{2.2-6}$$

where $T(k,v,p)$ is the Rayleigh function defined by

$$T(k,v,p) = [k_s^2 + 2(k^2+v^2)]^2 - 4\eta_s\eta_d(k^2+v^2) \ . \qquad (2.2\text{-}7)$$

Then substitution from (2.2-6) into a transformed statement of (2.1-2) and use of the Fourier inversion formula (2.2-1) give the Laplace transformed displacements

$$\bar{u}_j(x,y,z,p) = \bar{u}_{jd}(x,y,z,p) + \bar{u}_{js}(x,y,z,p) \quad , \quad (j = x,y,z) \ , \qquad (2.2\text{-}8)$$

where

$$\bar{u}_{j\alpha}(x,y,z,p) = \frac{1}{(2\pi)^2\mu}\iint_{-\infty}^{\infty} F_{j\alpha}(k,v,p)\, e^{-\eta_\alpha z + i(kx+vy)}\, dk\, dv, \ (\alpha = d,s) \qquad (2.2\text{-}9)$$

and

$$\left.\begin{aligned}
F_{xd}(k,v,p) &= \frac{-ik[k_s^2+2(k^2+v^2)]}{(ick+p)T(k,v,p)} \quad , \quad F_{xs}(k,v,p) = \frac{2ik\eta_d\eta_s}{(ick+p)T(k,v,p)} \\
F_{yd}(k,v,p) &= \frac{-iv[k_s^2+2(k^2+v^2)]}{(ick+p)T(k,v,p)} \quad , \quad F_{ys}(k,v,p) = \frac{2iv\eta_d\eta_s}{(ick+p)T(k,v,p)} \\
F_{zd}(k,v,p) &= \frac{\eta_d[k_s^2+2(k^2+v^2)]}{(ick+p)T(k,v,p)} \quad , \quad F_{zs}(k,v,p) = \frac{-2\eta_d(k^2+v^2)}{(ick+p)T(k,v,p)} \ .
\end{aligned}\right\} (2.2\text{-}10)$$

$\bar{u}_j$ in (2.2-8), written this way, reflects the fact that it can be expressed as the sum of its dilatational and equivoluminal contributions. The integrals in (2.2-9) converge because $\mathrm{Re}\,\eta_d > 0$ and $\mathrm{Re}\,\eta_s > 0$. It still remains to invert the Laplace transform. It is sufficient for the subsequent calculations to assume that the Laplace transform

parameter is a real, positive number. For such values of p, Lerch's theorem (see Carslaw and Jaeger[21], p. 345) guarantees us that if $u_j(x,y,z,t)$ exists it is unique.

When the displacements in (2.2-8) with (2.2-9) and (2.2-10) are evaluated for $c = 0$ and $z = 0$, and then expressed in terms of the cylindrical geometry shown in Fig. 2, they compare exactly with those computed by Pekeris [3] for the stationary point load.

2.3. TRANSFORMATION OF THE FORMAL SOLUTION

Although (2.2-8) with (2.2-9) and (2.2-10) is a formal solution of this problem for the displacements, its form is practically useless. By a sequence of transformations and contour integrations the integrals in (2.2-9) will be converted into a form that allows the Laplace transform to be inverted by inspection. In this way the exact inversion of each $\bar{u}_j$ will be obtained as a sum of single integrals and algebraic terms.

In this section two successive variable transformations are made in (2.2-9) to simplify the dependence of $\bar{u}_{j\alpha}$ on $\underline{x}$ and p. The first follows because $F_{j\alpha}(k,v,p)$ and $-\eta_\alpha z + i(kx+vy)$ are homogeneous functions of the Laplace transform variable p. Let

$$k = \frac{p}{c_d}\beta \quad , \qquad v = \frac{p}{c_d}\sigma \quad , \tag{2.3-1}$$

where $dk\,dv = (p/c_d)^2\, d\beta\, d\sigma$. The second one is designed to simplify the argument of the exponentials. Let

$$\beta = q\cos\theta - w\sin\theta \quad , \quad \sigma = q\sin\theta + w\cos\theta \quad , \tag{2.3-2}$$

where $\beta^2 + \sigma^2 = q^2 + w^2$, $\beta x + \sigma y = qr$, $d\beta\, d\sigma = dq\, dw$, and (r,θ) are the cylindrical coordinates shown in Fig. 2. Then the substitution of (2.3-1) and (2.3-2) into (2.2-8) - (2.2-10) and the reflection of -w into w yield

$$\bar{u}_j(r,\theta,z,p) = \bar{u}_{jd}(r,\theta,z,p) + \bar{u}_{js}(r,\theta,z,p) \quad , \quad (j = x,y,z), \qquad (2.3\text{-}3)$$

where

$$\bar{u}_{j\alpha}(r,\theta,z,p) = \frac{1}{2}\int_0^{\infty}\int_{-\infty}^{\infty} K_{j\alpha}(q,w,\theta)\, e^{-\frac{p}{c_d}(m_\alpha z - iqr)}\, dq\, dw, \quad (\alpha = d,s) \qquad (2.3\text{-}4)$$

and

$$\left.\begin{aligned} K_{xd}(q,w,\theta) &= \frac{-[iq\cos\theta(iq\cos\theta+\gamma) + w^2\sin^2\theta][\ell^2 + 2(q^2+w^2)]}{\pi^2 c\mu[(iq\cos\theta+\gamma)^2 + w^2\sin^2\theta]\, R(q,w)} \\ K_{xs}(q,w,\theta) &= \frac{2[iq\cos\theta(iq\cos\theta+\gamma) + w^2\sin^2\theta]\, m_d m_s}{\pi^2 c\mu[(iq\cos\theta+\gamma)^2 + w^2\sin^2\theta]\, R(q,w)} \end{aligned}\right\} \qquad (2.3\text{-}5a)$$

$$\left.\begin{aligned} K_{yd}(q,w,\theta) &= \frac{-\sin\theta[iq(iq\cos\theta+\gamma) - w^2\cos\theta][\ell^2 + 2(q^2+w^2)]}{\pi^2 c\mu[(iq\cos\theta+\gamma)^2 + w^2\sin^2\theta]\, R(q,w)} \\ K_{ys}(q,w,\theta) &= \frac{2\sin\theta[iq(iq\cos\theta+\gamma) - w^2\cos\theta]\, m_d m_s}{\pi^2 c\mu[(iq\cos\theta+\gamma)^2 + w^2\sin^2\theta]\, R(q,w)} \end{aligned}\right\} \qquad (2.3\text{-}5b)$$

$$\left.\begin{aligned} K_{zd}(q,w,\theta) &= \frac{(iq\cos\theta+\gamma) m_d[\ell^2 + 2(q^2+w^2)]}{\pi^2 c\mu[(iq\cos\theta+\gamma)^2 + w^2\sin^2\theta]\, R(q,w)} \\ K_{zs}(q,w,\theta) &= \frac{-2(iq\cos\theta+\gamma) m_d (q^2+w^2)}{\pi^2 c\mu[(iq\cos\theta+\gamma)^2 + w^2\sin^2\theta]\, R(q,w)} \end{aligned}\right\} \qquad (2.3\text{-}5c)$$

$$R(q,w) = [\ell^2 + 2(q^2+w^2)]^2 - 4m_d m_s (q^2+w^2), \qquad (2.3\text{-}6)$$

$$m_d = (q^2+w^2+1)^{\frac{1}{2}} \quad , \quad m_s = (q^2+w^2+\ell^2)^{\frac{1}{2}}, \qquad (2.3\text{-}7)$$

$$\ell = \frac{c_d}{c_s} \quad , \quad \gamma = \frac{c_d}{c} \quad . \qquad (2.3\text{-}8)$$

As first noted by DeHoop [10], the transformation (2.3-2) brings a two-dimensional resemblance to the $\bar{u}_j$. By holding w fixed in (2.3-4) and considering only the q integration variable, the exponentials have exactly the same form as those found in the stationary line load problem where exact inversions are obtained easily (see DeHoop [22]).

The $\bar{u}_j$ have the following symmetry property

$$\left.\begin{aligned} &\bar{u}_j(r,\theta,z,p) = \bar{u}_j(r,-\theta,z,p) \quad , \quad (j = x,z) \\ &\bar{u}_y(r,\theta,z,p) = -\bar{u}_y(r,-\theta,z,p) \end{aligned}\right\}, \qquad (2.3\text{-}9)$$

where $\theta \rightarrow -\theta$ implies $x \rightarrow x$, $y \rightarrow -y$, $z \rightarrow z$; a reflection over the axis that the load moves along. This result is expected physically and it is used in the subsequent calculations.

Finally, it remains to convert the integrals in (2.3-4) into a form that contains the Laplace transform integral. This essentially involves replacing $\frac{1}{c_d}(m_\alpha z - iqr)$ with the real variable t. This complex variable change is effected by a contour integration in a complex q-plane. In section 2.4 the contour integration for $\bar{u}_z$ is carried through in detail for $z > 0$, resulting in the exact inversion of the

vertical displacement for the interior of the half-space. In section 2.5 the exact inversion of $\bar{u}_x$ and $\bar{u}_y$ for $z > 0$ is computed in short order by using the results in section 2.4. Then in section 2.6 the surface $(z = 0)$ displacements, less the Rayleigh waves, are obtained as a limit case of the interior results. The Rayleigh waves are computed by returning to the contour integration planes and assessing the Rayleigh poles. Allowance is made in each of these sections for the variable load speed. To complete Chapter 2, in section 2.7 the displacements appropriate to a stationary point load are obtained as a special case of the results in the preceding sections.

2.4. EXACT INVERSION OF THE VERTICAL DISPLACEMENT FOR THE INTERIOR OF THE HALF-SPACE

Anticipating the fact that the solution takes different forms depending on the speed of the load relative to the body wave speeds (c_d, c_s), the contour integration for $\bar{u}_z$ is separated into three cases. In particular the terms supersonic, transonic, and subsonic refer to the cases when the load speed is greater than the dilatational wave speed, between the dilatational and equivoluminal wave speeds, and less than the equivoluminal wave speed respectively. As shown in this section, one single expression represents the exact inversion of $\bar{u}_z$ in the interior of the half-space for all load speeds.

The inversion of $\bar{u}_z$ is given in detail for the case of supersonic load motion. The dilatational contribution is treated in subsection 2.4.1 and the equivoluminal contribution in 2.4.2. Then in

subsections 2.4.3 and 2.4.4 the cases of transonic and subsonic load motion are handled briefly, only indicating the differences with the supersonic case. In view of the reflection property in (2.3-9), the calculations in subsections 2.4.1 - 2.4.4 are only done for $\theta \geq 0$. Finally, in subsection 2.4.5 the results are summarized for all load speeds and extended to include $\theta < 0$.

2.4.1. Dilatational Contribution for Supersonic Load Motion.

From (2.3-4)

$$\bar{u}_{zd}(\underline{x},p) = \frac{1}{2} \int_0^{\infty}\int_{-\infty}^{\infty} K_{zd}(q,w,\theta) e^{-\frac{p}{c_d}(m_d z - iqr)}\, dq\, dw, \qquad (2.4\text{-}1)$$

where K_{zd} and m_d are given by (2.3-5c) and (2.3-7). Since several different sets of coordinates are employed in this section, $\bar{u}_{zd}$ is only shown as a function of the position vector $\underline{x}$. For the computations that follow involving the q-integral it is convenient to restrict w to the bounded interval 0 to M, where M is a large, positive number. Then, after assessing the q-integral, one lets M tend towards infinity. With this in mind (2.4-1) is written as

$$\bar{u}_{zd}(\underline{x},p) = \frac{1}{2} \lim_{M\to\infty} \int_0^{M}\int_{-\infty}^{\infty} K_{zd}(q,w,\theta) e^{-\frac{p}{c_d}(m_d z - iqr)}\, dq\, dw\,. \qquad (2.4\text{-}2)$$

In order to effect the desired contour integration, the integrand of (2.4-2) must be extended to being an analytic function of a complex variable q. The singularities of the integrand are branch points located at $q = \pm i(w^2+1)^{\frac{1}{2}}$ and $q = \pm i(w^2+\ell^2)^{\frac{1}{2}}$, and simple poles at

$q = \pm i(w^2 + \gamma_R^2)^{\frac{1}{2}}$ and $q = \frac{\pm w \sin\theta + i\gamma}{\cos\theta}$. The poles located at $q = \pm i(w^2 + \gamma_R^2)^{\frac{1}{2}}$ correspond to the zeros of the Rayleigh function $R(q,w)$, where $\gamma_R = c_d/c_R$ and c_R is the Rayleigh wave speed. All of these singularities migrate in the q-plane as a function of w. However, since $w \in [0, M)$ they always lie in the finite q-plane as shown in Fig. 3. In addition, the manner in which the poles at $q = \frac{\pm w \sin\theta + i\gamma}{\cos\theta}$ migrate as a function of w depends on θ and c. The dependence of these poles on θ and c is carefully described in the subsequent material as the need arises to effect the contour integration.

In order to convert equation (2.4-2) into a form that contains the Laplace transform integral, one seeks a contour in the q-plane such that

$$t = \frac{1}{c_d}(m_d z - iqr) \quad , \tag{2.4-3}$$

where t is a real variable (eventually t will be identified as the time parameter). The solution of (2.4-3) for q yields

$$q_d(\pm) = \frac{c_d}{\rho^2}\left[itr \pm z(t^2 - t_{wd}^2)^{\frac{1}{2}}\right] \quad \text{for } t \geq t_{wd} \, , \tag{2.4-4}$$

where

$$t_{wd} = \frac{\rho}{c_d}(w^2 + 1)^{\frac{1}{2}}, \qquad \rho = (r^2 + z^2)^{\frac{1}{2}} \, . \tag{2.4-4a}$$

t_{wd} represents a "pseudo-time" of arrival because it is a function of the integration variable w and it is related to the time of arrival

of a hemispherical, dilatational wave, ρ/c_d (for $w = 0$, $t_{wd} = \rho/c_d$). ρ is a spherical radius as shown at the bottom of Fig. 2. $q_d(\pm)$ represents the particular q satisfying (2.4-3) and $(\pm)$ indicates the two possible roots. The contour $q_d(\pm)$ is shown in Fig. 3 and it is one branch of a hyperbola which is parametrically described by t as t varies monotonically from t_{wd} towards infinity. The hyperbola is symmetric about the imaginary q-axis and its vertex† lies on this axis at $q = \frac{ir}{\rho}(w^2+1)^{\frac{1}{2}}$ for $t = t_{wd}$. Since $\frac{r}{\rho} < 1$ (recall $z > 0$) the vertex never lies on the branch cuts. For $z = 0$, $q_d(\pm)$ wraps around the branch cuts and, in particular, the Rayleigh pole at $q = i(w^2+\gamma_R^2)^{\frac{1}{2}}$. The contribution of this pole is assessed in section 2.6 where the $z = 0$ case is considered. That a condition like $t \geq t_{wd}$ should arise is not surprising in view of the hyperbolic nature of the governing wave equations (2.1-3).

In order to construct a closed contour C, including $q_d(\pm)$, the arcs C_I and C_{II} are introduced as shown in Fig. 3 so that $C = C_I + C_{II} + q_d(-) + q_d(+) + \text{Re } q\text{-axis}$. The arcs C_I and C_{II} lie outside all the singularities in the q-plane and recede towards infinity. By comparing the relative position of the poles at $q = \frac{\pm w \sin\theta + i\gamma}{\cos\theta}$ and the contour $q_d(\pm)$ in the q-plane, one finds that these poles lie inside C if, and only if,‡

---

† The vertex at $q = \frac{ir}{\rho}(w^2+1)^{\frac{1}{2}}$ and the contour $q_d(\pm)$ represent the saddle point and the path of steepest descent associated with the q-integral for large p. However, an asymptotic expansion of the q-integral is not particularly useful because of the remaining w-integral.

‡ For simplicity consider only strict inequalities, then extend the results to include the cases of equality.

$$\left.\begin{array}{ll} (1) & -\frac{\pi}{2} < \theta < \frac{\pi}{2} \\ (2) & \frac{\nu}{\cos\theta} < \frac{c_d t r}{\rho^2} \\ (3) & w \tan\theta < \frac{c_d z}{\rho^2}\left(t^2 - t_{wd}^2\right)^{\frac{1}{2}} \end{array}\right\} , \qquad (2.4\text{-}5)$$

or equivalently (using coordinates shown in Fig. 2 and t_{wd} in (2.4-4a))

$$\left.\begin{array}{ll} (1) & x > 0 \\ (2) & t > t_L \quad \text{where} \quad t_L = \frac{\rho^2}{cx} \\ (3) & w^2 > w_o^2 \\ & \text{where} \quad w_o^2 = \left(\frac{\rho^2\nu^2}{x^2} - 1\right)\frac{z^2\cos^2\theta}{n^2} \ , \ n = (y^2+z^2)^{\frac{1}{2}}. \end{array}\right\} \qquad (2.4\text{-}6)$$

n is a radial coordinate measuring distance from the x-axis as shown at the bottom of Fig. 2. For fixed time, $t = t_L$ is the equation of a hemisphere (considering $z > 0$ only) with center $(x = \frac{ct}{2}, n = 0)$ and radius $\frac{ct}{2}$. The center of this hemisphere is always mid-way between the position of the load and the origin of the coordinates. The significance of this hemisphere will be apparent in the inverted displacement field.

In view of the conditions in (2.4-6) and the anticipation of applying the Cauchy-Goursat theorem along C, it is convenient to consider the following three cases:

Case I: $x > 0$, $\frac{x}{\rho} > \frac{c_d}{c}$

The poles at $q = \frac{\pm w \sin\theta + i\gamma}{\cos\theta}$ lie inside C for $w \in [0, M)$.

Case II: $x > 0$, $\frac{x}{\rho} < \frac{c_d}{c}$

The poles at $q = \frac{\pm w \sin\theta + i\gamma}{\cos\theta}$ lie inside C for $w \in (w_o, M)$ (2.4-7)

where $w_o = \left(\frac{\rho^2\gamma^2}{x^2} - 1\right)^{\frac{1}{2}} \frac{z \cos\theta}{n}$ and $w_o > 0$.

Case III: $x < 0$

No poles lie inside C for $w \in [0, M)$.

Each of these cases, while including a different part of the half-space, requires a different application of the Cauchy-Goursat theorem. Furthermore, excluding $x = 0$ and $\frac{x}{\rho} = \frac{c_d}{c}$, all positions in the interior of the half-space are included in these cases. For $x > 0$, $\frac{x}{\rho} = \frac{c_d}{c}$ defines a cone whose axis is the positive x-axis. As the solution will show, this cone separates the half-space into regions in which u_{zd} has distinctly different wave front patterns. The inversion of $\bar{u}_{zd}$ will be completed in each of these cases, with the results summarized at the end of this subsection.

Case I: $x > 0$, $\frac{x}{\rho} > \frac{c_d}{c}$

In view of the conditions for case I in (2.4-7), the Cauchy-Goursat theorem and residue theory applied to the integrand in (2.4-2) and C in Fig. 3 yield

$$\bar{u}_{zd}(\underline{x},p) = \bar{A}_{zd}(\underline{x},p) + \bar{B}_{zd}(\underline{x},p) , \qquad (2.4-8)$$

where

$$\overline{A}_{zd}(\underline{x},p) = \lim_{M\to\infty}\int_0^M \int_{t_{wd}}^{\infty} \mathrm{Re}\left[K_{zd}(q_d,w,\theta)\,\frac{dq_d}{dt}\right] e^{-pt}\,dt\,dw \qquad (2.4\text{-}9)$$

and

$$\overline{B}_{zd}(\underline{x},p) = \lim_{M\to\infty}\int_0^M \mathrm{Re}\left\{\left[\hat{K}_{zd}(q,w,\theta)\, e^{-\frac{p}{c_d}(m_d z - iqr)}\right]\Big|_{q=\frac{w\sin\theta+i\gamma}{\cos\theta}}\right\} dw \qquad (2.4\text{-}10)$$

with

$$\hat{K}_{zd}(q,w,\theta) = \frac{\sec\theta\, m_d[\ell^2 + 2(q^2+w^2)]}{\pi c\mu R(q,w)} \,. \qquad (2.4\text{-}10a)$$

$\overline{A}_{zd}$ is the contribution from $q_d(\pm)$ and the convention has been adopted that $q_d = q_d(+)$. Also, $\overline{B}_{zd}$ is the residue contribution from the poles at $q = \frac{\pm w\sin\theta + i\gamma}{\cos\theta}$ and $\hat{K}_{zd}$ is that part of K_{zd} which is left after the residue evaluation. The integrals that arise along C_I and C_{II} vanish in view of Jordan's lemma (see Copson [23], p. 137) and remark (3) under Fig. 3.

The integrals in (2.4-9) clearly converge uniformly for all $\underline{x}$ in the interior of the half-space (recall $z > 0$) as M tends towards infinity. This follows because t_{wd}, as given in (2.4-4a), also tends to infinity and the exponential in the integrand predominates (recall p is a real, positive number). In addition, the integral in (2.4-10) converges uniformly for all $\underline{x}$ in the interior of the half-space because $\mathrm{Re}\left[(m_d z - iqr)\Big|_{q=\frac{w\sin\theta+i\gamma}{\cos\theta}}\right] > 0$ for all w. Therefore (2.4-9) and (2.4-10) become

$$\overline{A}_{zd}(\underline{x},p) = \int_0^\infty \int_{t_{wd}}^\infty \mathrm{Re}\left[K_{zd}(q_d,w,\theta) \frac{dq_d}{dt} \right] e^{-pt}\, dt\, dw \qquad (2.4\text{-}11)$$

and

$$\overline{B}_{zd}(\underline{x},p) = \int_0^\infty \mathrm{Re}\left\{ \left[\hat{K}_{zd}(q,w,\theta) e^{-\frac{p}{c_d}(m_d z - iqr)} \right] \Big|_{q = \frac{w\sin\theta + i\gamma}{\cos\theta}} \right\} dw \,. \qquad (2.4\text{-}12)$$

To complete the inversion of $\overline{A}_{zd}$, interchange the order of integration in (2.4-11). This is legitimate (see Jeffreys and Jeffreys [24], pp. 180-181) because the double integral in (2.4-11) is absolutely convergent. The absolute convergence follows because the only singularity in the integrand is the integrable one introduced by

$$\frac{dq_d}{dt} = \frac{c_d}{\rho^2} \left[ir + zt(t^2 - t_{wd}^2)^{-\frac{1}{2}} \right] \qquad (2.4\text{-}13)$$

at $t = t_{wd}$. Also, for large t and/or w the exponential in the integrand predominates (recall that t_{wd} goes to infinity as w goes to infinity). Then (2.4-11) becomes

$$\overline{A}_{zd}(\underline{x},p) = \int_{t_d}^\infty \int_0^{T_d} \mathrm{Re}\left[K_{zd}(q_d,w,\theta) \frac{dq_d}{dt} \right] dw\, e^{-pt}\, dt \,, \qquad (2.4\text{-}14)$$

where

$$T_d = \left(\frac{t^2}{t_d^2} - 1 \right)^{\frac{1}{2}} \,, \quad t_d = \frac{\rho}{c_d} \,. \qquad (2.4\text{-}14a)$$

The inversion of the Laplace transform in (2.4-14) yields

$$A_{zd}(\underline{x},t) = H(t - t_d)\int_0^{T_d} \mathrm{Re}\left[K_{zd}(q_d,w,\theta)\,\frac{dq_d}{dt}\right] dw \quad , \qquad (2.4\text{-}15)$$

where $H(\tau)$ is the Heaviside function defined by

$$H(\tau) = \begin{cases} 0 & \text{for } \tau < 0 \\ 1 & \text{for } \tau > 0 \end{cases} \qquad (2.4\text{-}16)$$

and t is now identified as the physical time parameter. t_d represents the arrival time† of a hemispherical, dilatational wave generated at the origin of the coordinates as shown in Fig. 7. Therefore A_{zd} represents a hemispherical, dilatational wave.

By inspection of (2.4-12) one sees that $\overline{B}_{zd}$ can also be converted into the Laplace transform integral by the same scheme as applied to the q-integral in (2.4-2). In fact $\overline{B}_{zd}$ has exactly the form found in two-dimensional problems where the Cagniard technique has well-known applicability (see, for example, DeHoop [22] where the stationary line load problem is inverted to algebraic form). Equation (2.4-12) is written as

$$\overline{B}_{zd}(\underline{x},p) = \mathrm{Re}\int_0^{\infty} \left[\hat{K}_{zd}(q,w,\theta)e^{-\frac{p}{c_d}(m_d z - iqr)}\right]\Big|_{q = \frac{w\sin\theta + i\gamma}{\cos\theta}} dw \, . \qquad (2.4\text{-}17)$$

To effect the desired contour integration, the integrand of (2.4-17) must be extended to being an analytic function of a complex variable w. The

†Arrival times are designated by the time parameter subscripted with lower case letters referring to the particular wave in question. In comparison, the time parameter subscripted with a capital letter designates a value of time which arises in constructing the solution, but is not related to a particular wave.

singularities of the integrand are branch points located at $w = -i\gamma \sin\theta \pm i(1-\gamma^2)^{\frac{1}{2}}\cos\theta$ and $w = -i\gamma \sin\theta \pm i(\ell^2-\gamma^2)^{\frac{1}{2}}\cos\theta$, and simple poles at $w = -i\gamma \sin\theta \pm i(\gamma_R^2-\gamma^2)^{\frac{1}{2}}\cos\theta$. These poles correspond to zeros of the Rayleigh function $R\left(\frac{w\sin\theta + i\gamma}{\cos\theta}, w\right)$ and, as previously defined, $\ell = \frac{c_d}{c_s}$, $\gamma = \frac{c_d}{c}$, and $\gamma_R = \frac{c_d}{c_R}$. The position of these singularities in the w-plane is shown in Fig. 4.

As done above, one seeks the particular contour in the w-plane such that

$$t = \frac{1}{c_d}(m_d z - iqr)\Big|_{q = \frac{w\sin\theta + i\gamma}{\cos\theta}}, \qquad (2.4\text{-}18)$$

where t is a real variable. The solution of (2.4-18) for w yields

$$w_d(\pm) = -i\gamma\sin\theta + \frac{\gamma\cos\theta}{n^2}(i\xi y \pm z\alpha_d) \quad \text{for} \quad t \geq t_{dc}, \qquad (2.4\text{-}19)$$

where

$$\left.\begin{aligned} t_{dc} &= \frac{1}{c}\left[\left(\frac{c^2}{c_d^2}-1\right)^{\frac{1}{2}} n + x\right] \\ \alpha_d &= \left[\xi^2 - \left(\frac{c^2}{c_d^2}-1\right)n^2\right]^{\frac{1}{2}} \\ \xi &= ct - x, \quad n = (y^2+z^2)^{\frac{1}{2}}. \end{aligned}\right\} \qquad (2.4\text{-}19a)$$

t_{dc} represents the arrival time of a conical, dilatational wave trailing behind the load as shown in Fig. 7. ξ is a coordinate measuring distance from the position of the load along the x-axis as shown at the bottom of Fig. 2 and n was introduced in (2.4-6). $w_d(\pm)$ represents the particular w satisfying (2.4-18) with $(\pm)$ indicating the two

possible roots. In view of the limits of integration in (2.4-17), only the plus root of (2.4-19) is needed and the convention is adopted that $w_d = w_d(+)$. The contour w_d is shown in Fig. 4. It is part of one branch of a hyperbola which is parametrically described by t as t varies monotonically from t_{dc} to infinity and its vertex† lies on the imaginary w-axis at $w = -i\gamma \sin\theta + i\frac{\gamma}{n}(1-\gamma^2)^{\frac{1}{2}}\cos\theta$ for $t = t_{dc}$. For case I the vertex lies between the Re w-axis and the branch point located at $w = -i\gamma \sin\theta + i(1-\gamma^2)^{\frac{1}{2}}\cos\theta$ (see remark (2) under Fig. 4). When z goes to zero, w_d collapses, in the limit, on the imaginary w-axis and, in particular, on the Rayleigh pole. The contribution of this pole is assessed in section 2.6 where the $z = 0$ solution is computed. Again, a condition like $t \geq t_{dc}$ reflects the hyperbolic nature of the governing equations.

In order to construct a closed contour $\mathcal{C}$, including w_d, the contours $\mathcal{C}_I$ and $\mathcal{C}_1$ are introduced as shown in Fig. 4 so that $\mathcal{C} = \mathcal{C}_I + w_d + \mathcal{C}_1 + \text{Re w-axis}$. Then the application of the Cauchy-Goursat theorem to the integrand in (2.4-17) and $\mathcal{C}$ produces

$$\overline{B}_{zd}(\underline{x},p) = \text{Re}\int_{t_{dc}}^{\infty} \hat{K}_{zd}(w_d,\theta)\frac{dw_d}{dt}e^{-pt}\,dt \quad , \tag{2.4-20}$$

where

$$\hat{K}_{zd}(w,\theta) = \hat{K}_{zd}\left(\frac{w\sin\theta + i\gamma}{\cos\theta}, w, \theta\right) \quad . \tag{2.4-20a}$$

† The vertex at $w = -i\gamma\sin\theta + \frac{i\gamma}{n}(1-\gamma^2)^{\frac{1}{2}}\cos\theta$ and the contour $w_d(\pm)$ represent the saddle point and the path of steepest descent associated with the w-integral in (2.4-17) for large p. By using the saddle point technique and a Tauberian limit theorem, a wave front expansion of B_{zd} can be computed. Such a technique has been used by Knopoff and Gilbert [13], but it is not employed in this thesis.

The integral that arises along C_I vanishes in view of Jordan's lemma and remark (3) under Fig. 4. The integral that arises along C_1 vanishes because its real part is zero. The inversion of the Laplace transform in (2.4-20) gives

$$B_{zd}(\underline{x},t) = \mathrm{Re}\left[\hat{K}_{zd}(w_d,\theta)\frac{dw_d}{dt} \right] H(t - t_{dc}) \ , \qquad (2.4\text{-}21)$$

where $H(\tau)$ is given by (2.4-16). In view of $H(t - t_{dc})$ in (2.4-21), B_{zd} is identified as a conical, dilatational wave trailing behind the load.

By combining expressions (2.4-8), (2.4-15), and (2.4-21), u_{zd} for case I becomes

$$u_z(\underline{x},t) = H(t - t_d)\int_0^{T_d} \mathrm{Re}\left[K_{zd}(q_d,w,\theta)\frac{dq_d}{dt} \right] dw + \mathrm{Re}\left[\hat{K}_{zd}(w_d,\theta)\frac{dw_d}{dt} \right] H(t - t_{dc}) \ , \qquad (2.4\text{-}22)$$

where the notation is defined in the text, $x > 0$, and $\frac{x}{\rho} > \frac{c_d}{c}$. The Roman numeral one in the diagrams at the bottom of Fig. 7 is located in the domain (all $\underline{x}$ such that $\frac{x}{\rho} > \frac{c_d}{c}$) of the half-space where (2.4-22) is pertinent.

Case II: $x > 0$, $\frac{x}{\rho} < \frac{c_d}{c}$

Returning to the contour integration in the q-plane and noting the conditions for case II in (2.4-7) suggest that equation (2.4-2) be written as

$$\bar{u}_{zd}(\underline{x},p) = \frac{1}{2}\lim_{\epsilon \to 0} (\bar{I}_1 + \bar{I}_2 + \bar{I}_3 + \bar{I}_4) \ , \qquad (2.4\text{-}23)$$

where

$$\left.\begin{aligned} \bar{I}_1 &= \int_0^{w_o-\epsilon}\int_{-\infty}^{\infty} K_{zd}(q,w,\theta)\, e^{-\frac{p}{c_d}(m_d z - iqr)}\, dq\, dw \\ \bar{I}_2 &= \int_{w_o-\epsilon}^{w_o} (\dot{\tilde{\cdot}})\, dw \quad , \quad \bar{I}_3 = \int_{w_o}^{w_o+\epsilon} (\dot{\tilde{\cdot}})\, dw \quad , \quad \bar{I}_4 = \lim_{M\to\infty} \int_{w_o+\epsilon}^{M} (\dot{\tilde{\cdot}})\, dw. \end{aligned}\right\} \quad (2.4\text{-}24)$$

The integrand in each $\bar{I}_\alpha$, $(\alpha = 1,2,3,4)$, is the same. The Cauchy-Goursat theorem can now be applied uniformly to each $\bar{I}_\alpha$ and the corresponding q-planes are shown in Fig. 5.

By calculations similar to those in case I, $\bar{I}_1$ and $\bar{I}_4$ become

$$\bar{I}_1 = 2\int_0^{w_o-\epsilon}\int_{t_{wd}}^{\infty} \mathrm{Re}\left[K_{zd}(q_d,w,\theta)\, \frac{dq_d}{dt} \right] e^{-pt}\, dt\, dw \quad , \qquad (2.2\text{-}25a)$$

$$\bar{I}_4 = 2\lim_{M\to\infty}\int_{w_o+\epsilon}^{M}\int_{t_{wd}}^{\infty} \mathrm{Re}\left[K_{zd}(q_d,w,\theta)\, \frac{dq_d}{dt} \right] e^{-pt}\, dt\, dw$$

$$+ 2\lim_{M\to\infty}\int_{w_o+\epsilon}^{M} \mathrm{Re}\left\{ \left[\hat{K}_{zd}(q,w,\theta)\, e^{-\frac{p}{c_d}(m_d z - iqr)} \right] \Big|_{q = \frac{w\sin\theta + iy}{\cos\theta}} \right\} dw \quad , (2.4\text{-}25b)$$

where $\hat{K}_{zd}(q,w,\theta)$ is given in (2.4-10a).

To evaluate the q-integrals in $\bar{I}_2$ and $\bar{I}_3$ assume that $w = w_o$. This means that the poles at $q = \frac{\pm w\sin\theta + iy}{\cos\theta}$ lie on $q_d(\pm)$ at $t = t_L$ and one must indent around them (see C_1 and C_2 in Fig. 5). Then the application of the Cauchy-Goursat theorem yields

$$\bar{I}_2 = 2\int_{w_o-\epsilon}^{w_o} P \int_{t'_{wd}}^{\infty} \mathrm{Re}\left[K_{zd}(q_d,w,\theta) \frac{dq_d}{dt} \right] \Big|_{w=w_o} e^{-pt}\, dt\, dw$$

$$+ \int_{w_o-\epsilon}^{w_o} \mathrm{Re}\left\{ \left[\hat{K}_{zd}(q,w,\theta) e^{-\frac{p}{c_d}(m_d z - iqr)} \right] \Big|_{q=\frac{w\sin\theta + i\gamma}{\cos\theta}} \right\} \Big|_{w=w_o} dw \,, \qquad (2.4\text{-}26a)$$

$$\bar{I}_3 = 2\int_{w_o}^{w_o+\epsilon} P \int_{t'_{wd}}^{\infty} (\dot{\tilde{\ }})\, dt\, dw \quad + \quad \int_{w_o}^{w_o+\epsilon} (\dot{\tilde{\ }})\, dw \,, \qquad (2.4\text{-}26b)$$

where t'_{wd} equals t_{wd} evaluated at $w = w_o$. The integrands in $\bar{I}_3$ are exactly the same as for $\bar{I}_2$. P precedes an improper integral to imply that it is interpreted in the sense of a Cauchy principal value (as defined in Copson [23], p. 133). Such integrals arise in (2.4-26) because of the poles lying on the contour $q_d(\pm)$ at $t = t_L$. The second term in $\bar{I}_2$ and $\bar{I}_3$ is the contribution from C_1 and C_2, which is essentially half of the residue evaluation of the poles. However, since each w-integrand in (2.4-26) is a bounded, constant function of w, it follows that $\bar{I}_2$ and $\bar{I}_3$ are linear functions of ϵ and vanish as ϵ goes to zero.

Then by substituting (2.4-25) and (2.4-26) into (2.4-23) and noting that the limit as M goes to infinity proceeds exactly as in Case I, one finds

$$\bar{u}_{zd}(\underline{x},p) = \lim_{\epsilon \to 0}\left[\int_0^{w_o-\epsilon} + \int_{w_o+\epsilon}^{\infty}\right]\int_{t_{wd}}^{\infty} \mathrm{Re}\left[K_{zd}(q_d,w,\theta)\frac{dq_d}{dt}\right] e^{-pt}\, dt\, dw$$

$$+ \lim_{\epsilon \to 0} \int_{w_o+\epsilon}^{\infty} \mathrm{Re}\left\{\left[\hat{K}_{zd}(q,w,\theta) e^{-\frac{p}{c_d}(m_d z - iqr)}\right]\Big|_{q = \frac{w\sin\theta + i\gamma}{\cos\theta}}\right\} dw \,. \qquad (2.4\text{-}27)$$

In the limit as $\epsilon \to 0$ the t-integral in the first term is interpreted in the sense of a Cauchy principal value because its integrand contains a simple pole† at $t = t_L$ for $w = w_o$. The second term in (2.4-27) converges to a regular integral as $\epsilon \to 0$. Therefore (2.4-27) becomes

$$\bar{u}_{zd}(\underline{x},p) = \bar{A}_{zd}(\underline{x},p) + \bar{B}_{zd}(\underline{x},p) \,, \qquad (2.4\text{-}28)$$

where

$$\bar{A}_{zd}(\underline{x},p) = \int_0^{\infty} P\int_{t_{wd}}^{\infty} \mathrm{Re}\left[K_{zd}(q_d,w,\theta)\frac{dq_d}{dt}\right] e^{-pt}\, dt\, dw \qquad (2.4\text{-}29)$$

and

$$\bar{B}_{zd}(\underline{x},p) = \int_{w_o}^{\infty} \mathrm{Re}\left\{\left[\hat{K}_{zd}(q,w,\theta) e^{-\frac{p}{c_d}(m_d z - iqr)}\right]\Big|_{q = \frac{w\sin\theta + i\gamma}{\cos\theta}}\right\} dw \,. \qquad (2.4\text{-}30)$$

The only difference in $\bar{A}_{zd}$ between cases I and II (compare equations (2.4-11) and (2.4-29)) is the simple pole in the integrand at ($t = t_L$, $w = w_o$). $\bar{B}_{zd}$ only differs in the lower limit (compare equations (2.4-12) and (2.4-30)).

---

† For integrals along the real line, a simple pole refers to a $\frac{1}{t-t_o}$ type singularity which lies on the real line at $t = t_o$.

Completing the inversion of $\overline{A}_{zd}$ in (2.4-29) is similar to case I, except when interchanging the order of integration one must account for the additional singularity in the integrand. The reference given in case I is still sufficient to guarantee the interchange since the double integral in (2.4-29) is absolutely convergent. Therefore, by interchanging the order of integration and inverting the Laplace transform one finds

$$A_{zd}(\underline{x},t) = H(t-t_d)P\int_0^{T_d} \mathrm{Re}\left[K_{zd}(q_d,w,\theta)\,\frac{dq_d}{dt}\right] dw \quad , \tag{2.4-31}$$

where T_d and t_d are given in (2.4-14a). This integral is interpreted as a Cauchy principal value for $t = t_L$. As in case I, A_{zd} is identified as a hemispherical, dilatational wave.

To complete the inversion of $\overline{B}_{zd}$ one proceeds exactly as in case I. The singularities that arise in the w-plane and the contour w_d remain the same except for their relative position with the real w-axis as shown in Fig. 6. The contour w_d intersects the real w-axis at $w = w_o$, the lower limit of the w-integral in $\overline{B}_{zd}$, for $t = t_L$. The application of the Cauchy-Goursat theorem to the integrand in (2.4-30) with the Re-operator taken outside the integral and $\mathcal{C}$ in Fig. 6 gives, upon inverting the Laplace transform,

$$B_{zd}(\underline{x},t) = \mathrm{Re}\left[\hat{K}_{zd}(w_d,\theta)\,\frac{dw_d}{dt}\right] H(t-t_L) \quad , \tag{2.4-32}$$

where $\hat{K}_{zd}(w,\theta)$ is given in (2.4-20a). B_{zd} has the same algebraic form as in case I (see (2.4-21)), but it lacks the conical, dilatational wave front.

By combining (2.4-31) and (2.4-32) with (2.4-28), u_{zd} for case II becomes

$$u_{zd}(\underline{x},t) = H(t-t_d)P\int_0^{T_d} \mathrm{Re}\left[K_{zd}(q_d,w,\theta)\frac{dq_d}{dt}\right] dw + \mathrm{Re}\left[\hat{K}_{zd}(w_d,\theta)\frac{dw_d}{dt}\right]H(t-t_L) \quad , \qquad (2.4\text{-}33)$$

where the notation is defined in the text, $x > 0$, and $\frac{x}{\rho} < \frac{c_d}{c}$. That the discontinuity in the second term of (2.4-33), which is caused by $H(t-t_L)$, coincides with the Cauchy principal value in the first term is consistent with the way the poles at $q = \frac{\pm w \sin\theta + i\gamma}{\cos\theta}$ migrate through $q_d(\pm)$. Therefore one should expect u_{zd} to be continuous over $t = t_L$. This is proven in section 3.3 for a special case (in fact all derivatives of u_{zd} should be continuous over $t = t_L$, implying that $t = t_L$ is not a wave front, but this is not proven). The Roman numeral two in the diagrams at the bottom of Fig. 7 is located in the domain (all $\underline{x}$ such that $x > 0$ and $\frac{x}{\rho} < \frac{c_d}{c}$) of the half-space where (2.4-33) is pertinent.

Case III: $x < 0$

As indicated in (2.4-7), no poles lie inside C. Therefore the computations proceed exactly as in case I, less the residue term $\overline{B}_{zd}$, and u_{zd} can be gotten from (2.4-22) by deleting the algebraic term. This case is also depicted in Fig. 7.

Summary:

By comparing the conditions underlying each case in (2.4-7)

and the results given for these cases, it follows that u_{zd} can be represented by one expression for all three cases. In particular, the dilatational contribution to the vertical displacement for supersonic load motion is

$$u_{zd}(\underline{x},t) = H(t-t_d)P\int_0^{T_d} \mathrm{Re}\left[K_{zd}(q_d,w,\theta)\frac{dq_d}{dt}\right]dw$$

$$+ \mathrm{Re}\left[\hat{K}_{zd}(w_d,\theta)\frac{dw_d}{dt}\right]H(t-t_{dc})H(t-t_L)H(x) \ , \qquad (2.4\text{-}34)$$

where the notation is given in the text, $\theta \geq 0$, $|x| > 0$, and $|\frac{x}{\rho} - \frac{c_d}{c}| > 0$. As shown in case II, the integral in the first term of (2.4-34) is interpreted as a Cauchy principal value for $t = t_L$ if $x > 0$. By inspection of equation (2.4-34) one sees that it is equally well valid for $\frac{x}{\rho} = \frac{c_d}{c}$ and $x = 0$. To assess u_{zd} at $t = t_d$, $t = t_{dc}$, and $t = t_L$, (2.4-34) must first be expanded near these surfaces. Then the value of u_{zd} at one of them is obtained as a limit of the corresponding expansion. In this way (2.4-34) is valid for all points in the interior of the half-space such that $\theta \geq 0$. By using the reflection property in (2.3-9), equation (2.4-34) can also be extended to include $\theta < 0$.

The wave fronts at $t = t_d$ and $t = t_{dc}$ are shown in Fig. 7. They intersect at $t = t_L$ for $\frac{x}{\rho} = \frac{c_d}{c}$. The spatial variation in the wave front pattern is clearly related to the cone $\frac{x}{\rho} = \frac{c_d}{c}$, which is indicated in Fig. 7 by dashed lines, and to the three cases considered in computing the solution. The Roman numerals in the diagrams at the bottom of Fig. 7 correspond to these cases. The integral contribution to u_{zd} in (2.4-34) is a hemispherical, dilatational wave

emanating from the origin of the coordinates, which is also the initial position of the load. The algebraic term in (2.4-34) is a conical, dilatational wave which trails behind the load. Both the integral and the algebraic term contain a singularity for $t = t_L$.

As mentioned under (2.4-6), for fixed time, $t=t_L$ is the equation of a hemisphere with the center ($x = \frac{ct}{2}$, $n = 0$) and radius $\frac{ct}{2}$. As shown in Fig. 7 and by (2.4-34), only the part of this hemisphere which is behind the wave front at $t = t_d$ is pertinent to u_{zd}. That this part of $t = t_L$ is not a wave front (i.e., u_{zd} and all derivatives of u_{zd} are continuous through $t = t_L$) seems obvious by the way it arose in constructing the solution (see case II and the remarks in the text under (2.4-33)) and by the following heuristic argument. The hemispherical wave front at $t = t_d$ is the characteristic surface associated with the wave equation for ϕ in (2.1-3). The conical wave front at $t = t_{dc}$ can be thought of as the envelope of a sequence of hemispherical, dilatational wave fronts generated by the load as it moves along the x-axis. But the surface at $t = t_L$ can not be constructed by a superposition of these hemispherical wave fronts, and therefore it is not expected to be a wave front.

The integral contribution to u_{zd} in (2.4-34) can easily be approximated at the hemispherical, dilatational wave front because its range of integration vanishes as t approaches t_d (i.e., $T_d \to 0$ as $t \to t_d$). The algebraic contribution can be assessed at the conical, dilatational wave front as well as any other place in the half-space.

These wave front expansions are given in section 3.1.

As one might expect, the wave front geometry associated with u_{zd} in (2.4-34) is peculiar to the case of supersonic load motion. The corresponding results for transonic and subsonic load motion are computed in subsections 2.4.3 and 2.4.4 respectively. In the next subsection the equivoluminal contribution to $\bar{u}_z$ is inverted for supersonic load motion.

2.4.2. Equivoluminal Contribution for Supersonic Load Motion.

From (2.3-4)

$$\bar{u}_{zs}(\underline{x},p) = \frac{1}{2}\int_0^\infty \int_{-\infty}^{\infty} K_{zs}(q,w,\theta) e^{-\frac{p}{c_d}(m_s z - iqr)}\, dq\, dw \ , \qquad (2.4\text{-}35)$$

where K_{zs} and m_s are given by (2.3-5c) and (2.3-7). The inversion of $\bar{u}_{zs}$ proceeds as for $\bar{u}_{zd}$, but the required contour integrations are more complicated due to the appearance of head waves. Since the behavior of the integrals in (2.4-35) near $w = \infty$ is exactly the same as those in (2.4-1), the computations involving the q-integral are done immediately for $w \in [0,\infty)$. As a function of complex q the singularities in the integrand of $\bar{u}_{zs}$ are the same as those for $\bar{u}_{zd}$ and they are shown again in Fig. 8.

As previously, by seeking the particular contour in the q-plane such that $t = \frac{1}{c_d}(m_s z - iqr)$, one finds

$$q_s(\pm) = \frac{c_d}{\rho^2}\left[itr \pm z(t^2 - t_{ws}^2)^{\frac{1}{2}}\right] \quad \text{for} \quad t \geq t_{ws} \ , \qquad (2.4\text{-}36)$$

where

$$t_{ws} = \frac{\rho}{c_d}(w^2 + \ell^2)^{\frac{1}{2}} \ , \quad \rho = (r^2 + z^2)^{\frac{1}{2}} \ . \qquad (2.4\text{-}36a)$$

t_{ws} represents a pseudo-arrival time which is related to the hemispherical, equivoluminal wave and ρ is the spherical radius introduced in (2.4-4). The other properties of $q_s(\pm)$ are similar to $q_d(\pm)$, except that the vertex, which is now located at $q = \frac{ir}{\rho}(w^2+\ell^2)^{\frac{1}{2}}$ where $t = t_{ws}$, can lie on the branch cut between $q = i(w^2+1)^{\frac{1}{2}}$ and $q = i(w^2+\ell^2)^{\frac{1}{2}}$. As follows from Figs. 8 and 9, this occurs if, and only if, $\frac{r}{\rho}(w^2+\ell^2)^{\frac{1}{2}} > (w^2+1)^{\frac{1}{2}}$. This inequality is equivalent to the conditions $\frac{r}{\rho} > \frac{c_s}{c_d}$ and $w < w_1$, where $w_1 = \frac{\rho}{z}\left(\frac{r^2\ell^2}{\rho^2} - 1\right)^{\frac{1}{2}}$. When the vertex lies on the branch cut, the particular contour wraps around the branch cut and it is given by (2.4-36) plus

$$q_{sd} = \frac{ic_d}{\rho^2}[tr - z(t_{ws}^2 - t^2)^{\frac{1}{2}}] \quad \text{for} \quad t_{ws} \geq t \geq t_{wsd} \quad , \qquad (2.4\text{-}37)$$

where

$$t_{wsd} = \frac{1}{c_d}[(\ell^2-1)^{\frac{1}{2}}z + (w^2+1)^{\frac{1}{2}}r] \quad , \qquad (2.4\text{-}37a)$$

and an identation C_1 around the branch point at $q = i(w^2+1)^{\frac{1}{2}}$. The contours C_1 and q_{sd} are shown in Fig. 9 where a $(\pm)$ notation has been added to q_{sd} to indicate whether the contour is on the right or left side of the branch cut. q_{sd} is parametrically described by t as t varies monotonically from t_{wsd}, the arrival time of a pseudo-head wave, to t_{ws}, the arrival time of the pseudo-hemispherical, equivoluminal wave introduced above. In two-dimensional problems (see, for example, DeHoop [22]) contributions from contours like q_{sd} are identified as headwaves, that is an equivoluminal disturbance which propagates in front of the two-sided, equivoluminal waves. But here, in view of the additional integration variable w, q_{sd} contributes pseudo-

head waves.

The q-plane for $\frac{r}{\rho} < \frac{c_s}{c_d}$ and $w \in [0,\infty)$ is shown in Fig. 8. When $\frac{r}{\rho} > \frac{c_s}{c_d}$, the q-plane is shown in Fig. 9 for $w \in [0,w_1)$ and in Fig. 8 for $w \in (w_1,\infty)$. The closed contour C is again constructed, but it varies depending on where the vertex lies. It is shown in Figs. 8 and 9. The conditions for the poles at $q = \frac{\pm w \sin\theta + iy}{\cos\theta}$ to be inside C are more complicated than for the dilatational computation. Not only can these poles migrate through $q_s(\pm)$, they can also intersect q_{sd}.

If $\frac{r}{\rho} < \frac{c_s}{c_d}$, these poles migrate through $q_s(\pm)$ and lie inside C if, and only if (compare the positions of $q = \frac{\pm w \sin\theta + iy}{\cos\theta}$ and $q_s(\pm)$ in the q-plane in Fig. 8),

$$\left.\begin{array}{ll} (1) & -\frac{\pi}{2} < \theta < \frac{\pi}{2} \\ (2) & \frac{y}{\cos\theta} < \frac{c_d t r}{\rho^2} \\ (3) & w \tan\theta > \frac{c_d z}{\rho^2}\,(t^2 - t_{ws}^2)^{\frac{1}{2}} \end{array}\right\}, \qquad (2.4\text{-}38)$$

or equivalently (using coordinates shown in Fig. 2 and t_{ws} in (2.4-36a))

$$\left.\begin{array}{ll} (1) & x > 0 \\ (2) & t > t_L \quad \text{where} \quad t_L = \frac{\rho^2}{cx} \\ (3) & w^2 > w_o^2 \end{array}\right\} \qquad (2.4\text{-}39)$$

$$\text{where} \quad w_o^2 = \left(\frac{\rho^2\gamma^2}{x^2} - \ell^2\right)\frac{z^2\cos^2\theta}{n^2}, \quad n = (y^2+z^2)^{\frac{1}{2}}.$$

n represents the radial coordinate introduced in (2.4-6) and $t = t_L$ is the same surface as found for the dilatational disturbance.

If $\frac{r}{\rho} > \frac{c_s}{c_d}$ the poles can migrate through $q_s(\pm)$ or intersect q_{sd}. By comparing the positions of the poles at $q = \frac{\pm w \sin\theta + i\gamma}{\cos\theta}$, the vertex at $q = \frac{ir}{\rho}(w^2 + \ell^2)^{\frac{1}{2}}$, and the branch point at $q = i(w^2+1)^{\frac{1}{2}}$ as w goes to zero (see Fig. 10), one concludes: if $\frac{r}{\rho} > \frac{c_s}{c_d}$ and $\frac{x}{r} > \frac{c_d}{c}$, then the poles lie inside C for $w \in [0,\infty)$; if $\frac{r}{\rho} > \frac{c_s}{c_d}$, $\frac{x}{r} < \frac{c_d}{c}$, and $\frac{x}{\rho} > \frac{c_s}{c}$, then the poles lie inside C for $w \in (0,\infty)$ and intersect q_{sd} for $w = 0$; if $\frac{r}{\rho} > \frac{c_s}{c_d}$ and $\frac{x}{\rho} < \frac{c_s}{c}$, then the poles migrate through $q_s(\pm)$ and conditions (2.4-39) determine when they lie inside C.

In view of the conditions regarding the position of the poles and the vertex in the q-plane, and the anticipation of using the Cauchy-Goursat theorem along C, it is convenient to consider the following seven cases:

Case I: $x > 0$, $\frac{x}{\rho} > \frac{c_s}{c}$, $\frac{r}{\rho} < \frac{c_s}{c_d}$, $\frac{x}{r} > \frac{c_d}{c}$

The poles lie inside C for $w \in [0,\infty)$.

The vertex does not lie on the branch cut for $w \in [0,\infty)$.

Case II: $x > 0$, $\frac{x}{\rho} > \frac{c_s}{c}$, $\frac{r}{\rho} > \frac{c_s}{c_d}$, $\frac{x}{r} > \frac{c_d}{c}$

The poles lie inside C for $w \in [0,\infty)$.

The vertex lies on the branch cut for $w \in [0, w_1)$.

Case III: $x > 0$, $\frac{x}{\rho} > \frac{c_s}{c}$, $\frac{r}{\rho} > \frac{c_s}{c_d}$, $\frac{x}{r} < \frac{c_d}{c}$

The poles lie inside C for $w \in (0,\infty)$ and intersect q_{sd} for $w = 0$.

The vertex lies on the branch cut for $w \in [0,w_1)$.

Case IV: $x > 0$, $\frac{x}{\rho} < \frac{c_s}{c}$, $\frac{r}{\rho} < \frac{c_s}{c_d}$

The poles lie inside C for $w \in (w_o,\infty)$.

The vertex does not lie on the branch cut for $w \in [0,\infty)$.

Case V: $x > 0$, $\frac{x}{\rho} < \frac{c_s}{c}$, $\frac{r}{\rho} > \frac{c_s}{c_d}$

The poles lie inside C for $w \in (w_o,\infty)$.

The vertex lies on the branch cut for $w \in [0,w_1)$.

Case VI: $x < 0$, $\frac{r}{\rho} < \frac{c_s}{c_d}$

No poles lie inside C for $w \in [0,\infty)$.

The vertex does not lie on the branch cut for $w \in [0,\infty)$.

Case VII: $x < 0$, $\frac{r}{\rho} > \frac{c_s}{c_d}$

No poles lie inside C for $w \in [0,\infty)$.

The vertex lies on the branch cut for $w \in [0,w_1)$.

(Cases I - VII are referred to in the text by (2.4-40))

The poles referred to in (2.4-40) are $q = \frac{\pm w \sin\theta + i\gamma}{\cos\theta}$; the vertex is $q = \frac{ir}{\rho}(w^2+\ell^2)^{\frac{1}{2}}$; $w_o = \left(\frac{\rho^2\gamma^2}{x^2} - \ell^2\right)^{\frac{1}{2}} \frac{z\cos\theta}{n}$, where $w_o > 0$; and $w_1 = \frac{\rho}{z}\left(\frac{r^2\ell^2}{\rho^2} - 1\right)^{\frac{1}{2}}$, where $w_1 > 0$. Each of these cases, while including

a different part of the half-space, requires a different application of the Cauchy-Goursat theorem. Furthermore, excluding $x = 0$, $\frac{x}{\rho} = \frac{c_s}{c}$, $\frac{x}{r} = \frac{c_d}{c}$, and $\frac{r}{\rho} = \frac{c_s}{c_d}$, all positions in the interior of the half-space are included in these cases. For $x > 0$, $\frac{x}{\rho} = \frac{c_s}{c}$ defines a cone, whose axis is the positive x-axis, which plays a similar role in the solution as $\frac{x}{\rho} = \frac{c_d}{c}$ for the dilatational contribution. Also, $\frac{r}{\rho} = \frac{c_s}{c_d}$ defines a cone, but whose axis is the positive z-axis. Finally, for $x > 0$, $\frac{x}{r} = \frac{c_d}{c}$ defines two planes, one for $y > 0$ and one for $y < 0$. The restrictions $\frac{x}{r} \gtrless \frac{c_d}{c}$ and $\frac{r}{\rho} \gtrless \frac{c_s}{c_d}$ in (2.4-40) introduce complications that were not present in the dilatational contribution. As the solution will show, these restrictions are related to the head waves. The inversion of $\bar{u}_{zs}$ will be completed in each of these cases, with the results summarized at the end of this subsection.

Case I: $x > 0$, $\frac{x}{\rho} > \frac{c_s}{c}$, $\frac{r}{\rho} < \frac{c_s}{c_d}$, $\frac{x}{r} > \frac{c_d}{c}$

By noting the conditions in (2.4-40) for case I and applying the Cauchy-Goursat theorem to the integrand in (2.4-35) with C in Fig. 8, one finds

$$\bar{u}_{zs}(\underline{x},p) = \bar{A}_{zs}(\underline{x},p) + \bar{B}_{zs}(\underline{x},p) \quad , \tag{2.4-41}$$

where

$$\bar{A}_{zs}(\underline{x},p) = \int_0^{\infty}\int_{t_{ws}}^{\infty} \mathrm{Re}\left[K_{zs}(q_s,w,\theta) \frac{dq_s}{dt} \right] e^{-pt}\, dt\, dw \tag{2.4-42}$$

and

$$\overline{B}_{zs}(\underline{x},p) = \int_0^\infty \mathrm{Re}\left\{\left[\hat{K}_{zs}(q,w,\theta)e^{-\frac{p}{c_d}(m_s z - iqr)}\right]\Big|_{q=\frac{w\sin\theta+iy}{\cos\theta}}\right\} dw \qquad (2.4\text{-}43)$$

with

$$\hat{K}_{zs}(q,w,\theta) = \frac{-2\sec\theta\, m_d(q^2+w^2)}{\pi c\mu R(q,w)} . \qquad (2.4\text{-}43a)$$

$\overline{A}_{zs}$ is the contribution from $q_s(\pm)$ and the convention has been adopted that $q_s = q_s(+)$. Also, $\overline{B}_{zs}$ is the residue contribution from the poles at $q = \frac{\pm w\sin\theta + iy}{\cos\theta}$ and $\hat{K}_{zs}$ is that part of K_{zs} which is left after the residue evaluation. The integrals that arise along C_I and C_{II} vanish in view of Jordan's lemma and remark (3) under Fig. 8.

The inversion of $\overline{A}_{zs}$ proceeds exactly as for $\overline{A}_{zd}$ in case I of subsection 2.4.1 and A_{zs} is given by

$$A_{zs}(\underline{x},t) = H(t-t_s)\int_0^{T_s} \mathrm{Re}\left[K_{zs}(q_s,w,\theta)\frac{dq_s}{dt}\right] dw , \qquad (2.4\text{-}44)$$

where

$$T_s = \left(\frac{t^2}{t_s^2} - 1\right)^{\frac{1}{2}} \ell \quad , \quad t_s = \frac{\rho}{c_s} . \qquad (2.4\text{-}44a)$$

t_s is the arrival time of a hemispherical, equivoluminal wave emanating from the origin of the coordinates as shown in Fig. 15. Therefore A_{zs} represents a hemispherical, equivoluminal wave.

The inversion of $\overline{B}_{zs}$ proceeds in a similar manner as for $\overline{B}_{zd}$ in case I of subsection 2.4.1. Formula (2.4-43) is written as

$$\overline{B}_{zs}(\underline{x},p) = \mathrm{Re}\int_0^\infty \left[\hat{K}_{zs}(q,w,\theta)e^{-\frac{p}{c_d}(m_s z - iqr)}\right]\Big|_{q=\frac{w\sin\theta + i\gamma}{\cos\theta}} dw \quad . \qquad (2.4\text{-}45)$$

As a function of complex w the singularities in the integrand of $\overline{B}_{zs}$ are the same as those for $\overline{B}_{zd}$ and they are shown again in Fig. 11.

As previously, by seeking the particular contour in the w-plane such that $t = \frac{1}{c_d}(m_s z - iqr)\Big|_{q=\frac{w\sin\theta + i\gamma}{\cos\theta}}$, one finds

$$w_s(\pm) = -i\gamma\sin\theta + \frac{\gamma\cos\theta}{n^2}(i\xi y \pm z\alpha_s) \quad \text{for } t \geq t_s \ , \qquad (2.4\text{-}46)$$

where

$$\left.\begin{aligned} t_{sc} &= \frac{1}{c}\left[\left(\frac{c^2}{c_s^2} - 1\right)^{\frac{1}{2}} n + x\right] \\ \alpha_s &= \left[\xi^2 - \left(\frac{c^2}{c_s^2} - 1\right)n^2\right]^{\frac{1}{2}} \\ \xi &= ct - x \quad , \quad n = (y^2 + z^2)^{\frac{1}{2}} . \end{aligned}\right\} \qquad (2.4\text{-}46a)$$

t_{sc} represents the arrival time of a conical, equivoluminal wave trailing behind the load as shown in Fig. 15. ξ is the coordinate introduced in (2.4-19). Again, only the plus root of $w_s(\pm)$ is needed and the convention is adopted that $w_s = w_s(+)$. The contour w_s is shown in Fig. 11. The other properties of w_s are similar to those of w_d in subsection 2.4.1, except for the position of the vertex, which is now located at $w = i\gamma\sin\theta + \frac{i\gamma}{n}(\ell^2 - \gamma^2)^{\frac{1}{2}}\cos\theta$ where $t = t_{sc}$. By comparing the position of the vertex and the branch points in the w-plane one finds that if $\frac{\gamma}{n} < \phi_c$, where $\phi_c = \left(\frac{c^2}{c_d^2} - 1\right)^{\frac{1}{2}} \Big/ \left(\frac{c^2}{c_s^2} - 1\right)^{\frac{1}{2}}$, the

vertex lies on the imaginary w-axis between the real w-axis and the branch point at $w = -i\gamma \sin\theta + i(1-\gamma^2)^{\frac{1}{2}}\cos\theta$. But, if $\frac{y}{n} > \phi_c$ it lies between the branch points at $w = -i\gamma \sin\theta + i(1-\gamma^2)^{\frac{1}{2}}\cos\theta$ and $w = -i\gamma \sin\theta + i(\ell^2-\gamma^2)^{\frac{1}{2}}\cos\theta$. As the solution will show, the angle ϕ_c is related to the head waves. However, the conditions $\frac{x}{\rho} > \frac{c_s}{c}$ and $\frac{r}{\rho} < \frac{c_s}{c_d}$, that underlie this case, imply that $\frac{y}{n} < \phi_c$.

Then, for $\frac{y}{n} < \phi_c$ the w-plane is given in Fig. 11. The application of the Cauchy-Goursat theorem to the integrand in (2.4-45) and $\mathcal{C}$ shown in Fig. 11 gives

$$\overline{B}_{zs}(\underline{x},p) = \mathrm{Re}\int_{t_{sc}}^{\infty} \hat{K}_{zs}(w_s,\theta)\frac{dw_s}{dt}\, e^{-pt}\, dt \ , \qquad (2.4\text{-}47)$$

where

$$\hat{K}_{zs}(w,\theta) = \hat{K}_{zs}\left(\frac{w\sin\theta + i\gamma}{\cos\theta}, w, \theta\right) \ . \qquad (2.4\text{-}47a)$$

The integral that arises along $\mathcal{C}_I$ vanishes in view of Jordan's lemma and remark (3) under Fig. 11, and the integral along $\mathcal{C}_1$ vanishes because its real part is zero. The inversion of the Laplace transform in (2.4-47) yields

$$B_{zs}(\underline{x},t) = \mathrm{Re}\left[\hat{K}_{zs}(w_s,\theta)\frac{dw_s}{dt}\right] H(t-t_{sc}) \ . \qquad (2.4\text{-}48)$$

In view of $H(t-t_{sc})$ in (2.4-48), B_{zs} represents a conical, equivoluminal wave trailing behind the load.

By combining (2.4-41), (2.4-44), and (2.4-48), u_{zs} for Case I becomes

$$u_{zs}(\underline{x},t) = H(t-t_s)\int_0^{T_s} \mathrm{Re}\left[K_{zs}(q_s,w,\theta)\,\frac{dq_s}{dt}\right] dw$$

$$+ \mathrm{Re}\left[\hat{K}_{zs}(w_s,\theta)\,\frac{dw_s}{dt}\right] H(t-t_{sc}), \qquad (2.4\text{-}49)$$

where the notation is given in the text, $x > 0$, $\frac{x}{\rho} > \frac{c_s}{c}$, $\frac{r}{\rho} < \frac{c_s}{c_d}$, $\frac{x}{r} > \frac{c_d}{c}$, and $\frac{y}{n} < \phi_c$. The Roman numeral one in Fig. 17[†] is located in the domain (all $\underline{x}$ satisfying the inequalities following (2.4-49)) of the half-space where (2.4-49) is pertinent.

Case II: $x > 0$, $\frac{x}{\rho} > \frac{c_s}{c}$, $\frac{r}{\rho} > \frac{c_s}{c_d}$, $\frac{x}{r} > \frac{c_d}{c}$

By noting the conditions in (2.4-40) for case II and applying the Cauchy-Goursat theorem to the integrand of (2.4-35) with C given in Fig. 9 for $w \in [0, w_1)$ and in Fig. 8 for $w \in (w_1, \infty)$, one finds

$$\overline{u}_{zs}(\underline{x},p) = \overline{A}_{zs}(\underline{x},p) + \overline{B}_{zs}(\underline{x},p) + \overline{D}_{zs}(\underline{x},p), \qquad (2.4\text{-}50)$$

where $\overline{A}_{zs}$ and $\overline{B}_{zs}$ are given by (2.4-42) and (2.4-45) respectively, and

$$\overline{D}_{zs}(\underline{x},p) = \int_0^{\infty}\int_{t_{wsd}}^{t_{ws}} \mathrm{Re}\left[K_{zs}(q_{sd},w,\theta)\,\frac{dq_{sd}}{dt}\right] e^{-pt}\,dt\,H(w_1 - w)\,dw\,. \qquad (2.4\text{-}51)$$

The contribution from C_1 in Fig. 9 vanishes because the integrand of (2.4-35) is regular at $q = i(w^2+1)^{\frac{1}{2}}$ and the radius of C_1 is assumed to go to zero. As mentioned previously, $\overline{D}_{zs}$, being the contribution

---

[†] In Figs. 16, 17, 18 and 20 the dilatational wave fronts are shown for reference in addition to the equivoluminal ones, even though only the latter are found in this subsection.

from q_{sd}, will contribute pseudo-head waves. The remaining details in deducing (2.4-50) are the same as in case I and they are deleted here.

The inversion of $\overline{A}_{zs}$ proceeds exactly as in case I with A_{zs} given by (2.4-44). The inversion of $\overline{B}_{zs}$ also proceeds as in Case I, except that both possibilities $\frac{y}{n} \gtrless \phi_c$ arise. The inversion of $\overline{B}_{zs}$ for $\frac{y}{n} < \phi_c$ remains exactly the same as in case I and B_{zs} is given by (2.4-48).

For the case $\frac{y}{n} > \phi_c$ the w-plane is given in Fig. 12 and an additional segment of contour must be included in $\mathcal{C}$, namely w_{sd} given by

$$w_{sd} = -i\gamma \sin\theta + \frac{i\gamma \cos\theta}{n^2}(\xi y - z\alpha_{sd}) \quad \text{for} \quad t_{sc} \geq t \geq t_{sdc}, \tag{2.4-52}$$

where

$$\left.\begin{aligned} t_{sdc} &= \frac{1}{c}\left[\left(\frac{c^2}{c_s^2} - \frac{c^2}{c_d^2}\right)^{\frac{1}{2}} z + \left(\frac{c^2}{c_d^2} - 1\right)^{\frac{1}{2}} y + x\right] \\ \alpha_{sd} &= \left[\left(\frac{c^2}{c_s^2} - 1\right)n^2 - \xi^2\right]^{\frac{1}{2}}, \quad \xi = ct - x, \quad n = (y^2 + z^2)^{\frac{1}{2}}. \end{aligned}\right\} \tag{2.4-52a}$$

w_{sd} is shown in Fig. 12 and it is monotonically described by t as t varies from t_{sdc} to t_{sc}. t_{sc} is given in (2.4-46a) and t_{sdc} is the arrival time of a head wave which has a plane wave front and trails behind the load as shown in Fig. 18. The application of the Cauchy-Goursat theorem to the integrand in (2.4-45) and $\mathcal{C}$ shown in Fig. 12 yields

$$\overline{B}_{zs}(\underline{x},p) = \mathrm{Re}\int_{t_{sc}}^{\infty} \hat{K}_{zs}(w_s,\theta)\frac{dw_s}{dt}e^{-pt}\,dt + \mathrm{Re}\int_{t_{sdc}}^{t_{sc}} \hat{K}_{zs}(w_{sd},\theta)\frac{dw_{sd}}{dt}e^{-pt}\,dt \quad , \tag{2.4-53}$$

where $\hat{K}_{zs}(w,\theta)$ is given in (2.4-47a). The integrals that arise along C_I and C_1 vanish as in case I. Then the inversion of the Laplace transform in (2.4-53) gives

$$B_{zs}(\underline{x},t) = \mathrm{Re}\left[\hat{K}_{zs}(w_s,\theta)\frac{dw_s}{dt}\right]H(t-t_{sc}) + \mathrm{Re}\left[\hat{K}_{zs}(w_{sd},\theta)\frac{dw_{sd}}{dt}\right]\left[H(t-t_{sdc})-H(t-t_{sc})\right] . \tag{2.4-54}$$

The first term in (2.4-54) is the same conical, equivoluminal wave given in (2.4-48) and the second term is a plane head wave which propagates in front of the conical, equivoluminal wave. Consequently, unlike case I, the conical, equivoluminal wave front is a two-sided wave front for $\frac{y}{n} > \phi_c$ as indicated in Fig. 18.

By combining the Heaviside function $H(\frac{y}{n} - \phi_c)$ with (2.4-48) and (2.4-54), B_{zs} for both $\frac{y}{n} > \phi_c$ and $\frac{y}{n} < \phi_c$ can be written as

$$B_{zs}(\underline{x},t) = \mathrm{Re}\left[\hat{K}_{zs}(w_s,\theta)\frac{dw_s}{dt}\right]H(t-t_{sc}) + \mathrm{Re}\left[\hat{K}_{zs}(w_{sd},\theta)\frac{dw_{sd}}{dt}\right]H\left(\frac{y}{n} - \phi_c\right)\left[H(t-t_{sdc})-H(t-t_{sc})\right] . \tag{2.4-55}$$

To invert $\overline{D}_{zs}$, (2.4-51) is written as

$$\overline{D}_{zs}(\underline{x},p) = \int_0^\infty \int_0^\infty \mathrm{Re}\left[K_{zs}(q_{sd},w,\theta)\,\frac{dq_{sd}}{dt}\right] e^{-pt}$$

$$\cdot[\,H(t-t_{wsd})-H(t-t_{ws})]\;dt\;H(w_1-w)\;dw\;. \qquad (2.4\text{-}56)$$

The function

$$\frac{dq_{sd}}{dt} = \frac{ic_d}{\rho^2}\left[\,r + zt(t_{ws}^2 - t^2)^{-\frac{1}{2}}\right] \qquad (2.4\text{-}57)$$

introduces an integrable singularity at $t = t_{ws}$ and a simple pole at $(t = t_s\,,\ w = 0)$ into the integrand of $\overline{D}_{zs}$. Also, the exponential in the integrand dominates near $t = \infty$ and/or $w = \infty$. Therefore the double integral in (2.4-56) is absolutely convergent and the order of integration can legitimately be interchanged (see Jeffreys and Jeffreys [24], pp. 180 - 181). Then the inversion of the Laplace transform in (2.4-56) gives

$$D_{zs}(\underline{x},t) = \int_0^\infty \mathrm{Re}\left[K_{zs}(q_{sd},w,\theta)\,\frac{dq_{sd}}{dt}\right][\,H(t-t_{wsd})-H(t-t_{ws})]\,H(w_1-w)\;dw\,, \qquad (2.4\text{-}58)$$

where the integral in (2.4-58) is improper for $t = t_s$ because its integrand contains a simple pole at $w = 0$ for $t = t_s$. By using the Heaviside function in the integrand of (2.4-58) to restrict the range of integration, D_{zs} can be written as

$$D_{zs}(\underline{x},t) = H(t-t_s)H(t_B-t)\int_{T_s}^{T_{sd}} \mathrm{Re}\left[K_{zs}(q_{sd},w,\theta)\,\frac{dq_{sd}}{dt}\right] dw$$

$$+[\,H(t-t_{sd})-H(t-t_s)]\int_0^{T_{sd}} \mathrm{Re}\left[K_{zs}(q_{sd},w,\theta)\frac{dq_{sd}}{dt}\right] dw\,, \qquad (2.4\text{-}59)$$

where

$$T_{sd}=\left[\left(\frac{c_d(t-t_{sd})}{r}+1\right)^2-1\right]^{\frac{1}{2}}, \quad t_{sd}=\frac{1}{c_d}\left[(\ell^2-1)^{\frac{1}{2}}z+r\right], \quad t_B=\frac{\rho^2(\ell^2-1)^{\frac{1}{2}}}{zc_d}, \tag{2.4-59a}$$

and T_s and t_s are given in (2.4-44a). t_{sd} is the arrival time of a head wave that has a conical wave front. This head wave emanates from the origin of the coordinates as shown in Fig. 17. Both integrals in (2.4-59) are improper for $t = t_s$ because their integrands contain a simple pole at $w = 0$ for $t = t_s$. As shown in section 3.1, an expansion of these improper integrals generates a two-sided, logarithmic singularity at the hemispherical, equivoluminal wave front.

The first term in (2.4-59) represents another hemispherical, equivoluminal wave (in addition to A_{zs}), but it has a "back" at $t = t_B$, or equivalently at $r^2+\left[z-\frac{c_dt}{2(\ell^2-1)^{\frac{1}{2}}}\right]^2=\frac{c_d^2t^2}{4(\ell^2-1)}$. For fixed time this contour is the equation of a sphere with center $\left(r=0,\ z=\frac{c_dt}{2(\ell^2-1)^{\frac{1}{2}}}\right)$ and radius $\frac{c_dt}{2(\ell^2-1)^{\frac{1}{2}}}$. The sphere is indicated in Fig. 17 and in subsection 2.4.5 the first term in (2.4-59) is shown to be continuous over it. The second term in (2.4-59) is a conical head wave which propagates in front of the hemispherical, equivoluminal waves. Consequently, unlike case I, the hemispherical equivoluminal wave front that arises in case II is a two-sided wave front as indicated in Fig. 17.

By combining (2.4-44), (2.4-50), (2.4-55), and (2.4-59), u_{zs} for case II becomes

$$u_{zs}(\underline{x},t) = H(t-t_s)\int_0^{T_s} \mathrm{Re}\left[K_{zs}(q_s,w,\theta)\,\frac{dq_s}{dt}\right] dw$$

$$+ H(t-t_s)H(t_B-t)\int_{T_s}^{T_{sd}} \mathrm{Re}\left[K_{zs}(q_{sd},w,\theta)\,\frac{dq_{sd}}{dt}\right] dw$$

$$+ \left[H(t-t_{sd})-H(t-t_s)\right]\int_0^{T_{sd}} \mathrm{Re}\left[K_{zs}(q_{sd},w,\theta)\,\frac{dq_{sd}}{dt}\right] dw$$

$$+ \mathrm{Re}\left[\hat{K}_{zs}(w_s,\theta)\,\frac{dw_s}{dt}\right] H(t-t_{sc})$$

$$+ \mathrm{Re}\left[\hat{K}_{zs}(w_{sd},\theta)\,\frac{dw_{sd}}{dt}\right] H\left(\frac{y}{n}-\phi_c\right)\left[H(t-t_{sdc})-H(t-t_{sc})\right] , \qquad (2.4\text{-}60)$$

where the notation is given in the text, $x > 0$, $\frac{x}{\rho} > \frac{c_s}{c}$, $\frac{r}{\rho} > \frac{c_s}{c_d}$, and $\frac{x}{r} > \frac{c_d}{c}$. The Roman numeral two in Figs. 16 and 17 is located in the domain (all $\underline{x}$ satisfying the inequalities following (2.4-60)) of the half-space where (2.4-60) is pertinent. The main difference between this case and case I is the appearance of the head waves and the additional hemispherical, equivoluminal wave.

Case III: $x > 0$, $\frac{x}{\rho} > \frac{c_s}{c}$, $\frac{r}{\rho} > \frac{c_s}{c_d}$, $\frac{x}{r} < \frac{c_d}{c}$

As displayed in (2.4-40) for case III, the poles at $q = \frac{\pm w \sin\theta + iy}{\cos\theta}$ intersect q_{sd} for $w = 0$. Therefore it is convenient to write $\bar{u}_{zs}$ in (2.4-35) as

$$\bar{u}_{zs}(\underline{x},p) = \frac{1}{2}\lim_{\epsilon \to 0}(\bar{I}_1 + \bar{I}_2) \quad , \qquad (2.4\text{-}61)$$

where

$$\left.\begin{aligned} \bar{I}_1 &= \int_0^{\epsilon}\int_{-\infty}^{\infty} K_{zs}(q,w,\theta)\, e^{-\frac{p}{c_d}(m_s z - iqr)}\, dq\, dw \\ \bar{I}_2 &= \int_{\epsilon}^{\infty}\int_{-\infty}^{\infty} K_{zs}(q,w,\theta)\, e^{-\frac{p}{c_d}(m_s z - iqr)}\, dq\, dw \ . \end{aligned}\right\} \qquad (2.4\text{-}62)$$

The Cauchy-Goursat theorem can now be applied uniformly to $\bar{I}_1$ and $\bar{I}_2$, and the corresponding q-planes are shown in Fig. 13.

To evaluate the q-integral in $\bar{I}_1$ one assumes that $w = 0$. This means that the poles at $q = \frac{\pm w \sin\theta + i\gamma}{\cos\theta}$ coalesce on the branch cut at $q = \frac{i\gamma}{\cos\theta}$ and $q_{sd}(\pm)$ must be indented around this position (see C_2 C_3 in Fig. 13). These indentations occur along q_{sd} at $t = t_E$, where $t_E = \frac{1}{cx}\left[\left(\frac{c^2}{c_s^2}x^2 - r^2\right)^{\frac{1}{2}} z + r^2\right]$ (t_E is found by evaluating $t = \frac{1}{c_d}(m_s z - iqr)$ at $q = \frac{i\gamma}{\cos\theta}$ and $w = 0$). The importance of the surface given by $t = t_E$ will be obvious in the solution. Then the application of the Cauchy-Goursat theorem to the integrand of $\bar{I}_1$ and C shown in the upper diagram of Fig. 13 yields

$$\begin{aligned} \bar{I}_1 = {} & 2\int_0^{\epsilon}\int_{t'_{ws}}^{\infty} \mathrm{Re}\left[K_{zs}(q_s,w,\theta)\frac{dq_s}{dt}\right]\Big|_{w=0} e^{-pt}\, dt\, dw \\ & + 2\int_0^{\epsilon} P\int_{t'_{wsd}}^{t'_{ws}} \mathrm{Re}\left[K_{zs}(q_{sd},w,\theta)\frac{dq_{sd}}{dt}\right]\Big|_{w=0} e^{-pt}\, dt\, H(w_1 - w)\, dw \\ & + 2\int_0^{\epsilon} \mathrm{Re}\left\{\left[\hat{K}_{zs}(q,w,\theta)\, e^{-\frac{p}{c_d}(m_s z - iqr)}\right]\Big|_{q=\frac{i\gamma}{\cos\theta}}\right\}\Big|_{w=0} dw \ , \end{aligned} \qquad (2.4\text{-}63)$$

where $\hat{K}_{zs}$ is given in (2.4-43a). Also, t'_{ws} and t'_{wsd} are t_{ws} and t_{wsd} evaluated at $w = 0$. The first and second terms in (2.4-63) are the contributions from $q_s(\pm)$ and $q_{sd}(\pm)$ respectively. The Cauchy principal value arises in the second term in (2.4-63) because of the poles on q_{sd}. The last term is the contribution from C_2 and C_3, which is really just the residue evaluation of the pole at $q = \frac{i\gamma}{\cos\theta}$. However, since each w-integrand in (2.4-63) is a bounded, constant function of w, it follows that $\bar{I}_1$ is a linear function of ϵ and vanishes as ϵ goes to zero.

The application of the Cauchy-Goursat theorem to the integrand of $\bar{I}_2$ in (2.4-62) and the contour C in the lower diagrams of Fig. 13 gives

$$\bar{I}_2 = 2\int_{\epsilon}^{\infty}\int_{t_{ws}}^{\infty} \mathrm{Re}\left[K_{zs}(q_s,w,\theta)\,\frac{dq_s}{dt}\right] e^{-pt}\,dt\,dw$$

$$+ 2\int_{\epsilon}^{\infty}\int_{t_{wsd}}^{t_{ws}} \mathrm{Re}\left[K_{zs}(q_{sd},w,\theta)\,\frac{dq_{sd}}{dt}\right] e^{-pt}dt\,H(w_1-w)\,dw$$

$$+ 2\int_{\epsilon}^{\infty} \mathrm{Re}\left\{\left[\hat{K}_{zs}(q,w,\theta)e^{-\frac{p}{c_d}(m_s z - iqr)}\right]\Big|_{q=\frac{w\sin\theta+i\gamma}{\cos\theta}}\right\} dw\,, \qquad (2.4\text{-}64)$$

where the details in computing (2.4-64) are the same as those in case I and they are deleted here.

Then the substitution of (2.4-63) and (2.4-64) into (2.4-61) produces

$$\bar{u}_{zs}(\underline{x},p) = \lim_{\epsilon \to 0} \int_{\epsilon}^{\infty} \int_{t_{ws}}^{\infty} \mathrm{Re}\left[K_{zs}(q_s,w,\theta) \frac{dq_s}{dt} \right] e^{-pt} dt\, dw$$

$$+ \lim_{\epsilon \to 0} \int_{\epsilon}^{\infty} \int_{t_{wsd}}^{t_{ws}} \mathrm{Re}\left[K_{zs}(q_{sd},w,\theta) \frac{dq_{sd}}{dt} \right] e^{-pt} dt\, H(w_1 - w)\, dw$$

$$+ \lim_{\epsilon \to 0} \int_{\epsilon}^{\infty} \mathrm{Re}\left\{ \left[\hat{K}_{zs}(q,w,\theta) e^{-\frac{p}{c_d}(m_s z - iqr)} \right] \Big|_{q = \frac{w \sin\theta + iy}{\cos\theta}} \right\} dw \quad . \qquad (2.4\text{-}65)$$

The limit as ϵ goes to zero follows immediately in the first and third terms of (2.4-65) because their integrands are regular at $w = 0$. However, the t-integral in the second term is interpreted as a Cauchy principal value as $\epsilon \to 0$ because its integrand has a simple pole at $t = t_E$ for $w = 0$. Therefore, completing the limit in (2.4-65) gives

$$\bar{u}_{zs}(\underline{x},p) = \bar{A}_{zs}(\underline{x},p) + \bar{B}_{zs}(\underline{x},p) + \bar{D}_{zs}(\underline{x},p) \ , \qquad (2.4\text{-}66)$$

where $\bar{A}_{zs}$ and $\bar{B}_{zs}$, being exactly the same as in cases I and II, are given by (2.4-42) and (2.4-45) respectively, and

$$\bar{D}_{zs}(\underline{x},p) = \int_0^{\infty} P \int_{t_{wsd}}^{t_{ws}} \mathrm{Re}\left[K_{zs}(q_{sd},w,\theta) \frac{dq_{sd}}{dt} \right] e^{-pt} dt\, H(w_1 - w)\, dw \ . \qquad (2.4\text{-}67)$$

The only difference in $\bar{D}_{zs}$ between this case and case II is interpreting the t-integral as a Cauchy principal value.

The inversion of $\bar{A}_{zs}$ proceeds exactly as in case I with A_{zs} given by (2.4-44). A_{zs} still represents a hemispherical, equivolu-

minal wave.

To complete the inversion of $\overline{B}_{zs}$ one proceeds exactly as in cases I and II. The conditions $\frac{x}{\rho} > \frac{c_s}{c}$ and $\frac{x}{r} < \frac{c_d}{c}$, that underlie this case, imply that $\frac{y}{n} > \phi_c$. The singularities that arise in the w-plane and the contours w_s and w_{sd} remain the same except for their relative position with the real w-axis as shown in Fig. 14. Then the application of the Cauchy-Goursat theorem to the integrand in (2.4-45) with C given in Fig. 14 and the inversion of the resulting Laplace transform yield

$$B_{zs}(\underline{x},t) = \mathrm{Re}\left[\hat{K}_{zs}(w_s,\theta)\frac{dw_s}{dt}\right] H(t-t_{sc})$$

$$+ \mathrm{Re}\left[\hat{K}_{zs}(w_{sd},\theta)\frac{dw_{sd}}{dt}\right]\left[H(t-t_E) - H(t-t_{sc})\right] . \qquad (2.4\text{-}68)$$

The first term in (2.4-68) is still the conical, equivoluminal wave as found in cases I and II. The second term has the algebraic form of the plane head wave in case II (see equation (2.4-54)), but it lacks the plane wave front at $t = t_{sdc}$.

To invert $\overline{D}_{zs}$ given in (2.4-67) one proceeds exactly as in case II. In this case the integrand contains simple poles at $(t = t_s, w = 0)$ and $(t = t_E,\ w = 0)$. For $\frac{x}{\rho} > \frac{c_s}{c}$, a condition underlying this case, these poles do not coincide, the double integral in (2.4-67) is absolutely convergent, and $\overline{D}_{zs}$ becomes

$$D_{zs}(\underline{x},t) = H(t-t_s)H(t_B-t)\int_{T_s}^{T_{sd}} \mathrm{Re}\left[K_{zs}(q_{sd},w,\theta)\,\frac{dq_{sd}}{dt}\right] dw$$

$$+\left[H(t-t_{sd})-H(t-t_s)\right]\int_{0}^{T_{sd}} \mathrm{Re}\left[K_{zs}(q_{sd},w,\theta)\,\frac{dq_{sd}}{dt}\right] dw\,, \qquad (2.4\text{-}69)$$

where both integrals are improper for $t = t_s$ and the last one is also improper for $t = t_E$. As given in (2.4-69), D_{zs} is the same as in case II (see (2.4-59)), except for the additional singularity when $t = t_E$.

By combining (2.4-44), (2.4-66), (2.4-68), and (2.4-69), u_{zs} for case III becomes

$$u_{zs}(\underline{x},t) = H(t-t_s)\int_{0}^{T_s} \mathrm{Re}\left[K_{zs}(q_s,w,\theta)\frac{dq_s}{dt}\right] dw$$

$$+ H(t-t_s)H(t_B-t)\int_{T_s}^{T_{sd}} \mathrm{Re}\left[K_{zs}(q_{sd},w,\theta)\,\frac{dq_{sd}}{dt}\right] dw$$

$$+\left[H(t-t_{sd})-H(t-t_s)\right]\int_{0}^{T_{sd}} \mathrm{Re}\left[K_{zs}(q_{sd},w,\theta)\,\frac{dq_{sd}}{dt}\right] dw$$

$$+ \mathrm{Re}\left[\hat{K}_{zs}(w_s,\theta)\,\frac{dw_s}{dt}\right] H(t-t_{sc})$$

$$+ \mathrm{Re}\left[\hat{K}_{zs}(w_{sd},\theta)\,\frac{dw_{sd}}{dt}\right]\left[H(t-t_E)-H(t-t_{sc})\right]\,, \qquad (2.4\text{-}70)$$

where the notation is given in the text, $x > 0$, $\frac{x}{\rho} > \frac{c_s}{c}$, $\frac{r}{\rho} > \frac{c_s}{c_d}$, $\frac{x}{r} < \frac{c_d}{c}$, and $\frac{y}{n} > \phi_c$. The Roman numeral three in Fig. 16 is located in the domain (all $\underline{x}$ satisfying the inequalities following (2.4-70)) of the half-space where (2.4-70) is pertinent.

The primary difference in u_{zs} between this case and case II is the disappearance of the plane head wave front. This occurs because the source of the plane head wave front, namely the surface intersection of the conical, dilatational wave front, does not exist for $\frac{x}{r} < \frac{c_d}{c}$, as shown in Fig. 16. Therefore the plane head wave must end, which is reflected by the fact that the third term in (2.4-70) is an improper integral for $t = t_E$ and that the last term is discontinuous at this time. The solution is expected to be continuous over $t = t_E$, which is proven in section 3.3 for a special case.

Case IV: $x > 0$, $\frac{x}{\rho} < \frac{c_s}{c}$, $\frac{r}{\rho} < \frac{c_s}{c_d}$

As indicated in (2.4-40) for case IV, the poles lie inside C for $w \in (w_o, \infty)$ and the vertex does not lie on the branch cut. Therefore the inversion of $\bar{u}_{zs}$ in this case proceeds exactly as for $\bar{u}_{zd}$ in case II of subsection 2.4.1, and u_{zs} can be written down by analogy to u_{zd} (compare equations (2.4-22) and (2.4-33), and use (2.4-49)). That is

$$u_{zs}(\underline{x},t) = H(t-t_s) P \int_0^{T_s} \mathrm{Re}\left[K_{zs}(q_s,w,\theta) \frac{dq_s}{dt} \right] dw + \mathrm{Re}\left[\hat{K}_{zs}(w_s,\theta) \frac{dw_s}{dt} \right] H(t-t_L) \quad , \qquad (2.4\text{-}71)$$

where the notation is the same as in case I, $x > 0$, $\frac{x}{\rho} < \frac{c_s}{c}$, and $\frac{r}{\rho} < \frac{c_s}{c_d}$. The integral in (2.4-71) is interpreted as a Cauchy principal value for $t = t_L$ because its integrand has a simple pole at $w = w_o$ for $t = t_L$. The behavior of u_{zs} over $t = t_L$ is the same as described for u_{zd} in case II of subsection 2.4.1. The Roman numeral four in Fig. 17 is

located in the domain (all $\underline{x}$ such that $x > 0$, $\frac{x}{\rho} < \frac{c_s}{c}$, and $\frac{r}{\rho} < \frac{c_s}{c_d}$) of the half-space where (2.4-71) is pertinent.

Case V: $x > 0$, $\frac{x}{\rho} < \frac{c_s}{c}$, $\frac{r}{\rho} > \frac{c_s}{c_d}$

As displayed in (2.4-40), the only difference between cases IV and V is that the vertex lies on the branch cut in the q-plane for $w \in [0, w_1)$. The contribution from the contours along the branch cut, namely D_{zs}, arises as in case II. Therefore u_{zs} for this case is obtained by adding D_{zs} for case II to u_{zs} for case IV. That is, by combining (2.4-59) and (2.4-71) one finds

$$
\begin{aligned}
u_{zs}(\underline{x},t) = {} & H(t-t_s) P \int_0^{T_s} \mathrm{Re}\left[K_{zs}(q_s,w,\theta) \frac{dq_s}{dt} \right] dw \\
& + H(t-t_s) H(t_B-t) \int_{T_s}^{T_{sd}} \mathrm{Re}\left[K_{zs}(q_{sd},w,\theta) \frac{dq_{sd}}{dt} \right] dw \\
& + \left[H(t-t_{sd}) - H(t-t_s) \right] \int_0^{T_{sd}} \mathrm{Re}\left[K_{zs}(q_{sd},w,\theta) \frac{dq_{sd}}{dt} \right] dw \\
& + \mathrm{Re}\left[\hat{K}_{zs}(w_s,\theta) \frac{dw_s}{dt} \right] H(t-t_L) \quad , \qquad (2.4\text{-}72)
\end{aligned}
$$

where $x > 0$, $\frac{x}{\rho} < \frac{c_s}{c}$, and $\frac{r}{\rho} > \frac{c_s}{c_d}$. The notation and a discussion of the singularities in the integrals are included with (2.4-59) and (2.4-71). The Roman numeral five in Fig. 16 is located in the domain (all $\underline{x}$ such that $x > 0$, $\frac{x}{\rho} < \frac{c_s}{c}$ and $\frac{r}{\rho} > \frac{c_s}{c_d}$) of the half-space where (2.4-72) is pertinent.

Case VI: $x < 0$, $\frac{r}{\rho} > \frac{c_s}{c_d}$

As indicated in (2.4-40), no poles lie inside C and the vertex does not lie on the branch cut in the q-plane. Therefore the computations proceed exactly as in case I, less the residue term $\overline{B}_{zs}$, and u_{zs} can be gotten from (2.4-49) by deleting the algebraic term. This case is depicted in Fig. 17 by a Roman numeral six.

Case VII: $x < 0$, $\frac{r}{\rho} > \frac{c_s}{c_d}$

As indicated in (2.4-40), no poles lie inside C, but the vertex lies on the branch cut in the q-plane for $w \in [0, w_1)$. Therefore the computations proceed exactly as in case II, less the residue term $\overline{B}_{zs}$, and u_{zs} can be gotten from (2.4-60) by deleting the algebraic terms. This case is depicted in Figs. 16 and 17 by a Roman numeral seven.

Summary:

By comparing the conditions underlying each case in (2.4-40) and the results given for these cases, it follows that u_{zs} can be represented by one expression for all seven cases. In particular, the equivoluminal contribution to the vertical displacement for supersonic load motion is

$$u_{zs}(\underline{x},t) = H(t-t_s)P\int_0^{T_s} \mathrm{Re}\left[K_{zs}(q_s,w,\theta)\,\frac{dq_s}{dt}\right]dw$$

$$+ H(t-t_s)H(t_B-t)H\left(\frac{r}{\rho}-\frac{c_s}{c_d}\right)\int_{T_s}^{T_{sd}} \mathrm{Re}\left[K_{zs}(q_{sd},w,\theta)\,\frac{dq_{sd}}{dt}\right]dw$$

$$+ \left[H(t-t_{sd})-H(t-t_s)\right]H\left(\frac{r}{\rho}-\frac{c_s}{c_d}\right)\int_0^{T_{sd}} \mathrm{Re}\left[K_{zs}(q_{sd},w,\theta)\,\frac{dq_{sd}}{dt}\right]dw$$

$$+ \mathrm{Re}\left[\hat{K}_{zs}(w_s,\theta)\frac{dw_s}{dt}\right]H(t-t_{sc})H(t-t_L)H(x)$$

$$+ \mathrm{Re}\left[\hat{K}_{zs}(w_{sd},\theta)\,\frac{dw_{sd}}{dt}\right]H\left(\frac{y}{n}-\phi_c\right)\left\{H(t-t_{sdc})H\left(\frac{x}{r}-\frac{c_d}{c}\right)\right.$$

$$\left. + H(t-t_E)\left[H\left(\frac{x}{\rho}-\frac{c_s}{c}\right)-H\left(\frac{x}{r}-\frac{c_d}{c}\right)\right]-H(t-t_{sc})H\left(\frac{x}{\rho}-\frac{c_s}{c}\right)\right\}H(x)\,, \tag{2.4-73}$$

where the notation is given in the text, $\theta \geq 0$, $|x| > 0$, $\left|\frac{x}{\rho}-\frac{c_s}{c}\right| > 0$, and $\left|\frac{r}{\rho}-\frac{c_s}{c_d}\right| > 0$. The integral in the first term of (2.4-73) is interpreted as a Cauchy principal value for $t = t_L$ if $x > 0$. In addition, the integrals in the second and third terms are improper for $t = t_s$, and the one in the third term is also improper for $t = t_E$ if $x > 0$. For a more detailed discussion of these improper integrals the reader is referred to cases II-IV above. By inspection of equation (2.4-73), one sees that it is equally well valid for $\frac{x}{\rho} = \frac{c_s}{c}$, $\frac{r}{\rho} = \frac{c_s}{c_d}$, and $x = 0$. To assess u_{zs} at $t = t_s$, $t = t_{sd}$, $t = t_{sc}$, $t = t_{sdc}$, $t = t_B$, $t = t_E$, and $t = t_L$, (2.4-73) must first be expanded near these surfaces. Then the value of u_{zs} at one of them is obtained as the limit of the corresponding expansion. In this way (2.4-73) is valid for all points in the interior of the half-space where $\theta \geq 0$. By using the reflection

property in (2.3-9), equation (2.4-73) can also be extended to include $\theta < 0$.

The first three terms in (2.4-73) represent waves that emanate from the origin of the coordinates, which is also the initial position of the load. The last two represent waves which trail behind the load. In particular, the first and fourth terms are analogous to the two terms in (2.4-34). The first is a hemispherical, equivoluminal wave and the fourth is a conical, equivoluminal wave. The corresponding wave fronts are shown in Fig. 15 along with diagrams that display their spatial variation with respect to the cone $\frac{x}{\rho} = \frac{c_s}{c}$. These waves coincide at the hemisphere $t = t_L$ in the same way as the dilatational waves and, as for u_{zd}, u_{zs} is expected to be continuous through $t = t_L$. The second term in (2.4-73) represents another hemispherical, equivoluminal wave. However, this one has a back at $t = t_B$. u_{zs} is expected to be continuous through $t = t_B$. This wave is displayed in Fig. 17, but it has nothing to do with the moving nature of the load, as is shown in section 2.7 where the stationary load solution is given.

The third term in (2.4-73) represents the conical head wave. It is generated by the surface intersection of the hemispherical, dilatational wave front. The conical head wave front is a truncated cone given by $t = t_{sd}$ for $\frac{r}{\rho} \geq \frac{c_s}{c_d}$; and it is tangent to the hemispherical, equivoluminal wave front at $t = t_s$ for $\frac{r}{\rho} = \frac{c_s}{c_d}$. These tangency points (which form a circle) are shown in the upper diagram of Fig. 15, and the conical head wave front is displayed in Fig. 17. It should be noted that this conical front is not related to the moving nature of the

load.

The last term in (2.4-73) is the plane head wave. It is generated by the surface intersection of the conical, dilatational wave front. The plane head wave front is that part of the plane given by $t = t_{sdc}$ for $\frac{y}{n} \geq \phi_c$ and $\frac{x}{r} \geq \frac{c_d}{c}$, and it is tangent to the conical, equivoluminal wave front at $t = t_{sc}$ for $\frac{y}{n} = \phi_c$. These tangency points (which form straight lines) are shown in the upper diagram of Fig. 15, and the plane head wave front is displayed in Fig. 18. It only exists for $\frac{x}{r} \geq \frac{c_d}{c}$ because the conical, dilatational wave front only intersects the surface for $\frac{x}{r} \geq \frac{c_d}{c}$, as shown in Fig. 16. In Fig. 19 both the conical and plane head wave fronts are shown, displaying their tangential intersection in the plane defined by $\frac{x}{r} = \frac{c_d}{c}$.

As mentioned in case III, in the region between the plane $\frac{x}{r} = \frac{c_d}{c}$ and the cone $\frac{x}{\rho} = \frac{c_s}{c}$, the plane head wave coincides with the conical head wave at the surface given by $t = t_E$ in such a way that the solution is expected to be continuous there. This surface extends from the end of the plane head wave front to the conical, equivoluminal wave front at the latters intersection with the cone $\frac{x}{\rho} = \frac{c_s}{c}$. This means that the surfaces $t = t_E$, $t = t_{L_c}$, $t = t_{sc}$, and $t = t_s$ coincide at their intersection with the cone $\frac{x}{\rho} = \frac{c_s}{c}$. The surface $t = t_E$ always lies inside the hemisphere $t = t_L$, and it coincides with the hemisphere on the surface of the half-space.

The Roman numerals in Figs. 16 and 17 correspond to the cases considered when inverting $\bar{u}_{zs}$. Although only the equivoluminal waves were computed in this subsection, the dilatational waves are

also shown for reference. In Fig. 16 the wave geometry in the surface plane is displayed. In this diagram the head waves are indistinguishable from the dilatational waves. Furthermore, since u_z has only been inverted for $z > 0$ thus far, the Rayleigh waves are not shown in this figure. Then, in Fig. 17 the wave geometry in the plane under the path of the load is portrayed. The diagram in Fig. 18 shows the geometry of the waves trailing behind the load at a cross section in front of the hemispherical, dilatational wave front. Finally, in Fig. 20 a three-dimensional perspective of the waves is displayed. However, the head wave fronts and the surfaces $t = t_B$, $t = t_E$, and $t = t_L$ are not shown in this last figure, leaving only the body wave fronts.

2.4.3. Transonic Load Motion.

In this subsection $\bar{u}_z$ is inverted for the case of transonic load motion, $c_s < c < c_d$. Since the computations for this case are similar to those given in subsections 2.4.1 and 2.4.2, only the differences between the supersonic and transonic cases are emphasized here.

Dilatational Contribution:

The inversion of the dilatational contribution to $\bar{u}_z$, namely $\bar{u}_{zd}$ in (2.4-1), proceeds exactly as in subsection 2.4.1. The geometry of the q-plane remains as shown in Fig. 3. The first important difference between the supersonic and transonic cases appears in the cases considered to apply the Cauchy-Goursat theorem in the q-plane. In particular, for transonic load motion $\frac{x}{\rho}$ is always less than $\frac{c_d}{c}$ and,

consequently, only cases II and III of (2.4-7) are applicable. Physically this is expected since the conical, dilatational wave front, which was found in case I for supersonic load motion, should not exist for transonic load motion. The conditions underlying cases II and III remain as given in (2.4-7).

The inversion of $\bar{u}_{zd}$ in case II proceeds exactly as in subsection 2.4.1, except that the geometry of the w-plane that arises is different. The w-plane in Fig. 6 must be replaced with the one in Fig. 21 where two of the branch points have real parts. The contour w_d no longer has a vertex for real t (consistent with the fact that we do not expect a wave front to be associated with B_{zd} when $c < c_d$), and only the part which lies above the real w-axis is shown. When θ goes to zero the branch points at $w = -i\gamma \sin\theta \pm (\gamma^2-1)^{\frac{1}{2}}\cos\theta$ migrate to $w = \pm(\gamma^2-1)^{\frac{1}{2}}$ on the real w-axis. But w_o, given in (2.4-7), is greater than $(\gamma^2 - 1)^{\frac{1}{2}}$, and therefore the branch points do not coincide with the w range of integration in $\bar{B}_{zd}$. By comparing the structure of the w-planes given in Figs. 6 and 21, one sees that a contour integration in either plane would yield the same result. Therefore u_{zd} for transonic load motion and case II remains exactly the same as for supersonic load motion, and it is given in (2.4-33).

The inversion of $\bar{u}_{zd}$ in case III is independent of the poles at $q = \frac{\pm w \sin\theta + i\gamma}{\cos\theta}$ and proceeds exactly as for the supersonic case. The results are the same as those in subsection 2.4.1.

Then the dilatational contribution to the vertical displacement for transonic load motion becomes

$$u_{zd}(\underline{x},t) = H(t-t_d)P\int_0^{T_d} \mathrm{Re}\left[K_{zd}(q_d,w,\theta)\,\frac{dq_d}{dt}\right] dw$$

$$+ \mathrm{Re}\left[\hat{K}_{zd}(w_d,\theta)\,\frac{dw_d}{dt}\right] H(t-t_L)H(x) \ , \qquad (2.4\text{-}74)$$

where the notation is given in subsection 2.4.1 and $\theta \geq 0$. The integral in the first term of (2.4-74) is interpreted as a Cauchy principal value for $t = t_L$ if $x > 0$. By comparing (2.4-34) and (2.4-74) one sees that the only difference in u_{zd} between the transonic and supersonic cases is that the conical, dilatational wave front no longer exists. Consequently, the result in (2.4-74) can be gotten from (2.4-34) by replacing $H(t-t_{dc})$ with one. For transonic load motion the entire hemisphere $t = t_L$ lies behind the hemispherical, dilatational wave front as shown in Fig. 22. Again, the solution is expected to be continuous over $t = t_L$ and in this case the second term in (2.4-74) should not be considered as a separate wave. The wave geometry in the surface plane and the plane under the path of the load is shown in the diagrams at the bottom of Fig. 22. The Roman numerals in these diagrams indicate where cases II and III are pertinent.

Equivoluminal Contribution:

The inversion of the equivoluminal contribution to $\bar{u}_z$, namely $\bar{u}_{zs}$ in (2.4-35), proceeds as in subsection 2.4.2. However, when $\theta = 0$, the relative position of the poles at $q = \frac{\pm w \sin\theta + i\gamma}{\cos\theta}$, the branch points, and the contours in the q-plane must be reviewed. In partic-

ular, for $\theta = 0$ the poles at $q = \frac{\pm w \sin\theta + i\gamma}{\cos\theta}$ coalesce at $q = i\gamma$. For $c_s < c < c_d$ and certain values of w, $q = i\gamma$ lies on the branch cut between the branch points at $q = i(w^2+1)^{\frac{1}{2}}$ and $q = i(w^2+\ell^2)^{\frac{1}{2}}$. In addition, for certain values of $\underline{x}$, the poles at $q = i\gamma$ intersect the contour q_{sd}. As shown in Fig. 9 and described in the text above equation (2.4-37), the contour q_{sd} only arises if $\frac{r}{\rho} > \frac{c_s}{c_d}$ and $w \in [0, w_1)$. Then, by comparing the position of the poles at $q = \frac{\pm w \sin\theta + i\gamma}{\cos\theta}$, the vertex at $q = \frac{ir}{\rho}(w^2+\ell^2)^{\frac{1}{2}}$, and the branch point at $q = i(w^2+1)^{\frac{1}{2}}$ as θ goes to zero (see Fig. 23), one sees that these poles lie on q_{sd} if, and only if, $\frac{x}{\rho}(w^2+\ell^2)^{\frac{1}{2}} > \gamma$ and $(w^2+1)^{\frac{1}{2}} < \gamma$ or, by expanding these inequalities, $w^2 > \left(\frac{\rho^2\gamma^2}{x^2} - \ell^2\right)$ and $w^2 < (\gamma^2 - 1)$. These conditions correspond to the following two possibilities in the half-space:

$$\left.\begin{aligned} &\text{(1) if } \theta = 0,\ \frac{r}{\rho} > \frac{c_s}{c_d},\ \frac{x}{\rho} > \frac{c_s}{c}, \\ &\quad \text{the poles lie on } q_{sd} \text{ for } w \in [0, (\gamma^2-1)^{\frac{1}{2}}); \\ &\text{(2) if } \theta = 0,\ \frac{r}{\rho} > \frac{c_s}{c_d},\ \frac{x}{\rho} < \frac{c_s}{c}, \\ &\quad \text{the poles lie on } q_{sd} \text{ for } w \in \left(\left(\frac{\rho^2\gamma^2}{x^2} - \ell^2\right)^{\frac{1}{2}}, (\gamma^2-1)^{\frac{1}{2}}\right). \end{aligned}\right\} \quad (2.4\text{-}75)$$

The most convenient way to invert $\bar{u}_{zs}$ in the transonic case is to hold $\theta > 0$, but otherwise arbitrary. Then the structure of the q-plane remains exactly the same as in subsection 2.4.2. After inverting $\bar{u}_{zs}$ for $\theta > 0$, the solution is extended to include $\theta = 0$, which involves identifying the singularities that arise in the integrals along q_{sd} as θ goes to zero. The limit as θ goes to zero is

expected to be proper (not to omit a contribution to u_{zs}) because physically the total solution is expected to vary continuously as θ goes to zero and the limit should exist.

Of the cases considered in subsection 2.4.2 to apply the Cauchy-Goursat theorem in the q-plane, only the last five of them (III-VII in (2.4-40)) are applicable for transonic load motion because $\frac{x}{r}$ is always less than $\frac{c_d}{c}$. The inversion of $\bar{u}_{zs}$ in case III proceeds exactly as in subsection 2.4.2, except that the geometry of the w-plane that arises is different. In particular, the w-plane in Fig. 14 must be replaced with the one in Fig. 24 where two of the branch points have a real part. By comparing the structure of the w-planes, one sees that a contour integration in either plane would yield the same result. Therefore u_{zs} for transonic load motion and case III is given by the same expression as for supersonic load motion, namely equation (2.4-70), only now we require $\theta > 0$.

The inversion of $\bar{u}_{zs}$ in case IV also proceeds as in subsection 2.4.2. The analogy found in that subsection between $\bar{u}_{zs}$ for case IV and $\bar{u}_{zd}$ for case II remains valid in this subsection. Therefore u_{zs} for transonic load motion and case IV is given by the same expression as for supersonic load motion, namely equation (2.4-71), but with $\theta > 0$. Furthermore, the similarity between cases IV and V for supersonic load motion holds over here. Therefore u_{zs} for transonic load motion and case V is given by equation (2.4-72), only with $\theta > 0$. Finally, the inversion of $\bar{u}_{zs}$ in cases VI and VII is independent of the poles at $q = \frac{\pm w \sin\theta + iy}{\cos\theta}$ and it proceeds exactly as for super-

sonic load motion. The results for these cases are the same as those in subsection 2.4.2.

Then, by combining the results for cases III-VII the equivoluminal contribution to the vertical displacement for transonic load motion becomes

$$u_{zs}(\underline{x},t) = H(t-t_s)P\int_0^{T_s} \mathrm{Re}\Big[K_{zs}(q_s,w,\theta)\,\frac{dq_s}{dt}\Big]\,dw$$

$$+ H(t-t_s)H(t_B-t)H\Big(\frac{r}{\rho}-\frac{c_s}{c_d}\Big)\int_{T_s}^{T_{sd}} \mathrm{Re}\Big[K_{zs}(q_{sd},w,\theta)\,\frac{dq_{sd}}{dt}\Big]\,dw$$

$$+ \Big[H(t-t_{sd})-H(t-t_s)\Big]H\Big(\frac{r}{\rho}-\frac{c_s}{c_d}\Big)\int_0^{T_{sd}} \mathrm{Re}\Big[K_{zs}(q_{sd},w,\theta)\,\frac{dq_{sd}}{dt}\Big]\,dw$$

$$+ \mathrm{Re}\Big[\hat{K}_{zs}(w_s,\theta)\,\frac{dw_s}{dt}\Big]H(t-t_{sc})H(t-t_L)H(x)$$

$$+ \mathrm{Re}\Big[\hat{K}_{zs}(w_{sd},\theta)\,\frac{dw_{sd}}{dt}\Big]\Big[H(t-t_E)-H(t-t_{sc})\Big]\,H\Big(\frac{x}{\rho}-\frac{c_s}{c}\Big)\,H(x), \qquad (2.4\text{-}76)$$

where the notation is given in subsection 2.4.2 and $\theta > 0$. The integral in the first term of (2.4-76) is interpreted as a Cauchy principal value for $t = t_L$ if $x > 0$. Furthermore, the integrals in the second and third terms are improper for $t = t_s$, and the one in the third term is also improper for $t = t_E$ if $x > 0$. A detailed discussion of these improper integrals is given in subsection 2.4.2 and it is not repeated here. In addition to being valid for $\theta > 0$, equation (2.4-76) can be extended to include $\theta < 0$ by using the reflection property in (2.3-9).

To facilitate the extension of (2.4-76) to $\theta = 0$, it is first discussed for $\theta > 0$. The main difference between u_{zs} in the transonic and supersonic cases is that the plane head wave front no longer exists. Physically this is expected since its generator, the conical, dilatational wave front, no longer exists. The last term in (2.4-76), formerly identified as the plane head wave, is still an equivoluminal disturbance propagating ahead of the conical, equivoluminal wave front. However, in the transonic case it coincides with the conical head wave, making it indistinguishable as a separate wave.

The remaining differences between u_{zs} in the transonic and supersonic cases are changes in the relative positions of the wave fronts. Pictorially these can be seen by comparing Figs. 25-28 for transonic load motion to Figs. 15-17 and 20 for supersonic load motion. In Fig. 25 the conical and hemispherical, equivoluminal wave fronts are displayed, showing their relative position with respect to the line where the conical head wave front is tangent to the hemispherical, equivoluminal wave front. The dilatational and equivoluminal wave fronts are displayed in Fig. 26 for the surface plane and in the upper diagram of Fig. 27 for the plane under the path of the load (assume $\theta > 0$). The Roman numerals in Figs. 26 and 27 correspond to the cases considered to invert $\bar{u}_{zs}$ and they are located in the domain of the half-space where each case is pertinent. Finally, in Fig. 28 a three-dimensional perspective of the waves is shown. However, the conical head wave front and the surfaces $t = t_B$, $t = t_E$, and $t = t_L$ are not indicated in this figure, leaving only the body wave fronts.

To extend (2.4-76) to include $\theta = 0$ the conditions in (2.4-75) must be incorporated into (2.4-76). When $\theta = 0$ the integrands of the second and third terms in (2.4-76), which are the contributions from the contour q_{sd} in the q-plane, contain a simple pole which is the zero of $q_{sd} = i\gamma$. In particular, by using q_{sd} in (2.4-37) with $\theta = 0$, one finds that the simple pole is located at $w = \frac{\gamma}{z}\alpha_s$ where α_s is given in (2.4-46a). The conditions in (2.4-75) which determine when $q_{sd} = i\gamma$ has a zero are expressed in terms of the half-space parameters by using the mapping $t = \frac{1}{c_d}(m_s z - iqr)$, and they are

$$\left.\begin{array}{l} \text{(1) if } \theta = 0,\ \frac{r}{\rho} > \frac{c_s}{c_d},\ \frac{x}{\rho} > \frac{c_s}{c}, \text{ the integrand} \\ \quad \text{of the integrals along } q_{sd} \text{ has a simple} \\ \quad \text{pole at } w = \frac{\gamma}{z}\alpha_s \text{ for } t_{sc} < t < t^o_{sdc}\ ; \\ \text{(2) if } \theta = 0,\ \frac{r}{\rho} > \frac{c_s}{c_d},\ \frac{x}{\rho} < \frac{c_s}{c}, \text{ the integrand} \\ \quad \text{of the integrals along } q_{sd} \text{ has a simple} \\ \quad \text{pole at } w = \frac{\gamma}{z}\alpha_s \text{ for } t_L < t < t^o_{sdc}\ . \end{array}\right\} \qquad (2.4\text{-}77)$$

The article t^o_{sdc} equals $\frac{1}{c}\left[\left(\frac{c^2}{c_s^2} - \frac{c^2}{c_d^2}\right)^{\frac{1}{2}} z + x\right]$, or equivalently t_{sdc} in (2.4-52a) evaluated at $\theta = 0$. In addition, t_L and t_{sc} are given in (2.4-39) and (2.4-46a) respectively. In the lower diagram in Fig. 27 the $\theta = 0$ plane (or the $y = 0$ plane for $x > 0$) is shown in which the thatched area displays the bounds of the conditions in (2.4-77). Then, by using (2.4-77), u_{zs} is formally extended to include $\theta = 0$ by noting that the integral in the second term in (2.4-76) is interpreted as a Cauchy principal value for $t_L < t < t^o_{sdc}$ if $\theta = 0$. In addition, the integral in the third term is interpreted as a Cauchy principal

value for $t_{sc} < t < t^{o}_{sdc}$ if $\theta = 0$. In each of these cases the integrand contains a simple pole at $w = \frac{\gamma}{z}\alpha_s$. In section 3.3 a technique is given to show, particularly in the thatched region in Fig. 27, that u_{zs} varies continuously as θ goes to zero. With these modifications, u_{zs} as given in (2.4-76) represents the equivoluminal contribution to the vertical displacement for transonic load motion and the interior of the half-space where $\theta \geq 0$. Finally, by comparing (2.4-73) and (2.4-76) one sees that u_{zs} for transonic load motion can be obtained from u_{zs} for supersonic load motion by replacing $H\left(\frac{\gamma}{n} - \phi_c\right)$ with one and identifying the Cauchy principal values of the improper integrals that arise for $\theta = 0$.

2.4.4. Subsonic Load Motion.

In this subsection $\bar{u}_z$ is inverted for the case of subsonic load motion, $c < c_s$. The geometry of the contour integration planes depends on whether the load speed is greater or less than the Rayleigh wave speed. However, as expected for $z > 0$, the computations are invariant to this variation, unlike in section 2.6 where the surface ($z = 0$) solution is obtained.

Dilatational Contribution:

The inversion of $\bar{u}_{zd}$ proceeds exactly as for the transonic case, which is expected since u_{zd} for $z > 0$ should be the same for all c less than c_d. The w-plane that arises is slightly different than in the transonic case, but the difference has no effect on the computations. However, for reference in section 2.6, the w-plane

for the subsonic case is given in Fig. 29. Finally, u_{zd} for subsonic load motion is given by equation (2.4-74) and the remarks following that equation, along with Fig. 22, remain valid here.

Equivoluminal Contribution:

The inversion of $\bar{u}_{zs}$ proceeds as for supersonic load motion with the same type of modifications as for transonic load motion. The variation in the q-plane for $\theta = 0$ mentioned in subsection 2.4.3 also arises in this subsection. However, for subsonic load motion only condition (2) of (2.4-75) is possible because $\frac{x}{\rho}$ is always less than $\frac{c_s}{c}$. The technique used in the preceding subsection of holding $\theta > 0$, inverting $\bar{u}_{zs}$, and then extending the solution to include $\theta = 0$ is employed here.

Of the cases considered in subsection 2.4.2 to apply the Cauchy-Goursat theorem in the q-plane, only the last four of them (IV - VII in (2.4-40)) are applicable for subsonic load motion because $\frac{x}{\rho}$ and $\frac{x}{r}$ are always less than $\frac{c_s}{c}$ and $\frac{c_d}{c}$ respectively. The inversion of $\bar{u}_{zs}$ in case IV proceeds as in subsections 2.4.2 and 2.4.3. In particular, the analogy made previously between $\bar{u}_{zs}$ for case IV and $\bar{u}_{zd}$ for case II remains valid here. Therefore u_{zs} for subsonic load motion and case IV is given by the same expression as for supersonic load motion, namely equation (2.4-71), only now we require $\theta > 0$. Furthermore, the similarity between cases IV and V in the supersonic and transonic cases holds here also. Therefore u_{zs} for subsonic load motion and case V is given by (2.4-72), only now $\theta > 0$. Finally, the inversion of $\bar{u}_{zs}$ in cases VI and VII is

independent of the poles at $q = \frac{\pm w \sin\theta + iy}{\cos\theta}$ and it proceeds exactly as in subsection 2.4.2. The results are the same as those given in that subsection.

Then, by combining the results for cases IV - VII the equivoluminal contribution to the vertical displacement for subsonic load motion becomes

$$u_{zs}(\underline{x},t) = H(t-t_s)P\int_0^{T_s} \mathrm{Re}\left[K_{zs}(q_s,w,\theta)\frac{dq_s}{dt}\right] dw$$

$$+ H(t-t_s)H(t_B-t)H\left(\frac{r}{\rho}-\frac{c_s}{c_d}\right)\int_{T_s}^{T_{sd}} \mathrm{Re}\left[K_{zs}(q_{sd},w,\theta)\frac{dq_{sd}}{dt}\right] dw$$

$$+ \left[H(t-t_{sd}) - H(t-t_s)\right] H\left(\frac{r}{\rho}-\frac{c_s}{c_d}\right)\int_0^{T_{sd}} \mathrm{Re}\left[K_{zs}(q_{sd},w,\theta)\frac{dq_{sd}}{dt}\right] dw$$

$$+ \mathrm{Re}\left[\hat{K}_{zs}(w_s,\theta)\frac{dw_s}{dt}\right] H(t-t_L)H(x) , \qquad (2.4\text{-}78)$$

where the notation is given in subsection 2.4.2 and $\theta > 0$. The integral in the first term is interpreted as a Cauchy principal value for $t = t_L$ if $x > 0$. In addition, the integrals in the second and third terms are improper for $t = t_s$. Equation (2.4-78) can also be extended to include $\theta < 0$ by using the reflection property in (2.3-9).

By comparing u_{zs} for supersonic and transonic load motion in (2.4-73) and (2.4-76) to the result in (2.4-78) for subsonic load motion, one sees that the plane head wave and the conical, equivoluminal wave front no longer exist. Physically this is expected for $c < c_s$. For subsonic load motion the entire hemisphere $t = t_L$ lies behind the hemispherical, equivoluminal wave front as shown in

Fig. 30. As previously, the solution is expected to be continuous over $t = t_L$ and the last term in (2.4-78) should not be considered as a separate wave. The wave geometry is shown in Fig. 31 for the surface plane and in the upper diagram of Fig. 32 for the plane under the path of the load (assume $\theta > 0$). The Roman numerals in Figs. 31 and 32 correspond to the cases considered to invert $\bar{u}_{zs}$ and they are located in the domain of the half-space where each case is pertinent. Finally, in Fig. 33 a three-dimensional perspective of the waves is shown. However, the conical head wave front and the surfaces $t = t_B$ and $t = t_L$ are not displayed in this figure, leaving only the body waves.

To extend (2.4-78) to include $\theta = 0$ one proceeds exactly as in the transonic case. For subsonic load motion only condition (2) of (2.4-77) is applicable and its domain of influence is shown as the thatched area in the lower diagram of Fig. 32. Therefore u_{zs} in (2.4-78) is extended to include $\theta = 0$ by noting that the integral in the second term of (2.4-78) is interpreted as a Cauchy principal value for $t_L < t < t^o_{sdc}$ if $\theta = 0$. For these values of the physical parameters the integrand in the second term of u_{zs} has a simple pole at $w = \frac{\gamma}{z}\alpha_s$. In section 3.3 a technique is given to show that u_{zs} varies continuously as $\theta \to 0$. With this modification, u_{zs} as given in (2.4-78) represents the equivoluminal contribution to the vertical displacement for subsonic load motion and the interior of the half-space where $\theta \geq 0$. Finally, by comparing (2.4-73) and (2.4-78) one sees that u_{zs} for subsonic load motion can be obtained from u_{zs} for supersonic load motion by replacing $H(t-t_{sc})$ with one and

identifying the Cauchy principal value of the improper integral that arises for $\theta = 0$.

2.4.5. Summary of the Results for all Load Speeds.

As noted in subsections 2.4.3 and 2.4.4, u_{zd} and u_{zs} for transonic and subsonic load motion can be obtained from the corresponding results for supersonic load motion in subsections 2.4.1 and 2.4.2. Then, by using this fact and substituting u_{zd} and u_{zs} for supersonic load motion (use (2.4-34) and (2.4-73)) into

$$u_z(\underline{x},t) = u_{zd}(\underline{x},t) + u_{zs}(\underline{x},t) \qquad (2.4\text{-}79)$$

one finds a single expression for u_z which is valid for all points in the interior of the half-space and for all load speeds. In particular,

$$u_z(\underline{x},t) = \sum_{j=1}^{7} u_z^j(\underline{x},t) \qquad (2.4\text{-}80)$$

for $0 \leq r < \infty$, $0 \leq \theta \leq \pi$ (or $-\infty < x < \infty$, $0 \leq y < \infty$), $0 < z < \infty$, and $0 \leq c < \infty$. The u_z^j represent waves emanating from the initial position of the load (which is also the origin of the coordinates) and disturbances† trailing behind the load.

The waves emanating from the initial position of the load are

---

†The terminology 'disturbances' is used here in place of waves to emphasize the fact that these contributions to u_z are only interpreted as separate waves for certain ranges of values of the load speed.

$$u_z^1(\underline{x},t) = H(t-t_d)P\int_0^{T_d} Re\left[K_{zd}(q_d,w,\theta)\frac{dq_d}{dt}\right]dw \quad , \tag{2.4-81a}$$

$$u_z^2(\underline{x},t) = H(t-t_s)P\int_0^{T_s} Re\left[K_{zs}(q_s,w,\theta)\frac{dq_s}{dt}\right]dw \quad , \tag{2.4-81b}$$

$$u_z^3(\underline{x},t) = H(t-t_s)H(t_B-t)H\left(\frac{r}{\rho}-\frac{c_s}{c_d}\right)P\int_{T_s}^{T_{sd}} Re\left[K_{zs}(q_{sd},w,\theta)\frac{dq_{sd}}{dt}\right]dw \quad , \tag{2.4-81c}$$

$$u_z^4(\underline{x},t) = \left[H(t-t_{sd})-H(t-t_s)\right]H\left(\frac{r}{\rho}-\frac{c_s}{c_d}\right)P\int_0^{T_{sd}} Re\left[K_{zs}(q_{sd},w,\theta)\frac{dq_{sd}}{dt}\right]dw \quad , \tag{2.4-81d}$$

where K_{zd} and K_{zs} are given in (2.3-5c). The integrands in (2.4-81) have singularities of the simple pole type at

$$\left.\begin{array}{ll}
\text{(1)} & w = w_{od} \text{ for } t = t_L \text{ if } x > 0 \\
\text{(2)} & w = w_{os} \text{ for } t = t_L \text{ if } x > 0 \\
\text{(3a)} & w = 0 \text{ for } t = t_s \\
\text{(3b)} & w = \frac{\gamma}{z}\alpha_s \text{ for } t_L < t < t^o_{sdc} \text{ if } \theta = 0 \text{ and } c < c_d \\
\text{(4a)} & w = 0 \text{ for } t = t_s \\
\text{(4b)} & w = 0 \text{ for } t = t_E \text{ if } x > 0 \text{ and } c > c_s \\
\text{(4c)} & w = \frac{\gamma}{z}\alpha_s \text{ for } t_{sc} < t < t^o_{sdc} \text{ if } \theta = 0 \text{ and } c_s < c < c_d,
\end{array}\right\} \tag{2.4-82}$$

where the numbers in parentheses on the left correspond to the integrand of the particular u_z^j, $(j = 1, \ldots, 4)$, in which the pole appears. The factors w_{od}, w_{os}, and α_s used in (2.4-82) are

$$\left.\begin{aligned} w_{od} &= \left(\frac{\rho^2\gamma^2}{x^2} - 1\right)^{\frac{1}{2}} \frac{z\cos\theta}{n} \quad , \quad w_{os} = \left(\frac{\rho^2\gamma^2}{x^2} - \ell^2\right)^{\frac{1}{2}} \frac{z\cos\theta}{n} \\ \alpha_s &= \left[\xi^2 - \left(\frac{c^2}{c_s^2} - 1\right)n^2\right]^{\frac{1}{2}} \end{aligned}\right\} \quad (2.4\text{-}82a)$$

(w_{od} and w_{os} represent w_o as defined in subsections 2.4.1 and 2.4.2 respectively). Therefore the integrals in (2.4-81) are improper for those values of $\underline{x}$, t, and c in (2.4-82). For the cases when the simple pole is not located at one of the limits of integration, the improper integral is interpreted as a Cauchy principal value (indicated by a P preceding the integral in question). The q-transformations and the limits of integration appearing in (2.4.81) are

$$\left.\begin{aligned} q_\beta &= \frac{c_d}{\rho^2}\left[itr + z(t^2 - t_{w\beta}^2)^{\frac{1}{2}}\right] \quad , \quad (\beta = d, s) \\ q_{sd} &= i\frac{c_d}{\rho^2}\left[tr - z(t_{ws}^2 - t^2)^{\frac{1}{2}}\right] \end{aligned}\right\} \quad , \quad (2.4\text{-}83)$$

where

$$t_{wd} = \frac{\rho}{c_d}(w^2 + 1)^{\frac{1}{2}} \quad , \quad t_{ws} = \frac{\rho}{c_d}(w^2 + \ell^2)^{\frac{1}{2}} \quad , \quad (2.4\text{-}83a)$$

and

$$\left.\begin{aligned} T_d &= \left(\frac{t^2}{t_d^2} - 1\right)^{\frac{1}{2}} \quad , \quad T_s = \left(\frac{t^2}{t_s^2} - 1\right)^{\frac{1}{2}}\ell \\ T_{sd} &= \left[\left(\frac{c_d(t - t_{sd})}{r} + 1\right)^2 - 1\right]^{\frac{1}{2}} \end{aligned}\right\} \quad . \quad (2.4\text{-}84)$$

The arrival times in (2.4-81) - (2.4-84) are

$$\left.\begin{aligned} t_\beta &= \frac{\rho}{c_\beta}\,, \qquad (\beta = d, s) \\ t_{sd} &= \frac{1}{c_d}\left[(\ell^2-1)^{\frac{1}{2}}z + r\right] \end{aligned}\right\} \tag{2.4-85}$$

and the remaining subscripted time parameters take the form

$$\left.\begin{aligned} t_L = \frac{\rho^2}{cx}\,, \quad t_B = \frac{\rho^2(\ell^2-1)^{\frac{1}{2}}}{zc_d}\,, \quad t_E = \frac{1}{cx}\left[\left(\frac{c^2}{c_s^2}x^2 - r^2\right)^{\frac{1}{2}}z + r^2\right] \\ t^o_{sdc} = \frac{1}{c}\left[\left(\frac{c^2}{c_s^2} - \frac{c^2}{c_d^2}\right)^{\frac{1}{2}}z + x\right] \quad . \end{aligned}\right\} \tag{2.4-86}$$

The disturbances trailing behind the load that contribute to u_z are

$$u_z^5(\underline{x},t) = \mathrm{Re}\left[\hat{K}_{zd}(w_d,\theta)\frac{dw_d}{dt}\right]H(t-t_{dc})H(t-t_L)H(x)\,, \tag{2.4-87a}$$

$$u_z^6(\underline{x},t) = \mathrm{Re}\left[\hat{K}_{zs}(w_s,\theta)\frac{dw_s}{dt}\right]H(t-t_{sc})H(t-t_L)H(x)\,, \tag{2.4-87b}$$

$$\begin{aligned} u_z^7(\underline{x},t) = \mathrm{Re}\left[\hat{K}_{zs}(w_{sd},\theta)\frac{dw_{sd}}{dt}\right]H\left(\frac{y}{n}-\phi_c\right)\left\{H(t-t_{sdc})H\left(\frac{x}{r}-\frac{c_d}{c}\right)\right. \\ \left. +H(t-t_E)\left[H\left(\frac{x}{\rho}-\frac{c_s}{c}\right)-H\left(\frac{x}{r}-\frac{c_d}{c}\right)\right]-H(t-t_{sc})H\left(\frac{x}{\rho}-\frac{c_s}{c}\right)\right\}H(x)\,, \end{aligned} \tag{2.4-87c}$$

where the hat functions are

$$\hat{K}_{zd}(w,\theta) = \frac{\sec\theta}{\pi c\mu}\left[\frac{m_d\left[\ell^2+2(q^2+w^2)\right]}{R(q,w)}\right]\Bigg|_{q=\frac{w\sin\theta+i\gamma}{\cos\theta}}\,, \tag{2.4-88a}$$

$$\hat{K}_{zs}(w,\theta) = \frac{-2\sec\theta}{\pi c\mu}\left[\frac{m_d(q^2+w^2)}{R(q,w)}\right]\Bigg|_{q=\frac{w\sin\theta+i\gamma}{\cos\theta}}\,, \tag{2.4-88b}$$

and the Heaviside function is restricted by

$$\left.\begin{aligned} &H(t-t_{\beta c}) = 1 \quad \text{if} \quad c < c_\beta \,, \quad (\beta = d,s) \\ &H\left(\frac{y}{n} - \phi_c\right) = 1 \quad \text{if} \quad c < c_d \,. \end{aligned}\right\} \tag{2.4-89}$$

The w-transformations appearing in (2.4-87) are

$$\left.\begin{aligned} w_\beta &= -i\gamma \sin\theta + \frac{\gamma \cos\theta}{n^2}\,(i\xi y + z\alpha_\beta) \,, \quad (\beta = d,s) \\ w_{sd} &= -i\gamma \sin\theta + \frac{i\gamma \cos\theta}{n^2}\,(\xi y - z\alpha_{sd}) \end{aligned}\right\} , \tag{2.4-90}$$

where

$$\alpha_\beta = \left[\xi^2 - \left(\frac{c^2}{c_\beta^2} - 1\right)n^2\right]^{\frac{1}{2}} \,, \quad \alpha_{sd} = \left[\left(\frac{c^2}{c_s^2} - 1\right)n^2 - \xi^2\right]^{\frac{1}{2}} . \tag{2.4-90a}$$

In addition, the arrival times in (2.4-87) - (2.4-89) are

$$\left.\begin{aligned} t_{\beta c} &= \frac{1}{c}\left[\left(\frac{c^2}{c_\beta^2} - 1\right)^{\frac{1}{2}} n + x\right] \,, \quad (\beta = d,s) \\ t_{sdc} &= \frac{1}{c}\left[\left(\frac{c^2}{c_s^2} - \frac{c^2}{c_d^2}\right)^{\frac{1}{2}} z + \left(\frac{c^2}{c_d^2} - 1\right)^{\frac{1}{2}} y + x\right] \end{aligned}\right\} \tag{2.4-91}$$

and t_L and t_B are given in (2.4-86). Finally,

$$\phi_c = \frac{\left(\frac{c^2}{c_d^2} - 1\right)^{\frac{1}{2}}}{\left(\frac{c^2}{c_s^2} - 1\right)^{\frac{1}{2}}} \,. \tag{2.4-92}$$

The remaining notation used in formulas (2.4-80) - (2.4-92) is given in the preceding subsections. Thus far the terms contributing

to u_z are only valid for $\theta \geq 0$. However, by the reflection property in (2.3-9) one sees that u_z is valid for all θ and y such that $-\pi \leq \theta < \pi$ and $-\infty < y < \infty$ if θ and y are replaced with $|\theta|$ and $|y|$ in the formulas above. The waves emanating from the initial position of the load are invariant to interchanging θ and $|\theta|$. Therefore they are valid as given in (2.4-81) - (2.4-86) for $-\pi \leq \theta < \pi$.

The time dependence in the limits of the integrals composing the waves emanating from the initial position of the load can be removed by the transformations

$$\left.\begin{aligned} &(1)\quad w = T_d \sin\alpha \\ &(2)\quad w = T_s \sin\alpha \\ &(3)\quad w = \left[T_s^2 + (T_{sd}^2 - T_s^2)\sin^2\alpha\right]^{\frac{1}{2}} \\ &\qquad = \left[T_s^2 + (t_B - t)^2 h^2 \sin^2\alpha\right]^{\frac{1}{2}}, \qquad h = \frac{zc_d}{\rho r} \\ &(4)\quad w = T_{sd}\sin\alpha\ , \end{aligned}\right\} \qquad (2.4\text{-}93)$$

where the numbers in parentheses on the left correspond to the particular u_z^j, $(j = 1, \ldots, 4)$, where the transformation is applicable. Then the substitution of (2.4-93) into (2.4-81) yields

$$u_z^1(\underline{x},t) = H(t-t_d)P\int_0^{\frac{\pi}{2}} \hat{u}_z^1\, d\alpha\ , \qquad (2.4\text{-}94a)$$

$$u_z^2(\underline{x},t) = H(t-t_s)P\int_0^{\frac{\pi}{2}} \hat{u}_z^2\, d\alpha\ , \qquad (2.4\text{-}94b)$$

$$u_z^3(\underline{x},t) = H(t-t_s)H(t_B-t)H\left(\frac{r}{\rho}-\frac{c_s}{c_d}\right)P\int_0^{\frac{\pi}{2}} \hat{u}_z^3\, d\alpha \quad , \tag{2.4-94c}$$

$$u_z^4(\underline{x},t) = \left[H(t-t_{sd}) - H(t-t_s)\right]H\left(\frac{r}{\rho}-\frac{c_s}{c_d}\right)P\int_0^{\frac{\pi}{2}} \hat{u}_z^4\, d\alpha \quad , \tag{2.4-94d}$$

where

$$\hat{u}_z^1 = \frac{c_d}{\rho}\,\mathrm{Re}\left[K_{zd}(q_d,w,\theta)\Big|_{w=T_d\sin\alpha}\left(\frac{ir}{\rho}T_d\cos\alpha+\frac{zc_dt}{\rho^2}\right)\right] \quad , \tag{2.4-95a}$$

$$\hat{u}_z^2 = \frac{c_d}{\rho}\,\mathrm{Re}\left[K_{zs}(q_s,w,\theta)\Big|_{w=T_s\sin\alpha}\left(\frac{ir}{\rho}T_s\cos\alpha+\frac{zc_dt}{\rho^2}\right)\right] \quad , \tag{2.4-95b}$$

$$\hat{u}_z^3 = (t_B-t)\frac{c_dh^2r\cos\alpha}{\rho^2}\,\mathrm{Re}\left[K_{zs}(q_{sd},w,\theta)\Big|_{w=\left[T_s^2+(t_B-t)^2h^2\sin^2\alpha\right]^{\frac{1}{2}}} i\right]\frac{\left[t+(t_B-t)\sin\alpha\right]}{\left[T_s^2+(t_B-t)^2h^2\sin^2\alpha\right]^{\frac{1}{2}}} \quad , \tag{2.4-95c}$$

$$\text{with } h=\frac{zc_d}{\rho r}$$

$$\hat{u}_z^4 = T_{sd}\frac{c_d\cos\alpha}{\rho}\,\mathrm{Re}\left[K_{zs}(q_{sd},w,\theta)\Big|_{w=T_{sd}\sin\alpha} i\right]\left[\frac{r}{\rho}+\frac{zc_dt}{\rho^2}\left(T_{sd}^2\sin^2\alpha-T_s^2\right)^{-\frac{1}{2}}\right] . \tag{2.4-95d}$$

The position of the simple poles in the integrands in (2.4-94) can be found as a function of α by using the conditions in (2.4-82) along with the transformations in (2.4-93). By inspection of u_z^3 and $\hat{u}_z^3$ one sees that u_z^3 goes to zero as t approaches t_B, which shows that u_z^3, and therefore u_z, are continuous through $t = t_B$.

To display the disturbances trailing behind the load in a more useful form the cylindrical coordinates in (2.4-87) are replaced with their counterparts in terms of x, y, z, ξ, and n as shown in Fig. 2. At the same time, to obtain the solution for $-\infty < y < \infty$, y is replaced with $|y|$. Then (2.4-87) becomes

$$u_z^5(\underline{x},t) = \hat{u}_z^5 H(t-t_{dc})H(t-t_L)H(x) \quad , \tag{2.4-96a}$$

$$u_z^6(\underline{x},t) = \hat{u}_z^6 H(t-t_{sc})H(t-t_L)H(x) \quad , \tag{2.4-96b}$$

$$u_z^7(\underline{x},t) = \hat{u}_z^7 H\left(\frac{|y|}{n} - \phi_c\right)\left\{H(t-t_{sdc})H\left(\frac{x}{r} - \frac{c_d}{c}\right)\right.$$

$$\left. + H(t-t_E)\left[H\left(\frac{x}{\rho} - \frac{c_s}{c}\right) - H\left(\frac{x}{r} - \frac{c_d}{c}\right)\right] - H(t-t_{sc})H\left(\frac{x}{\rho} - \frac{c_s}{c}\right)\right\}H(x) \quad , \tag{2.4-96c}$$

where the hat functions are

$$\hat{u}_z^5 = \frac{1}{\alpha_d \pi\mu} \mathrm{Re}\left\{\frac{b_d^2\left[\left(\frac{c^2}{c_s^2} - 2\right)n^4 + 2a_d^2\right]}{\left[\left(\frac{c^2}{c_s^2} - 2\right)n^4 + 2a_d^2\right]^2 - 4b_d\left[b_d^2 + \left(\frac{c^2}{c_s^2} - \frac{c^2}{c_d^2}\right)n^4\right]^{\frac{1}{2}}(a_d^2 - n^4)}\right\} \quad , \tag{2.4-97a}$$

$$\hat{u}_z^6 = \frac{-2}{\alpha_s \pi\mu} \mathrm{Re}\left\{\frac{b_s(a_s^2 - n^4)\left[b_s^2 - \left(\frac{c^2}{c_s^2} - \frac{c^2}{c_d^2}\right)n^4\right]^{\frac{1}{2}}}{\left[\left(\frac{c^2}{c_s^2} - 2\right)n^4 + 2a_s^2\right]^2 - 4b_s\left[b_s^2 - \left(\frac{c^2}{c_s^2} - \frac{c^2}{c_d^2}\right)n^4\right]^{\frac{1}{2}}(a_s^2 - n^4)}\right\} \quad , \tag{2.4-97b}$$

$$\hat{u}{}_z^7 = \frac{-2}{\alpha_{sd}\pi\mu} \frac{b_{sd}(a_{sd}^2+n^4)\left[\left(\frac{c^2}{c_s^2}-\frac{c^2}{c_d^2}\right)n^4-b_{sd}^2\right]^{\frac{1}{2}}\left[\left(\frac{c^2}{c_s^2}-2\right)n^4-2a_{sd}^2\right]^2}{\left[\left(\frac{c^2}{c_s^2}-2\right)n^4-2a_{sd}^2\right]^4+16b_{sd}^2\left[\left(\frac{c^2}{c_s^2}-\frac{c^2}{c_d^2}\right)n^4-b_{sd}^2\right](a_{sd}^2+n^4)^2}, \tag{2.4-97c}$$

with

$$\left.\begin{aligned} a_\beta &= (i\xi|y|+z\alpha_\beta) \\ b_\beta &= (\xi z+i|y|\alpha_\beta) \\ \alpha_\beta &= \left[\xi^2-\left(\frac{c^2}{c_\beta^2}-1\right)n^2\right]^{\frac{1}{2}} \end{aligned}\right\}(\beta=d,s) \qquad \left.\begin{aligned} a_{sd} &= (\xi|y|-z\alpha_{sd}) \\ b_{sd} &= (\xi z+|y|\alpha_{sd}) \\ \alpha_{sd} &= \left[\left(\frac{c^2}{c_s^2}-1\right)n^2-\xi^2\right]^{\frac{1}{2}}. \end{aligned}\right\} \tag{2.4-98}$$

The restrictions in (2.4-89) on the Heaviside function become

$$\left.\begin{aligned} &H(t-t_{\beta c}) = 1 \quad \text{if} \quad c<c_\beta, \quad (\beta=d,s) \\ &H\left(\frac{|y|}{n}-\phi_c\right) = 1 \quad \text{if} \quad c<c_d \end{aligned}\right\} \tag{2.4-99}$$

and the arrival times in (2.4-91) take the form

$$\left.\begin{aligned} t_{\beta c} &= \frac{1}{c}\left[\left(\frac{c^2}{c_\beta^2}-1\right)^{\frac{1}{2}}n+x\right], \quad (\beta=d,s) \\ t_{sdc} &= \frac{1}{c}\left[\left(\frac{c^2}{c_s^2}-\frac{c^2}{c_d^2}\right)^{\frac{1}{2}}z+\left(\frac{c^2}{c_d^2}-1\right)^{\frac{1}{2}}|y|+x\right]. \end{aligned}\right\} \tag{2.4-100}$$

The parameters t_L, t_E, and ϕ_c remain as given in (2.4-86) and (2.4-92). Since the u_z^j in (2.4-96), less the Heaviside function, are only functions of the coordinates (ξ,n,y,z), they are constant at a fixed position in a coordinate system moving with the load. Therefore

the disturbances trailing behind the load represent steady-state contributions to u_z. In fact, in section 3.4 they are shown to constitute the entire steady-state displacement field for $c > c_d$. Furthermore, the wave front geometry associated with these terms depends on the load speed. That is, each of them is identified as a separate wave if, and only if, the load speed is sufficiently large that its wave front exists.

As the results in this section show, the vertical displacement for the interior of the half-space and for all load speeds can be represented as a sum of single integrals and algebraic terms. Each contribution is identified with a specific wave. In particular, the integrals represent a system of waves that emanate from the initial position of the load as if they were generated by a stationary point source. Three wave fronts distinguish this system: hemispherical fronts propagating with the dilatational and equivoluminal wave speeds, and a head wave front. The latter, which actually is the surface of a truncated cone, also propagates with the equivoluminal wave speed. On the other hand, the algebraic terms represent that part of the disturbance which trails behind the load. For supersonic load motion these terms display three wave fronts: conical fronts propagating with the dilatational and equivoluminal wave speeds, and another head wave front. The latter, which is part of a plane surface, also propagates with the equivoluminal wave speed. However, for transonic load motion the conical, dilatational wave front and the plane head wave front do not exist. Furthermore, for subsonic load motion the conical, equivo-

luminal wave front also disappears, leaving the disturbances trailing behind the load with no wave fronts.

For additional details concerning this representation of the vertical displacement, including diagrams of the wave fronts and their variation with different load speeds, the reader is referred to subsections 2.4.1-2.4.4. In the next section the horizontal displacements are represented in a similar way.

2.5. EXACT INVERSION OF THE HORIZONTAL DISPLACEMENTS FOR THE INTERIOR OF THE HALF-SPACE

Since K_{xd}, K_{xs}, K_{yd}, and K_{ys} as given in (2.3-5a) and (2.3-5b) have the same algebraic properties (square roots and poles) as K_{zd} and K_{zs} in (2.3-5c), the inversion of $\bar{u}_x$ and $\bar{u}_y$ proceeds exactly as for $\bar{u}_z$ in the preceding section. Then, without further deliberation, the results for u_x and u_y are stated. In particular,

$$u_\sigma(\underline{x},t) = \sum_{j=1}^{7} u_\sigma^j(\underline{x},t) \quad , \qquad (\sigma = x,y) \tag{2.5-1}$$

for $0 \leq r < \infty$, $-\pi \leq \theta < \pi$ (or $-\infty < x,y < \infty$), $0 < z < \infty$, and $0 \leq c < \infty$, where the u_σ^j represent waves emanating from the initial position of the load and disturbances trailing behind the load.

The waves emanating from the initial position of the load are

$$u_\sigma^1(\underline{x},t) = H(t-t_d)P\int_0^{T_d} \mathrm{Re}\left[K_{\sigma d}(q_d,w,\theta)\,\frac{dq_d}{dt} \right] dw \quad , \tag{2.5-2a}$$

$$u_\sigma^2(\underline{x},t) = H(t-t_s)P\int_0^{T_s} \mathrm{Re}\left[K_{\sigma s}(q_s,w,\theta)\,\frac{dq_s}{dt}\right] dw \quad , \tag{2.5-2b}$$

$$u_\sigma^3(\underline{x},t) = H(t-t_s)H(t_B-t)H\left(\frac{r}{\rho}-\frac{c_s}{c_d}\right)P\int_{T_s}^{T_{sd}} \mathrm{Re}\left[K_{\sigma s}(q_{sd},w,\theta)\,\frac{dq_{sd}}{dt}\right]dw, \tag{2.5-2c}$$

$$u_\sigma^4(\underline{x},t) = \left[H(t-t_{sd})-H(t-t_s)\right]H\left(\frac{r}{\rho}-\frac{c_s}{c_d}\right)P\int_0^{T_{sd}} \mathrm{Re}\left[K_{\sigma s}(q_{sd},w,\theta)\,\frac{dq_{sd}}{dt}\right]dw \quad , \tag{2.5-2d}$$

where the q-transformations, the limits of integration, the arrival times, and t_B are given in (2.4-83) - (2.4-86). In addition, the integral in each u_σ^j is improper in the same way as the corresponding u_z^j, as displayed by (2.4-82), with the following qualification. For conditions (3b) and (4c) in (2.4-82) the integrands of u_y^3 and u_y^4 do not have a simple pole, but rather an indeterminant form $(\frac{0}{0})$. In section 3.3, u_y^3 and u_y^4 are investigated further. The application of the transformations in (2.4-93) to the integrals in (2.5-2) brings these waves to the form

$$u_\sigma^1(\underline{x},t) = H(t-t_d)P\int_0^{\frac{\pi}{2}} \hat{u}_\sigma^1\, d\alpha \quad , \tag{2.5-3a}$$

$$u_\sigma^2(\underline{x},t) = H(t-t_s)\,P\int_0^{\frac{\pi}{2}} \hat{u}_\sigma^2\, d\alpha \quad , \tag{2.5-3b}$$

$$u_\sigma^3(\underline{x},t) = H(t-t_s)H(t_B-t)H\left(\frac{r}{\rho}-\frac{c_s}{c_d}\right)P\int_0^{\frac{\pi}{2}} \hat{u}_\sigma^3\, d\alpha \quad , \tag{2.5-3c}$$

$$u_\sigma^4(\underline{x},t) = \left[H(t-t_{sd}) - H(t-t_s)\right] H\left(\frac{r}{\rho} - \frac{c_s}{c_d}\right) P\int_0^{\frac{\pi}{2}} \hat{u}_\sigma^4 \, d\alpha \quad , \qquad (2.5\text{-}3d)$$

where

$$\hat{u}_\sigma^1 = \frac{c_d}{\rho} \mathrm{Re}\left[K_{\sigma d}(q_d,w,\theta)\Big|_{w = T_d \sin\alpha} \left(\frac{ir}{\rho} T_d \cos\alpha + \frac{zc_d t}{\rho^2}\right)\right] \quad , \qquad (2.5\text{-}4a)$$

$$\hat{u}_\sigma^2 = \frac{c_d}{\rho} \mathrm{Re}\left[K_{\sigma s}(q_s,w,\theta)\Big|_{w = T_s \sin\alpha} \left(\frac{ir}{\rho} T_s \cos\alpha + \frac{zc_d t}{\rho^2}\right)\right] \quad , \qquad (2.5\text{-}4b)$$

$$\hat{u}_\sigma^3 = (t_B - t) \frac{c_d h^2 r \cos\alpha}{\rho^2} \mathrm{Re}\left[K_{\sigma s}(q_{sd},w,\theta)\Big|_{w = \left[T_s^2 + (t_B-t)^2 h^2 \sin^2\alpha\right]^{\frac{1}{2}}} i\right] \frac{\left[t + (t_B - t)\sin\alpha\right]}{\left[T_s^2 + (t_B-t)^2 h^2 \sin^2\alpha\right]^{\frac{1}{2}}} \quad ,$$

$$\text{with } h = \frac{zc_d}{\rho r} \qquad (2.5\text{-}4c)$$

$$\hat{u}_\sigma^4 = T_{sd} \frac{c_d \cos\alpha}{\rho} \mathrm{Re}\left[K_{\sigma s}(q_{sd},w,\theta)\Big|_{w = T_{sd}\sin\alpha} i\right]\left[\frac{r}{\rho} + \frac{zc_d t}{\rho^2}\left(T_{sd}^2 \sin^2\alpha - T_s^2\right)^{-\frac{1}{2}}\right] . \qquad (2.5\text{-}4d)$$

The position of the simple poles of the integrands in (2.5-3) can be found as a function of α by using the conditions in (2.4-82) and the transformations in (2.4-93).

The disturbances trailing behind the load that contribute to u_σ are

$$u_\sigma^5(\underline{x},t) = \hat{u}_\sigma^5 H(t-t_{dc}) H(t-t_L) H(x) \quad , \qquad (2.5\text{-}5a)$$

$$u_\sigma^6(\underline{x},t) = \hat{u}_\sigma^6 H(t-t_{sc}) H(t-t_L) H(x) \quad , \qquad (2.5\text{-}5b)$$

$$\hat{u}_\sigma^7(\underline{x},t) = \hat{u}_\sigma^7 H\left(\frac{|y|}{n} - \phi_c\right)\left\{H(t-t_{sdc})H\left(\frac{x}{r} - \frac{c_d}{c}\right)\right.$$

$$\left. + H(t-t_E)\left[H\left(\frac{x}{\rho} - \frac{c_s}{c}\right) - H\left(\frac{x}{r} - \frac{c_d}{c}\right)\right] - H(t-t_{sc})H\left(\frac{x}{\rho} - \frac{c_s}{c}\right)\right\} H(x) \quad , \tag{2.5-5c}$$

where the Heaviside function is restricted by the conditions in (2.4-99) and the arrival times are given in (2.4-100). In addition, the parameters t_L, t_E, and ϕ_c are given in (2.4-86) and (2.4-92). The hat functions in (2.5-5) are, for $\sigma = x$

$$\hat{u}_x^5 = \frac{n^2}{\alpha_d \pi\mu} \mathrm{Re}\left\{ \frac{b_d\left[\left(\frac{c^2}{c_s^2} - 2\right)n^4 + 2a_d^2\right]}{\left[\left(\frac{c^2}{c_s^2} - 2\right)n^4 + 2a_d^2\right]^2 - 4b_d\left[b_d^2 + \left(\frac{c^2}{c_s^2} - \frac{c^2}{c_d^2}\right)n^4\right]^{\frac{1}{2}}(a_d^2 - n^4)} \right\} \tag{2.5-6a}$$

$$\hat{u}_x^6 = \frac{-2n^2}{\alpha_s \pi\mu} \mathrm{Re}\left\{ \frac{b_s^2\left[b_s^2 - \left(\frac{c^2}{c_s^2} - \frac{c^2}{c_d^2}\right)n^4\right]^{\frac{1}{2}}}{\left[\left(\frac{c^2}{c_s^2} - 2\right)n^4 + 2a_s^2\right]^2 - 4b_s\left[b_s^2 - \left(\frac{c^2}{c_s^2} - \frac{c^2}{c_d^2}\right)n^4\right]^{\frac{1}{2}}(a_s^2 - n^4)} \right\} \tag{2.5-6b}$$

$$\hat{u}_x^7 = \frac{2n^2}{\alpha_{sd} \pi\mu} \frac{b_{sd}^2\left[\left(\frac{c^2}{c_s^2} - \frac{c^2}{c_d^2}\right)n^4 - b_{sd}^2\right]^{\frac{1}{2}}\left[\left(\frac{c^2}{c_s^2} - 2\right)n^4 - 2a_{sd}^2\right]^2}{\left[\left(\frac{c^2}{c_s^2} - 2\right)n^4 - 2a_{sd}^2\right]^4 + 16b_{sd}^2\left[\left(\frac{c^2}{c_s^2} - \frac{c^2}{c_d^2}\right)n^4 - b_{sd}^2\right](a_{sd}^2 + n^4)^2} \tag{2.5-6c}$$

and for $\sigma = y$

$$\hat{u}_y^5 = \frac{-\mathrm{sgn}(y)}{\alpha_d \pi\mu} \mathrm{Re}\left\{ \frac{ia_d b_d\left[\left(\frac{c^2}{c_s^2} - 2\right)n^4 + 2a_d^2\right]}{\left[\left(\frac{c^2}{c_s^2} - 2\right)n^4 + 2a_d^2\right]^2 - 4b_d\left[b_d^2 + \left(\frac{c^2}{c_s^2} - \frac{c^2}{c_d^2}\right)n^4\right]^{\frac{1}{2}}(a_d^2 - n^4)} \right\} \tag{2.5-7a}$$

$$\hat{u}{}^{6}_{y} = \frac{2\,\mathrm{sgn}(y)}{\alpha_s \pi \mu}\,\mathrm{Re}\left\{\frac{i a_s b_s^2\left[b_s^2-\left(\frac{c^2}{c_s^2}-\frac{c^2}{c_d^2}\right)n^4\right]^{\frac{1}{2}}}{\left[\left(\frac{c^2}{c_s^2}-2\right)n^4+2a_s^2\right]^2-4b_s\left[b_s^2-\left(\frac{c^2}{c_s^2}-\frac{c^2}{c_d^2}\right)n^4\right]^{\frac{1}{2}}(a_s^2-n^4)}\right\} \tag{2.5-7b}$$

$$\hat{u}{}^{7}_{y} = \frac{2\,\mathrm{sgn}(y)}{\alpha_{sd} \pi \mu}\,\frac{a_{sd} b_{sd}^2\left[\left(\frac{c^2}{c_s^2}-\frac{c^2}{c_d^2}\right)n^4-b_{sd}^2\right]^{\frac{1}{2}}\left[\left(\frac{c^2}{c_s^2}-2\right)n^4-2a_{sd}^2\right]^2}{\left[\left(\frac{c^2}{c_s^2}-2\right)n^4-2a_{sd}^2\right]^4+16b_{sd}^2\left[\left(\frac{c^2}{c_s^2}-\frac{c^2}{c_d^2}\right)n^4-b_{sd}^2\right](a_{sd}^2+n^4)^2}\,, \tag{2.5-7c}$$

where the a's, b's, and α's are given in (2.4-98) and

$$\mathrm{sgn}(y) = \begin{cases} 1 & \text{for } y > 0 \\ -1 & \text{for } y < 0\,. \end{cases} \tag{2.5-8}$$

The remaining details concerning the structure (wave patterns, singularities, etc.) of u_x and u_y are the same as for u_z and they are discussed in the previous section.

2.6. EXACT INVERSION OF THE DISPLACEMENTS FOR THE SURFACE OF THE HALF-SPACE

The inversion scheme as developed in the preceding sections for $z > 0$ goes through for $z = 0$ also. In fact, the required contour integrations are much simpler, as is the structure of the solution. However, since the interior displacements have already been inverted, the surface displacements are obtained, in part, by assessing the interior ones for $z = 0$. In addition, an evaluation of the Rayleigh poles in the contour integration planes is included in the surface displacements. The latter contribution arises because as z goes to

zero, for certain values of $\underline{x}$ and c, the contours in the q and w-planes wrap around the Rayleigh poles. By inspection of the q-planes used in section 2.4 (see Figs. 3, 5, 8, 9, and 13), one sees that as $z \to 0$ the contours $q_d(\pm)$ and $q_s(\pm)$ wrap around the Rayleigh poles for all $\underline{x}$ and c. On the other hand, by inspecting the w-planes used in section 2.4 (see Figs. 4, 6, 11, 12, 14, 21, 24, and 29) one sees that as $z \to 0$ the contours w_d and w_s only wrap around the Rayleigh poles if $\tan\theta < \dfrac{(\gamma_R^2-\gamma^2)^{\frac{1}{2}}}{\gamma}$ (or $\dfrac{x}{r} > \dfrac{c_R}{c}$) and $c > c_R$.

An evaluation of a Rayleigh pole in either a q or w-plane produces (in the limit of the contour collapsing on the pole) a residue contribution from an arc around the pole plus an improper integral from the ends of the contours that shrink onto the pole. The improper integral is interpreted as a Cauchy principal value. For the residue contribution the Laplace transform is inverted to obtain the Rayleigh waves as a function of the space and time parameters. However, the improper integral appears in the interior solution when it is evaluated for $z = 0$.

In particular, for the vertical displacement the residue contribution of the Rayleigh poles in both the q and w-planes is zero. Then the substitution of $z = 0$ into formulas (2.4-80)-(2.4-86) and (2.4-96) - (2.4-100) yields

$$u_z(\underline{X},t) = \sum_{j=1}^{4} U_z^j(\underline{X},t) \qquad (2.6\text{-}1)$$

where $\underline{X}$ is the position vector in the surface plane of the half-space.

In this section the surface coordinates (x,y) are used with $r = (x^2+y^2)^{\frac{1}{2}}$ and $\xi = ct - x$, as shown in Fig. 2. Equation (2.6-1) is valid for $-\infty < x,y < \infty$ and $0 \leq c < \infty$. The $U_z^{j\,\dagger}$ represent circular waves (surface intersection of the hemispherical waves) emanating from the initial position of the load and disturbances trailing behind the load.

The circular waves are

$$U_z^1(\underline{X},t) = \frac{\ell^2\gamma^2}{\pi^2\mu r} H(t-t_d)\left(\frac{t}{t_L}-1\right) P\int_0^{T_d} \frac{(T_d^2-w^2)^{\frac{1}{2}}(2w^2-2T_s^2-\ell^2)^2\,dw}{\left[\gamma^2\left(\frac{t}{t_L}-1\right)^2+\frac{w^2\gamma^2}{r^2}\right]G(t^2,w^2)} \qquad (2.6\text{-}2a)$$

$$U_z^2(\underline{X},t) = \frac{4\ell^2\gamma^2}{\pi^2\mu r} H(t-t_s)\left(\frac{t}{t_L}-1\right) P\int_0^{T_s} \frac{(T_s^2-w^2)^{\frac{1}{2}}(T_d^2-w^2)(T_d^2+1-w^2)\,dw}{\left[\gamma^2\left(\frac{t}{t_L}-1\right)^2+\frac{w^2\gamma^2}{r^2}\right]G(t^2,w^2)} \qquad (2.6\text{-}2b)$$

where

$$G(t^2,w^2) = (2w^2-2T_s^2-\ell^2)^4 - 16(T_d^2-w^2)(T_s^2-w^2)(T_d^2+1-w^2)^2 . \qquad (2.6\text{-}3)$$

The factors T_d and T_s are given in (2.4-84) and the arrival times of the circular waves and t_L take the form

$$\left.\begin{aligned} t_\beta &= \frac{r}{c_\beta} \quad , \quad (\beta = d,s) \\ t_L &= \frac{r^2}{cx} \quad . \end{aligned}\right\} \qquad (2.6\text{-}4)$$

The integrals in (2.6-2) are improper[‡] for $t = t_L$ because their

[†] A capital letter is used to designate the components of $u_z(\underline{X},t)$ to emphasize that there is not a one-to-one relationship between the components of u_z for $z > 0$ and $z = 0$.

[‡] For the surface displacements, whenever a reference is made to t_L in connection with an improper integral, it is assumed that $x > 0$.

integrands have a non-integrable singularity at $w = 0$ for $t = t_L$. In order to assess U_z^1 and U_z^2 at $t = t_L$, the integrals in (2.6-2) must first be evaluated for t near t_L; then the limit as $t \to t_L$ is computed in U_z^1 and U_z^2. In addition, these integrals are interpreted as Cauchy principal values for $t \geq t_R$ because their integrands have a simple pole at $w = \left(\frac{t^2}{t_R^2} - 1\right)^{\frac{1}{2}} \gamma_R$ for $t \geq t_R$, where

$$t_R = \frac{r}{c_R} \tag{2.6-5}$$

and t_R is the arrival time of the circular Rayleigh wave.

The time dependence of the integrals in (2.6-2) is simplified by the transformation $w = \left(\frac{t^2}{t_d^2} - k^2\right)^{\frac{1}{2}}$ and it reduces (2.6-2) to

$$U_z^1(\underline{X},t) = \frac{\ell^2\gamma^2}{\pi^2\mu r} H(t-t_d)\left(\frac{t}{t_L}-1\right) P\int_1^{t/t_d} \frac{(k^2-1)^{\frac{1}{2}}(\ell^2-2k^2)^2\, k\, dk}{\left[\gamma^2\left(\frac{t}{t_L}-1\right)^2 + \frac{\gamma^2}{r^2}\left(\frac{t^2}{t_d^2}-k^2\right)\right]\left(\frac{t^2}{t_d^2}-k^2\right)^{\frac{1}{2}} G(k^2)}\,, \tag{2.6-6a}$$

$$U_z^2(\underline{X},t) = \frac{4\ell^2\gamma^2}{\pi^2\mu r} H(t-t_s)\left(\frac{t}{t_L}-1\right) P\int_\ell^{t/t_d} \frac{(k^2-\ell^2)^{\frac{1}{2}}(k^2-1)\, k^3\, dk}{\left[\gamma^2\left(\frac{t}{t_L}-1\right)^2 + \frac{\gamma^2}{r^2}\left(\frac{t^2}{t_d^2}-k^2\right)\right]\left(\frac{t^2}{t_d^2}-k^2\right)^{\frac{1}{2}} G(k^2)}\,, \tag{2.6-6b}$$

where G becomes

$$G(k^2) = (\ell^2-2k^2)^4 - 16(k^2-1)(k^2-\ell^2)k^4\,. \tag{2.6-7}$$

The integrals in (2.6-6) are still improper for $t = t_L$ and $t = t_R$. In particular, the Rayleigh pole in each integrand is located at $k = \gamma_R$ for $t \geq t_R$.

The disturbances trailing behind the load that contribute to u_z are

$$U_z^3(\underline{X},t) = \frac{-c^2y^2}{\pi c_s^2\mu} \frac{\alpha_d\left[\left(\frac{c^2}{c_s^2}-2\right)y^2-2\xi^2\right]^2 H(t-t_L)}{\left[\left(\frac{c^2}{c_s^2}-2\right)y^2-2\xi^2\right]^4 -16\alpha_d^2\alpha_s^2(\xi^2+y^2)^2} H(t-t_{dc})H(x), \quad (2.6\text{-}8a)$$

$$U_z^4(\underline{X},t) = \frac{-4c^2y^2}{\pi c_s^2\mu} \frac{\alpha_d^2\alpha_s(\xi^2+y^2)H(t-t_L)}{\left[\left(\frac{c^2}{c_s^2}-2\right)y^2-2\xi^2\right]^4 -16\alpha_d^2\alpha_s^2(\xi^2+y^2)^2} H(t-t_{sc})H(x), \quad (2.6\text{-}8b)$$

where the Heaviside function is restricted by

$$H(t-t_{\beta c}) = 1 \text{ if } c < c_\beta , \quad (\beta = d,s) . \quad (2.6\text{-}9)$$

The arrival times of the triangular waves (surface intersection of the conical waves) are

$$t_{\beta c} = \frac{1}{c}\left[\left(\frac{c^2}{c_\beta^2}-1\right)^{\frac{1}{2}}|y| + x\right], \quad (\beta = d,s) \quad (2.6\text{-}10)$$

and

$$\alpha_\beta = \left[\xi^2 - \left(\frac{c^2}{c_\beta^2}-1\right)y^2\right]^{\frac{1}{2}} , \quad (\beta = d,s) . \quad (2.6\text{-}11)$$

Both U_z^3 and U_z^4 are singular for $t = t_{Rc}$ when $c > c_R$ and $\frac{x}{r} > \frac{c_R}{c}$, where

$$t_{Rc} = \frac{1}{c}\left[\left(\frac{c^2}{c_R^2}-1\right)^{\frac{1}{2}}|y| + x\right] . \quad (2.6\text{-}12)$$

t_{Rc} is the arrival time of the triangular Rayleigh wave trailing behind the load.

In section 3.2 the behavior of u_z near the arrival of the circular and triangular Rayleigh waves is determined. In addition, in section 3.3, u_z is evaluated near $t = t_L$, showing that the total displacement is continuous through $t = t_L$. For fixed time, $t = t_L$ is the equation of a circle with center $\left(x = \frac{ct}{2}, y = 0\right)$ and radius $\frac{ct}{2}$, which is the surface intersection of the hemisphere $t = \frac{\rho^2}{cx}$ found in u_z for $z > 0$. In Fig. 34 the wave geometry in the surface plane is displayed for all load speeds.

For u_x the Rayleigh poles in both the q and w-planes contribute residue terms which, when their Laplace transforms are inverted, give the Rayleigh waves. Then, by adding the Rayleigh waves to formulas (2.5-1), (2.5-2), (2.5-5), and (2.5-6) assessed for $\sigma = x$ and $z = 0$, one finds

$$u_x(\underline{X},t) = \sum_{j=1}^{5} U_x^j(\underline{X},t) \qquad (2.6\text{-}13)$$

for $-\infty < x,y < \infty$ and $0 \leq c < \infty$. The U_x^j represent circular waves emanating from the initial position of the load and disturbances trailing behind the load.

The circular waves are

$$U_x^1(\underline{X},t) = \left[H(t-t_d) - H(t-t_s)\right] \int_0^{T_d} V_x \, dw \quad , \qquad (2.6\text{-}14a)$$

$$U_x^2(\underline{X},t) = H(t-t_s) \int_{T_s}^{T_d} V_x \, dw \quad , \qquad (2.6\text{-}14b)$$

$$U_x^3(\underline{X},t) = \frac{-c_R\Phi}{4\pi c\mu r}\,\frac{\left[\frac{tc_R x}{t_R cr}\left(\frac{t}{t_L}-1\right)+\frac{y^2}{r^2}\left(\frac{t^2}{t_R^2}-1\right)\right]}{\left[\frac{c_R^2}{c^2}\left(\frac{t}{t_L}-1\right)^2+\frac{y^2}{r^2}\left(\frac{t^2}{t_R^2}-1\right)\right]}\,\frac{H(t-t_R)}{\left(\frac{t^2}{t_R^2}-1\right)^{\frac{1}{2}}}\,, \qquad (2.6\text{-}14c)$$

where

$$V_x = \frac{\frac{-2\ell^2\gamma}{\pi^2\mu r}\left[\frac{t\gamma x}{t_d r}\left(\frac{t}{t_L}-1\right)+\frac{w^2y^2}{r^2}\right]\left(T_d^2-w^2\right)^{\frac{1}{2}}\left(w^2-T_s^2\right)^{\frac{1}{2}}(2w^2-2T_s^2-\ell^2)}{\left[\gamma^2\left(\frac{t}{t_L}-1\right)^2+\frac{w^2y^2}{r^2}\right]G(t^2,w^2)}\,, \qquad (2.6\text{-}15a)$$

$$\tilde{\Phi} = \frac{\left(\frac{c_R^2}{c_s^2}-2\right)+2\left(1-\frac{c_R^2}{c_d^2}\right)^{\frac{1}{2}}\left(1-\frac{c_R^2}{c_s^2}\right)^{\frac{1}{2}}}{2\left(\frac{c_R^2}{c_s^2}-2\right)+2\left(1-\frac{c_R^2}{c_d^2}\right)^{\frac{1}{2}}\left(1-\frac{c_R^2}{c_s^2}\right)^{\frac{1}{2}}+\left(1-\frac{c_R^2}{c_s^2}\right)^{\frac{1}{2}}\left(1-\frac{c_R^2}{c_d^2}\right)^{-\frac{1}{2}}+\left(1-\frac{c_R^2}{c_d^2}\right)^{\frac{1}{2}}\left(1-\frac{c_R^2}{c_s^2}\right)^{-\frac{1}{2}}}\,, \qquad (2.6\text{-}15b)$$

with $G(t^2,w^2)$ given in (2.6-3) and T_d and T_s in (2.4-84). The arrival times and t_L are given in (2.6-4) and (2.6-5). It is not proper to take the limit as $t \to t_L$ through the integral in (2.6-14a) because its integrand has an indeterminant form $(\frac{0}{0})$ for $t = t_L$ and $w = 0$. Instead, the integral should first be evaluated for t near t_L, and then the limit as $t \to t_L$ taken. The circular Rayleigh wave in (2.6-14c) has the one-sided, $(t-t_R)^{-\frac{1}{2}}$ singularity which is typical of horizontal displacements in three-dimensional problems. Pekeris [3], for example, obtained this type of result for the stationary point load.

By the transformation $w = \left(\frac{t^2}{t_d^2}-k^2\right)^{\frac{1}{2}}$, U_x^1 and U_x^2 become

$$U_x^1(\underline{X},t) = \left[H(t-t_d) - H(t-t_s)\right]\int_1^{t/t_d} \hat{V}_x \, dk \quad , \tag{2.6-16a}$$

$$U_x^2(\underline{X},t) = H(t-t_s)\int_1^{\ell} \hat{V}_x \, dk \quad , \tag{2.6-16b}$$

where

$$\hat{V}_x = \frac{-2\ell^2\gamma\left[\frac{t\gamma x}{t_d r}\left(\frac{t}{t_L}-1\right)+\frac{y^2}{r^2}\left(\frac{t^2}{t_d^2}-k^2\right)\right](k^2-1)^{\frac{1}{2}}(\ell^2-k^2)^{\frac{1}{2}}(\ell^2-2k^2)k}{\pi^2\mu r\left[\gamma^2\left(\frac{t}{t_L}-1\right)^2+\frac{y^2}{r^2}\left(\frac{t^2}{t_d^2}-k^2\right)\right]\left(\frac{t^2}{t_d^2}-k^2\right)^{\frac{1}{2}}G(k^2)} \tag{2.6-17}$$

and $G(k^2)$ is given in (2.6-7). It still is not proper to take the limit as $t \to t_L$ through the integral in U_x^1.

The disturbances trailing behind the load are

$$U_x^4(\underline{X},t) = \frac{2|y|c^2y^2}{\pi c_s^2\mu} W\left[H(t-t_{dc}) - H(t-t_{sc})\right]H(t-t_L)H(x) \quad , \tag{2.6-18a}$$

$$U_x^5(\underline{X},t) = \frac{\Phi}{4c\mu}\left(\frac{c^2}{c_R^2}-1\right)^{-\frac{1}{2}}\delta(t-t_{Rc})H\left(\frac{x}{r}-\frac{c_R}{c}\right)H(x) \quad , \tag{2.6-18b}$$

where

$$W = \frac{\alpha_d\alpha_{sd}\left[\left(\frac{c^2}{c_s^2}-2\right)y^2-2\xi^2\right]}{\left[\left(\frac{c^2}{c_s^2}-2\right)y^2-2\xi^2\right]^4-16\alpha_d^2\alpha_s^2(\xi^2+y^2)^2} \tag{2.6-19}$$

with

$$\alpha_{sd} = \left[\left(\frac{c^2}{c_s^2}-1\right)y^2-\xi^2\right]^{\frac{1}{2}} \tag{2.6-20}$$

and α_s, α_d, and Φ given in (2.6-11) and (2.6-15b). $\delta(\sim)$ is the Dirac delta function and the Heaviside function in (2.6-18a) is restricted by (2.6-9). The arrival times of the triangular waves and t_L are displayed in (2.6-10), (2.6-12), and (2.6-4). The time dependence of the triangular Rayleigh wave in (2.6-18b) is typical of that found for horizontal displacements in two-dimensional problems. DeHoop [22], for example, obtained this type of result for the line load problem. The magnitude of the triangular Rayleigh wave becomes unbounded as c approaches c_R. But, as c approaches c_R the domain of the half-space surface where U_x^5 is pertinent shrinks to the position of the load and the circular Rayleigh wave (when $c = c_R$ the load travels on the circular Rayleigh wave). Therefore $u_x(\underline{X},t)$ remains bounded for $c = c_R$, except in the neighborhood of the load and the circular Rayleigh wave where the solution is unbounded for all c.

The expansion of u_y for $z = 0$ proceeds exactly as for u_x, including the Rayleigh waves, and one finds

$$u_y(\underline{X},t) = \sum_{j=1}^{5} U_y^j(\underline{X},t) \qquad (2.6\text{-}21)$$

for $-\infty < x,y < \infty$ and $0 \leq c < \infty$. The circular waves are

$$U_y^1(\underline{X},t) = \left[H(t-t_d) - H(t-t_s)\right] \int_0^{T_d} V_y \, dw \quad , \qquad (2.6\text{-}22a)$$

$$U_y^2(\underline{X},t) = H(t-t_s) \int_{T_s}^{T_d} V_y \, dw \quad , \qquad (2.6\text{-}22b)$$

$$U_y^3(\underline{X},t) = \frac{c_R \Phi y}{4\pi c \mu r^2} \frac{\left[\frac{-tc_R}{t_R c}\left(\frac{t}{t_L}-1\right)+\frac{x}{r}\left(\frac{t^2}{t_R^2}-1\right)\right] H(t-t_R)}{\left[\frac{c_R^2}{c^2}\left(\frac{t}{t_L}-1\right)^2+\frac{y^2}{r^2}\left(\frac{t^2}{t_R^2}-1\right)\right]\left(\frac{t^2}{t_R^2}-1\right)^{\frac{1}{2}}} \quad , \qquad (2.6\text{-}22c)$$

where

$$V_y = \frac{2\ell^2\gamma y\left[\frac{-t\gamma}{t_d}\left(\frac{t}{t_L}-1\right)+\frac{w^2 x}{r}\right](T_d^2-w^2)^{\frac{1}{2}}(w^2-T_s^2)^{\frac{1}{2}}(2w^2-2T_s^2-\ell^2)}{\pi^2\mu r^2\left[\gamma^2\left(\frac{t}{t_L}-1\right)^2+\frac{w^2y^2}{r^2}\right] G(t^2,w^2)} \; . \qquad (2.6\text{-}23)$$

By using the transformation $w = \left(\frac{t^2}{t_d^2}-k^2\right)^{\frac{1}{2}}$, U_y^1 and U_y^2 become

$$U_y^1(\underline{X},t) = \left[H(t-t_d)-H(t-t_s)\right]\int_1^{t/t_d} \hat{V}_y \, dk \quad , \qquad (2.6\text{-}24a)$$

$$U_y^2(\underline{X},t) = H(t-t_s)\int_1^{\ell} \hat{V}_y \, dk \quad , \qquad (2.6\text{-}24b)$$

where

$$\hat{V}_y = \frac{2\ell^2\gamma y\left[\frac{-t\gamma}{t_d}\left(\frac{t}{t_L}-1\right)+\frac{x}{r}\left(\frac{t^2}{t_d^2}-k^2\right)\right](k^2-1)^{\frac{1}{2}}(\ell^2-k^2)^{\frac{1}{2}}(\ell^2-2k^2)k}{\pi^2\mu r^2\left[\gamma^2\left(\frac{t}{t_L}-1\right)^2+\frac{y^2}{r^2}\left(\frac{t^2}{t_d^2}-k^2\right)\right]\left(\frac{t^2}{t_d^2}-k^2\right)^{\frac{1}{2}} G(k^2)} \; . \qquad (2.6\text{-}25)$$

The disturbances trailing behind the load are

$$U_y^4(\underline{X},t) = \frac{2\xi c^2 y^2}{\pi c_s^2 \mu} W \, \mathrm{sgn}(y)\left[H(t-t_{dc})-H(t-t_{sc})\right] H(t-t_L)H(x) \; , \qquad (2.6\text{-}26a)$$

$$U_y^5(\underline{X},t) = \frac{\Phi}{4c\mu} \, \mathrm{sgn}(y) \, \delta(t-t_{Rc}) H\left(\frac{x}{r}-\frac{c_R}{c}\right) H(x) \; . \qquad (2.6\text{-}26b)$$

The arrival times, G, W, Φ, T_d, T_s, and t_L appearing in (2.6-22) - (2.6-26) are the same as those in u_x above. The Heaviside function in (2.6-26a) is subject to the conditions in (2.6-9). Unlike for u_x, the magnitude of the triangular Rayleigh wave for u_y is bounded as c approaches c_R. The remaining details concerning the structure of u_y are analogous to u_x and they are given above.

The disturbances trailing behind the load that arise in this section, as in the previous sections, represent steady-state contributions to the displacements. Furthermore, each of them is identified as a separate wave if, and only if, the load speed is sufficiently large that its wave front exists.

The results given above for the surface displacements are not new as Payton [1] and Lansing [2] have given them in closed form (algebraic terms and elliptic integrals) for $\lambda = \mu$. The integrals in the circular waves above can be reduced when $\lambda = \mu$ to closed form by partial fraction decomposition. However, since the behavior of the circular waves near their wave fronts and the Rayleigh arrival time can be computed easily from these integrals for all λ and μ, as shown in Chapter 3, this last integration is not undertaken here.

2.7. EXACT INVERSION OF THE DISPLACEMENTS FOR A STATIONARY POINT LOAD

A special case of the thesis problem is that of a half-space whose surface is excited by a stationary, but impulsive, point load.

As mentioned in Chapter I, many authors have contributed to this problem, but much work can still be done for the interior of the half-space. In this section a new representation of the interior displacements is obtained which is a sum of integrals. Each integral is identified as the disturbance behind a particular wave front. Furthermore, as shown in section 3.1, these integrals lend themselves to wave front expansions that display, amongst other discontinuities, the logarithmic discontinuity mentioned previously. Also, the surface displacements for the stationary point load problem are given in this section.

Before displaying the displacements, it should be noted that a point load with step time dependence and unit magnitude is obtained from the moving load problem formulated in section 2.1 for $c = 0$. Therefore all of the results given in this section correspond to such a surface load.

Now the interior displacements for the stationary point load problem are obtained from the results in subsection 2.4.5 and section 2.5. In particular, by expanding equations (2.4-80) - (2.4-92), (2.5-1), (2.5-2), and (2.5-5) - (2.5-7) for $c = 0$, and using the cylindrical geometry in Fig. 2, one finds u_r, u_θ, and u_z for $c = 0$ to be

$$u_\sigma(\underline{x},t) = \sum_{j=1}^{4} u_\sigma^j(\underline{x},t) \quad , \quad (\sigma = r,z) \quad , \qquad (2.7\text{-}1)$$

$$u_\theta(\underline{x},t) = 0 \quad , \qquad (2.7\text{-}2)$$

where $0 \leq r < \infty$, $-\pi \leq \theta < \pi$, $0 < z < \infty$, and

$$u_\sigma^1(\underline{x},t) = H(t-t_d)\int_0^{T_d} \mathrm{Re}\left[K_{\sigma d}^o(q_d,w)\,\frac{dq_d}{dt}\right]dw \quad , \tag{2.7-3a}$$

$$u_\sigma^2(\underline{x},t) = H(t-t_s)\int_0^{T_s} \mathrm{Re}\left[K_{\sigma s}^o(q_s,w)\,\frac{dq_s}{dt}\right]dw \quad , \tag{2.7-3b}$$

$$u_\sigma^3(\underline{x},t) = H(t-t_s)H(t_B-t)H\left(\frac{r}{\rho}-\frac{c_s}{c_d}\right)\int_{T_s}^{T_{sd}} \mathrm{Re}\left[K_{\sigma s}^o(q_{sd},w)\,\frac{dq_{sd}}{dt}\right]dw \quad , \tag{2.7-3c}$$

$$u_\sigma^4(\underline{x},t) = \left[H(t-t_{sd}) - H(t-t_s)\right]H\left(\frac{r}{\rho}-\frac{c_s}{c_d}\right)\int_0^{T_{sd}} \mathrm{Re}\left[K_{\sigma s}^o(q_{sd},w)\,\frac{dq_{sd}}{dt}\right]dw \quad . \tag{2.7-3d}$$

The functions $K_{\sigma d}^o$ and $K_{\sigma s}^o$ are

$$\left.\begin{aligned} K_{r\beta}^o(q,w) &= \left[\cos\theta K_{x\beta}(q,w,\theta) + \sin\theta K_{y\beta}(q,w,\theta)\right]\Big|_{c=0} \\ K_{z\beta}^o(q,w) &= K_{z\beta}(q,w,\theta)\Big|_{c=0} \qquad (\beta = d,s) \end{aligned}\right\} \tag{2.7-4}$$

and by using $K_{x\beta}$, $K_{y\beta}$, and $K_{z\beta}$ as given in (2.3-5), they become

$$\left.\begin{aligned} K_{rd}^o(q,w) &= \frac{-iq\left[\ell^2+2(q^2+w^2)\right]}{\pi^2 c_d \mu R(q,w)}, \qquad K_{rs}^o(q,w) = \frac{2iqm_d m_s}{\pi^2 c_d \mu R(q,w)} \\ K_{zd}^o(q,w) &= \frac{m_d\left[\ell^2+2(q^2+w^2)\right]}{\pi^2 c_d \mu R(q,w)}, \qquad K_{zs}^o(q,w) = \frac{-2m_d(q^2+w^2)}{\pi^2 c_d \mu R(q,w)} \end{aligned}\right\} \tag{2.7-5}$$

where $R(q,w)$, m_d, and m_s are given in (2.3-6) and (2.3-7). The q-transformations, the limits of integration, the arrival times, and t_B appearing in (2.7-3) are given in (2.4-83)-(2.4-86). The integrals in

(2.7-3c) and (2.7-3d) are improper for $t = t_s$ because their integrands have a simple pole at $w = 0$ for $t = t_s$. As shown in section 3.1, these improper integrals generate the logarithmic singularity mentioned in Chapter 1. The time parameters can be removed from the limits of the integrals in (2.7-3) by the variable transformations in (2.4-93), but the resulting integrals are not displayed.

The functions u_σ^j, $(j = 1,\ldots,4)$ and $(\sigma = r,z)$, represent a system of waves emanating from the load at the origin of the coordinates. In particular, u_σ^1 and u_σ^2 are hemispherical, dilatational and equivoluminal waves respectively. In addition, u_σ^3 represents a hemispherical, equivoluminal wave. But, unlike u_σ^2, it has a back at $t = t_B$. As shown for the moving load solution in subsection 2.4.5 (the computation given there is actually valid for $0 \leq c < \infty$), u_σ^3 and u_σ vary continuously through $t = t_B$. The function u_σ^4 represents the conical head wave generated by the surface intersection of the hemispherical, dilatational wave front. The wave fronts corresponding to these waves are displayed in the upper diagram of Fig. 35.

The surface displacements for the stationary point load problem are obtained from the results in section 2.6. In particular, by expanding equations (2.6-1, 6, 8, 13, 14c, 16, 18, 21, 22c, 24, and 26) for $c = 0$, and using the cylindrical geometry in Fig. 2, one finds u_r, u_θ, and u_z for $c = 0$ and $z = 0$ to be

$$u_r(r,\theta,0,t) = \sum_{j=1}^{3} U_r^j(r,\theta,0,t) \quad , \tag{2.7-6}$$

$$u_\theta(r,\theta,0,t) = 0 \quad , \tag{2.7-7}$$

$$u_z(r,\theta,0,t) = \sum_{j=1}^{2} U_z^j(r,\theta,0,t) \quad , \tag{2.7-8}$$

for $0 \leq r < \infty$ and $-\pi \leq \theta < \pi$. The circular waves take the form

$$U_r^1(r,\theta,0,t) = \left[H(t-t_d) - H(t-t_s)\right] \int_1^{t/t_d} \hat{V}_r \, dk \quad , \tag{2.7-9a}$$

$$U_r^2(r,\theta,0,t) = H(t-t_s) \int_1^{\ell} \hat{V}_r \, dk \quad , \tag{2.7-9b}$$

$$U_r^3(r,\theta,0,t) = \frac{t\Phi}{4\pi\mu r t_R} \frac{H(t-t_R)}{\left(\frac{t^2}{t_R^2} - 1\right)^{\frac{1}{2}}} \quad , \tag{2.7-9c}$$

$$U_z^1(r,\theta,0,t) = \frac{-\ell^2}{\pi^2 \mu r} H(t-t_d) P \int_1^{t/t_d} \frac{(k^2-1)^{\frac{1}{2}}(\ell^2-2k^2)^2 k \, dk}{G(k^2)\left(\frac{t^2}{t_d^2} - k^2\right)^{\frac{1}{2}}} \quad , \tag{2.7-10a}$$

$$U_z^2(r,\theta,0,t) = \frac{-4\ell^2}{\pi^2 \mu r} H(t-t_s) P \int_{\ell}^{t/t_d} \frac{(k^2-\ell^2)^{\frac{1}{2}}(k^2-1)k^3 \, dk}{G(k^2)\left(\frac{t^2}{t_d^2} - k^2\right)^{\frac{1}{2}}} \quad , \tag{2.7-10b}$$

where

$$\hat{V}_r = \frac{2\ell^2 t(k^2-1)^{\frac{1}{2}}(\ell^2-k^2)^{\frac{1}{2}}(\ell^2-2k^2)k}{\pi^2 \mu r t_d G(k^2)\left(\frac{t^2}{t_d^2} - k^2\right)^{\frac{1}{2}}} \tag{2.7-11}$$

and $G(k^2)$ and Φ are given in (2.6-7) and (2.6-15b) respectively. The arrival times are displayed in (2.6-4) and (2.6-5). The integrals in (2.7-10) are interpreted as Cauchy principal values for $t \geq t_R$

because their integrands have a simple pole at $k = \gamma_R$ for $t \geq t_R$. The surface wave geometry associated with these displacements is shown in the lower diagram of Fig. 35. If these surface displacements are assessed for $\lambda = \mu$ they become those computed by Pekeris [3] (see equations (33) - (36) and (57) - (59) of this reference). In addition, Pekeris reduced these displacements to closed form for $\lambda = \mu$. However, a comparable computation is not made in this investigation.

CHAPTER 3

EVALUATION OF THE RESPONSE

3.1. WAVE FRONT EXPANSIONS

In this section each wave, as identified in Chapter 2, that contributes to the displacements is evaluated near its wave front. Each wave front expansion is an asymptotic expansion as time approaches the particular arrival time and physically it represents the change in the displacements as the wave front passes a fixed point in the half-space. The wave front expansions are computed for $z > 0$ in subsection 3.1.1 and for $z = 0$ in subsection 3.1.2. The computations in these subsections are given for $0 \leq c < \infty$ with the expansions corresponding to $c = 0$ displayed at the end of each subsection.

3.1.1. Interior of the Half-Space.

The wave front expansions for u_z are computed and discussed in detail in this subsection while only the results are given for u_x and u_y.

Vertical Displacement, u_z:

1) Hemispherical, Dilatational Wave, u_z^1.

A wave front expansion of u_z^1 as $t \to t_d$ is obtained from equations (2.4-94a) and (2.4-95a) by computing an asymptotic expansion of $\hat{u}_z^1$ as $t \to t_d$ and then integrating this expansion with respect to α from 0 to $\frac{\pi}{2}$. To apply this technique properly the expansion of

$\hat{u}_z^1$ must be uniformly valid in α for $\alpha \in [0, \frac{\pi}{2}]$ and its regions of uniform validity with respect to $\underline{x}$ and c must be determined. In particular, one must take into consideration the simple pole in $\hat{u}_z^1$ for $t = t_L$ when $x > 0$. When $c > c_d$, $t = t_L$ coincides with $t = t_d$ along the rays defined by $\frac{x}{\rho} = \frac{c_d}{c}$ at the intersection of the conical and hemispherical, dilatational wave fronts. These rays form the cone mentioned in subsection 2.4.1 and shown in Fig. 7 as the dashed lines. The expansion given here is not valid along these rays. For $c < c_d$, $t = t_L$ and $t = t_d$ do not coincide, as shown in Fig. 22, and this pole does not interfere with the wave front expansion.

By expanding $\hat{u}_z^1$ in (2.4-95a) as $t \to t_d$, one finds

$$\hat{u}_z^1 = \frac{2}{\pi} N^1 z \left(1 - \frac{cx}{c_d \rho}\right)^{-1} + O(t-t_d) \qquad (3.1\text{-}1)$$

as $t \to t_d$ for $z > 0$, $\left| \frac{c_d}{c} - \frac{x}{\rho} \right| > 0$, $0 \leq c < \infty$, and $\alpha \in [0, \frac{\pi}{2}]$, where

$$N^1 = \frac{(z/2\pi\mu\rho)(\ell^2\rho^2 - 2r^2)}{(\ell^2\rho^2 - 2r^2)^2 + 4r^2 z(\ell^2\rho^2 - r^2)^{\frac{1}{2}}} \, . \qquad (3.1\text{-}2)$$

The conditions following (3.1-1) arise naturally in the computations and define the regions of uniform validity of the expansion. The symbol $O(\tau)$ is used to imply that $f = O(\tau)$ as $\tau \to 0$ if $\left| \frac{f}{\tau} \right| < M$ as $\tau \to 0$, where M is a real, positive constant which is bounded. Then the substitution of (3.1-1) into (2.4-94a) yields

$$u_z^1 = N^1 z \left(1 - \frac{cx}{c_d \rho}\right)^{-1} + O(t-t_d) \qquad (3.1\text{-}3)$$

as $t \to t_d$ for $t > t_d$, $z > 0$, $\left| \frac{c_d}{c} - \frac{x}{\rho} \right| > 0$, and $0 \leq c < \infty$. A definite inequality like $z > 0$, but z otherwise arbitrary, means that a limit as $t \to t_d$ can not be interchanged with $z \to 0$. Therefore a wave front expansion of u_z^1 for $z > 0$ can not be extended to obtain the corresponding expansion for $z = 0$. Likewise, the condition $\left| \frac{x}{\rho} - \frac{c_d}{c} \right| > 0$, which is only non-trivial if $c > c_d$, means that this expansion is not valid along the rays $\frac{x}{\rho} = \frac{c_d}{c}$. However, for $0 \leq c < \infty$ a limit as $t \to t_d$ can be interchanged with $c \to 0$ to obtain the corresponding wave front expansion for a stationary point load. From (3.1-3) one sees that there is a step discontinuity in u_z^1, and therefore u_z, across the hemispherical, dilatational wave front.

2) Hemispherical, Equivoluminal Wave, u_z^2.

A wave front expansion of u_z^2 as $t \to t_s$ can be computed from (2.4-94b) and (2.4-95b) by the same technique as used for u_z^1 with the result

$$u_z^2 = \begin{cases} N_\ell^2 r^2 \left(1 - \frac{cx}{c_s \rho}\right)^{-1} + O(t-t_s) & \text{for } \frac{r}{\rho} < \frac{c_s}{c_d} \\ N_g^2 r^2 \left(1 - \frac{cx}{c_s \rho}\right)^{-1} + O\left((t-t_s)^{\frac{1}{2}}\right) & \text{for } \frac{r}{\rho} > \frac{c_s}{c_d} \end{cases} \qquad (3.1\text{-}4)$$

as $t \to t_s$ for $t > t_s$, $z > 0$, $\left| \frac{c_s}{c} - \frac{x}{\rho} \right| > 0$, and $0 \leq c < \infty$, where

$$N_\ell^2 = \frac{(z/\pi\mu\rho)(\ell^{-2}\rho^2 - r^2)^{\frac{1}{2}}}{(\rho^2 - 2r^2)^2 + 4r^2 z(\ell^{-2}\rho^2 - r^2)^{\frac{1}{2}}} , \qquad (3.1\text{-}5a)$$

$$N_g^2 = \frac{(4r^2z^2/\pi\mu\rho)(r^2 - \ell^{-2}\rho^2)}{(\rho^2 - 2r^2)^4 + 16r^4z^2(\ell^{-2}\rho^2 - r^2)} . \qquad (3.1\text{-}5b)$$

As mentioned in subsection 2.4.2 and shown in Figs. 15 and 25 by the dashed lines, for $c > c_s$, $\frac{x}{\rho} = \frac{c_s}{c}$ defines a cone that denotes where the conical and hemispherical, equivoluminal wave fronts intersect. Also, as mentioned in subsection 2.4.2 and shown in Figs. 17, 27, 32, and 35 by dashed lines, $\frac{r}{\rho} = \frac{c_s}{c_d}$ defines a cone that denotes where the conical head wave front is tangent to the hemispherical, equivoluminal wave front. The expansion in (3.1-4) is not valid along the rays given by $\frac{x}{\rho} = \frac{c_s}{c}$ and $\frac{r}{\rho} = \frac{c_s}{c_d}$. As in the case of the hemispherical, dilatational wave front, there is a step discontinuity in u_z^2 and u_z across the hemispherical, equivoluminal wave front for $\frac{r}{\rho} < \frac{c_s}{c_d}$. However, for $\frac{r}{\rho} > \frac{c_s}{c_d}$, u_z^3 also contributes behind this wave front and u_z^4 ahead. These waves are expanded next.

3) Hemispherical, Equivoluminal Wave, u_z^3.

As displayed by (2.4-94c) with (2.4-82), (2.4-93), and (2.4-95c), the integral in u_z^3 is improper for $t = t_s$ because $\hat{u}_z^3$ has a simple pole at $\alpha = 0$. To obtain a wave front expansion of u_z^3 as $t \to t_s$ this improper integral must be assessed. For this purpose the integral in u_z^3 is written as

$$\int_0^{\frac{\pi}{2}} \hat{u}_z^3 \, d\alpha = \int_0^{\epsilon} \hat{u}_z^3 \, d\alpha + \int_{\epsilon}^{\frac{\pi}{2}} \hat{u}_z^3 \, d\alpha \quad , \tag{3.1-6}$$

where ϵ is an arbitrarily small, positive number. The integral from ϵ to $\frac{\pi}{2}$ is $O(1)$ and the one from 0 to ϵ must be approximated for t near t_s. By substituting $t = t_s(1 + \Delta)$ into $\hat{u}_z^3$, expanding it for small α and Δ, and combining the results with (3.1-6),

one finds

$$\int_0^{\frac{\pi}{2}} \hat{u}_z^3 \, d\alpha = -2N^3 r^2 \left(1 - \frac{cx}{c_s \rho}\right)^{-1} [1 + O(\Delta)] \int_0^{\epsilon} \frac{d\alpha}{(\alpha^2 + a^2)^{\frac{1}{2}}} + O(1) \qquad (3.1\text{-}7)$$

as $\Delta \to 0$ for $z > 0$, $\frac{r}{\rho} > \frac{c_s}{c_d}$, $\left|\frac{c_s}{c} - \frac{x}{\rho}\right| > 0$, and $0 \leq c < \infty$, where

$$N^3 = \frac{(z/\pi^2 \mu \rho)(r^2 - \ell^{-2}\rho^2)^{\frac{1}{2}}(\rho^2 - 2r^2)^2}{(\rho^2 - 2r^2)^4 + 16 r^4 z^2 (r^2 - \ell^{-2}\rho^2)}, \qquad (3.1\text{-}8a)$$

$$a = \ell r (2\Delta)^{\frac{1}{2}} [(\ell^2 - 1)^{\frac{1}{2}} \rho - \ell z]^{-1} . \qquad (3.1\text{-}8b)$$

By substituting the auxilliary result

$$\int_0^{\epsilon} \frac{d\alpha}{(\alpha^2 + a^2)^{\frac{1}{2}}} = -\log a + O(1) , \qquad (3.1\text{-}9)$$

where the integral is tabulated in reference [25] (p. 255, formula (20)), into (3.1-7), one finds

$$\int_0^{\frac{\pi}{2}} \hat{u}_z^3 \, d\alpha = N^3 r^2 \left(1 - \frac{cx}{c_s \rho}\right)^{-1} \log \Delta + O(1) \qquad (3.1\text{-}10)$$

as $\Delta \to 0$ for $z > 0$, $\frac{r}{\rho} > \frac{c_s}{c_d}$, $\left|\frac{c_s}{c} - \frac{x}{\rho}\right| > 0$, and $0 \leq c < \infty$. Then the substitution of (3.1-10) into (2.4-94c) with $\Delta = \frac{t}{t_s} - 1$ gives

$$u_z^3 = N^3 r^2 \left(1 - \frac{cx}{c_s \rho}\right)^{-1} \log \left(\frac{t}{t_s} - 1\right) + O(1) \qquad (3.1\text{-}11)$$

as $t \to t_s$ for $t > t_s$, $z > 0$, $\frac{r}{\rho} > \frac{c_s}{c_d}$, $\left|\frac{c_s}{c} - \frac{x}{\rho}\right| > 0$, and $0 \leq c < \infty$. The conditions following this expansion are the same as those following the expansion of u_z^2, and they are discussed in the text beneath

(3.1-5b). To find the total singularity across the hemispherical, equivoluminal wave front for $\frac{r}{\rho} > \frac{c_s}{c_d}$, u_z^4 must be expanded for $t < t_s$, which is undertaken next.

4) Conical Head Wave, u_z^4.

The function u_z^4 can be evaluated ahead of the hemispherical, equivoluminal wave front and behind the conical head wave front. As displayed by (2.4-94d) with (2.4-82), (2.4-93), and (2.4-95d), the integral in u_z^4 is improper for $t = t_s$ because $\hat{u}_z^4$ has a simple pole at $\alpha = 0$. The corresponding wave front expansion can be computed in the same way as for u_z^3 with the result

$$u_z^4 = N^3 r^2 \left(1 - \frac{cx}{c_s \rho}\right)^{-1} \log\left(1 - \frac{t}{t_s}\right) + O(1) \qquad (3.1\text{-}12)$$

as $t \to t_s$ for $t < t_s$, $z > 0$, $\frac{r}{\rho} > \frac{c_s}{c_d}$, $\left|\frac{c_s}{c} - \frac{x}{\rho}\right| > 0$, and $0 \leq c < \infty$, where N^3 is given in (3.1-8a). This wave front expansion along with the one for u_z^3 in (3.1-11) displays a logarithmic singularity in u_z across the two-sided, hemispherical, equivoluminal wave front. This singularity is symmetric about $t = t_s$.

The wave front expansion of u_z^4 as $t \to t_{sd}$ can be computed from (2.4-94d) and (2.4-95d) by the same technique used for u_z^1 with the result

$$u_z^4 = -N^4 r \left(1 - \frac{cx}{c_d r}\right)^{-1} (t - t_{sd}) + O\left((t - t_{sd})^2\right) \qquad (3.1\text{-}13)$$

as $t \to t_{sd}$ for $t > t_{sd}$, $\frac{z}{r} < (\ell^2 - 1)^{\frac{1}{2}}$, $\left|\frac{c_d}{c} - \frac{x}{r}\right| > 0$, and $0 \leq c < \infty$, where

$$N^4 = \frac{c_d(\ell^2 - 1)^{\frac{3}{4}}}{\pi\mu r^{\frac{3}{2}}(\ell^2 - 2)^2[(\ell^2 - 1)^{\frac{1}{2}}r - z]^{\frac{3}{2}}} \quad . \tag{3.1-14}$$

The condition $\frac{z}{r} = (\ell^2 - 1)^{\frac{1}{2}}$ implies that $\frac{r}{\rho} = \frac{c_s}{c_d}$, which is discussed in the text under (3.1-5b). As mentioned in subsection 2.4.2 and shown in Fig. 19, $\frac{x}{r} = \frac{c_d}{c}$ defines a plane which denotes where the plane head wave front is tangent to the conical head wave front. As (3.1-13) shows, u_z^4, and hence u_z, are continuous through the conical head wave front.

5) Conical, Dilatational Wave, u_z^5.

The function u_z^5 is only identified as a separate wave when $c > c_d$ and then its conical, dilatational wave front is located at $t = t_{dc}$. The corresponding wave front expansion, which is an algebraic computation from (2.4-96a), is

$$u_z^5 = zN^5 M_{dc}(t-t_{dc})^{-\frac{1}{2}} + O\left((t-t_{dc})^{\frac{1}{2}}\right) \tag{3.1-15}$$

as $t \to t_{dc}$ for $t > t_{dc}$, $n > 0$, $z > 0$, $\frac{x}{\rho} \geq \frac{c_d}{c}$ and $c > c_d$, where

$$N^5 = \frac{(z/\pi\mu)(2cn)^{-\frac{1}{2}}M_{dc}^{\frac{1}{2}}[n^2(M_{sc}^2 - 1) - 2y^2M_{dc}^2]}{[n^2(M_{sc}^2 - 1) - 2y^2M_{dc}^2]^2 + 4zM_{dc}(z^2M_{dc}^2 + n^2M_{sdc}^2)^{\frac{1}{2}}(y^2M_{dc}^2 + n^2)} \tag{3.1-16}$$

and

$$\left.\begin{aligned} M_{\beta c} &= \left(\frac{c^2}{c_\beta^2} - 1\right)^{\frac{1}{2}}, \quad (\beta = d, s) \\ M_{sdc} &= \left(\frac{c^2}{c_s^2} - \frac{c^2}{c_d^2}\right)^{\frac{1}{2}}. \end{aligned}\right\} \tag{3.1-16a}$$

The restrictions following (3.1-15) arise naturally when expanding u_z^5 and they determine where the expansion is uniformly valid. In particular, $t = t_{dc}$ and $n = 0$ imply that $\xi = 0$ or $ct = x$. Therefore $n > 0$ implies that (3.1-15) is not valid at the position of the load, as one might expect due to the singular nature of the load. The restriction $c > c_d$ arises because, as c approaches c_d, the conical, dilatational wave front collapses to the position of the load, where the expansion has already been excluded. As for the hemispherical waves, $z > 0$ means that this wave front expansion can not be extended to include $z = 0$. Finally, $\frac{x}{\rho} \geq \frac{c_d}{c}$ means that a limit as $t \to t_{dc}$ can be interchanged with $\frac{x}{\rho} \to \frac{c_d}{c}$, so that (3.1-15) is valid along the ray $\frac{x}{\rho} = \frac{c_d}{c}$ as well as for $\frac{x}{\rho} > \frac{c_d}{c}$. As (3.1-15) shows, u_z^5 and hence u_z have a one-sided $(t - t_{dc})^{-\frac{1}{2}}$ singularity at the conical, dilatational wave front.

6) Conical, Equivoluminal Wave, u_z^6.

The function u_z^6 has a wave front at $t = t_{sc}$ for $c > c_s$. The corresponding wave front expansion, which is an algebraic computation from (2.4-96b), is

$$u_z^6 = \begin{cases} N_g^6(y^2M_{sc}^2 + n^2)(t-t_{sc})^{-\frac{1}{2}} + O\left((t-t_{sc})^{\frac{1}{2}}\right) & \text{for } \frac{z}{n} > \frac{M_{sdc}}{M_{sc}},\ c > c_d \\ N_\ell^6(y^2M_{sc}^2 + n^2)(t-t_{sc})^{-\frac{1}{2}} + O(1) & \text{for } \frac{z}{n} < \frac{M_{sdc}}{M_{sc}} \end{cases} \tag{3.1-17}$$

as $t \to t_{sc}$ for $t > t_{sc}$, $n > 0$, $z > 0$, $\frac{x}{\rho} \geq \frac{c_s}{c}$, and $c > c_s$, where

$$N_g^6 = \frac{(2z/\pi\mu)(2cn)^{-\frac{1}{2}} M_{sc}^{\frac{1}{2}} (z^2M_{sc}^2 - n^2M_{sdc}^2)^{\frac{1}{2}}}{[\,n^2(M_{sc}^2-1) - 2y^2M_{sc}^2\,]^2 + 4zM_{sc}(z^2M_{sc}^2 - n^2M_{sdc}^2)^{\frac{1}{2}}(y^2M_{sc}^2+n^2)}\,, \tag{3.1-18a}$$

$$N_\ell^6 = \frac{(8z^2/\pi\mu)(2cn)^{-\frac{1}{2}} M_{sc}^{\frac{3}{2}} (y^2M_{sc}^2+n^2)(n^2M_{sdc}^2 - z^2M_{sc}^2)}{[\,n^2(M_{sc}^2-1) - 2y^2M_{sc}^2\,]^4 + 16z^2M_{sc}^2(n^2M_{sdc}^2 - z^2M_{sc}^2)(y^2M_{sc}^2+n^2)^2}\,. \tag{3.1-18b}$$

When $c < c_d$, $\frac{z}{n}$ is always less than $\frac{M_{sdc}}{M_{sc}}$ and only the lower term in (3.1-17) is pertinent to the expansion of u_z^6. Also, for $c > c_d$ the condition $\frac{z}{n} = \frac{M_{sdc}}{M_{sc}}$ is equivalent to $\frac{|y|}{n} = \phi_c$, where ϕ_c is given in (2.4-92). This angle is shown in Fig. 18 by dashed lines that denote where the plane head wave front is tangent to the conical, equivoluminal wave front. As (3.1-15) and (3.1-17) show, u_z has the same time dependence at the conical, equivoluminal wave front as at the conical, dilatational wave front.

7) Plane Head Wave, u_z^7.

The function u_z^7 can be expanded both ahead of the conical, equivoluminal wave front and behind the plane head wave front. The former front exists if $c > c_s$ while the latter only exists if $c > c_d$. The evaluation of u_z^7 at either front is just an algebraic asymptotic expansion from equation (2.4-96c) and the results are

$$u_z^7 = -N_b^7(y^2M_{sc}^2+n^2)(t_{sc}-t)^{-\frac{1}{2}} + O(1) \tag{3.1-19}$$

as $t \to t_{sc}$ for $t < t_{sc}$, $n > 0$, $z > 0$, $\frac{x}{\rho} \geq \frac{c_s}{c}$, $\frac{z}{n} < \frac{M_{sdc}}{M_{sc}}$ and $c > c_s$,

where

$$N_b^7 = \frac{(2z/\pi\mu)(2cn)^{-\frac{1}{2}} M_{sc}^{\frac{1}{2}} (n^2 M_{sdc}^2 - z^2 M_{sc}^2)^{\frac{1}{2}} [\, n^2(M_{sc}^2 - 1) - 2y^2 M_{sc}^2 \,]^2}{[\, n^2(M_{sc}^2 - 1) - 2y^2 M_{sc}^2 \,]^4 + 16 z^2 M_{sc}^2 (n^2 M_{sdc}^2 - z^2 M_{sc}^2)(y^2 M_{sc}^2 + n^2)^2} \qquad (3.1\text{-}20)$$

and

$$u_z^7 = - N_f^7 (t - t_{sdc})^{\frac{1}{2}} + O\left((t - t_{sdc})^{\frac{3}{2}}\right) \qquad (3.1\text{-}21)$$

as $t \to t_{sdc}$ for $t > t_{sdc}$, $n > 0$, $\frac{z}{|y|} < \frac{M_{sdc}}{M_{dc}}$, $\frac{x}{r} \geq \frac{c_d}{c}$, and $c > c_d$, where

$$N_f^7 = \frac{2(2c_d)^{\frac{1}{2}} (\ell^2 - 1)^{\frac{3}{4}} M_{dc}^{\frac{1}{2}}}{\pi\mu(\ell^2 - 2)^2 \left(|y| M_{sdc} - z M_{dc} \right)^{\frac{3}{2}}} \quad . \qquad (3.1\text{-}22)$$

The condition $\frac{z}{|y|} = \frac{M_{sdc}}{M_{dc}}$ implies that $\frac{|y|}{n} = \phi_c$, which was discussed with the expansion of u_z^6 above. The wave front expansion in (3.1-19) and the lower one in (3.1-17) give a $\pm(|t - t_{sc}|)^{-\frac{1}{2}}$ singularity (+ for $t > t_{sc}$ and - for $t < t_{sc}$) in u_z across the two-sided, conical, equivoluminal wave front. This two-sided singularity, which is not antisymmetric, exists in u_z for both transonic and supersonic load motion. As (3.1-21) shows, u_z^7, and hence u_z, are continuous through the plane head wave front.

It should be noted that the disturbance near the wave fronts trailing behind the load is a half-order stronger than near the corresponding wave fronts emanating from the initial position of the load (compare wave fronts involving the same type of disturbance). This can be seen, for example, by comparing the wave front expansions of u_z^1 as $t \to t_d$ and u_z^5 as $t \to t_{dc}$.

Horizontal Displacements, u_x and u_y:

The algebraic properties of the waves composing the horizontal displacements as given in (2.5-3) and (2.5-5) are exactly the same as those for the vertical displacement. Therefore the wave front expansions of u_x and u_y for $z > 0$ can be obtained by comparison to u_z. Without further computations, the results are stated. [In the following formulas the wave front expansions for u_x^j and u_y^j are presented in one expression with the upper character in $\{\ \}$ corresponding to u_x^j and the lower one to u_y^j.]

1) Hemispherical, Dilatational Waves, u_x^1 and u_y^1.

$$\begin{Bmatrix} u_x^1 \\ u_y^1 \end{Bmatrix} = N^1 \begin{Bmatrix} x \\ y \end{Bmatrix} \left(1 - \frac{cx}{c_d \rho}\right)^{-1} + O(t-t_d) \qquad (3.1\text{-}23)$$

as $t \to t_d$ for $t > t_d$, $z > 0$, $\left| \frac{c_d}{c} - \frac{x}{\rho} \right| > 0$, and $0 \le c < \infty$, where N^1 is given by (3.1-2).

2) Hemispherical, Equivoluminal Waves, u_x^2 and u_y^2.

$$\begin{Bmatrix} u_x^2 \\ u_y^2 \end{Bmatrix} = \begin{cases} -N_\ell^2 z \begin{Bmatrix} x \\ y \end{Bmatrix} \left(1 - \frac{cx}{c_s \rho}\right)^{-1} + O(t-t_s) & \text{for } \frac{r}{\rho} < \frac{c_s}{c_d} \\ -N_g^2 z \begin{Bmatrix} x \\ y \end{Bmatrix} \left(1 - \frac{cx}{c_s \rho}\right)^{-1} + O\left((t-t_s)^{\frac{1}{2}}\right) & \text{for } \frac{r}{\rho} > \frac{c_s}{c_d} \end{cases} \qquad (3.1\text{-}24)$$

as $t \to t_s$ for $t > t_s$, $z > 0$, $\left| \frac{c_s}{c} - \frac{x}{\rho} \right| > 0$, and $0 \le c < \infty$, where N_ℓ^2 and N_g^2 are given by (3.1-5).

3) Hemispherical, Equivoluminal Waves, u_x^3 and u_y^3.

$$\begin{Bmatrix} u_x^3 \\ u_y^3 \end{Bmatrix} = -N^3 z \begin{Bmatrix} x \\ y \end{Bmatrix} \left(1 - \frac{cx}{c_s \rho}\right)^{-1} \log\left(\frac{t}{t_s} - 1\right) + O(1) \qquad (3.1\text{-}25)$$

as $t \to t_s$ for $t > t_s$, $z > 0$, $\frac{r}{\rho} > \frac{c_s}{c_d}$, $\left|\frac{c_s}{c} - \frac{x}{\rho}\right| > 0$, and $0 \leq c < \infty$, where N^3 is given by (3.1-8a).

4) Conical Head Waves, u_x^4 and u_y^4.

$$\begin{Bmatrix} u_x^4 \\ u_y^4 \end{Bmatrix} = -N^3 z \begin{Bmatrix} x \\ y \end{Bmatrix} \left(1 - \frac{cx}{c_s \rho}\right)^{-1} \log\left(1 - \frac{t}{t_s}\right) + O(1) \qquad (3.1\text{-}26)$$

as $t \to t_s$ for $t < t_s$, $z > 0$, $\frac{r}{\rho} > \frac{c_s}{c_d}$, $\left|\frac{c_s}{c} - \frac{x}{\rho}\right| > 0$, and $0 \leq c < \infty$, where N^3 is given by (3.1-8a).

$$\begin{Bmatrix} u_x^4 \\ u_y^4 \end{Bmatrix} = N^4 \begin{Bmatrix} x \\ y \end{Bmatrix} (\ell^2 - 1)^{\frac{1}{2}} \left(1 - \frac{cx}{c_d r}\right)^{-1} (t - t_{sd}) + O\left((t - t_{sd})^2\right) \qquad (3.1\text{-}27)$$

as $t \to t_{sd}$ for $t > t_{sd}$, $\frac{z}{r} < (\ell^2 - 1)^{\frac{1}{2}}$, $\left|\frac{c_d}{c} - \frac{x}{r}\right| > 0$, and $0 \leq c < \infty$, where N^4 is given by (3.1-14).

5) Conical, Dilatational Waves, u_x^5 and u_y^5.

$$\begin{Bmatrix} u_x^5 \\ u_y^5 \end{Bmatrix} = N^5 \begin{Bmatrix} n \\ y M_{dc} \end{Bmatrix} (t - t_{dc})^{-\frac{1}{2}} + O\left((t - t_{dc})^{\frac{1}{2}}\right) \qquad (3.1\text{-}28)$$

as $t \to t_{dc}$ for $t > t_{dc}$, $n > 0$, $z > 0$, $\frac{x}{\rho} \geq \frac{c_d}{c}$, and $c > c_d$, where N^5 is given by (3.1-16).

6) Conical, Equivoluminal Waves, u_x^6 and u_y^6.

$$\begin{Bmatrix} u_x^6 \\ u_y^6 \end{Bmatrix} = \begin{cases} -zN_g^6 M_{sc} \begin{Bmatrix} n \\ yM_{sc} \end{Bmatrix} (t-t_{sc})^{-\frac{1}{2}} + O\left((t-t_{sc})^{\frac{1}{2}}\right) & \text{for } \frac{z}{n} > \frac{M_{sdc}}{M_{sc}},\ c > c_d \\ -zN_\ell^6 M_{sc} \begin{Bmatrix} n \\ yM_{sc} \end{Bmatrix} (t-t_{sc})^{-\frac{1}{2}} + O(1) & \text{for } \frac{z}{n} < \frac{M_{sdc}}{M_{sc}} \end{cases} \tag{3.1-29}$$

as $t \to t_{sc}$ for $t > t_{sc}$, $n > 0$, $z > 0$, $\frac{x}{\rho} \geq \frac{c_s}{c}$, and $c > c_s$, where N_g^6 and N_ℓ^6 are given by (3.1-18).

7) Plane Head Waves, u_x^7 and u_y^7.

$$\begin{Bmatrix} u_x^7 \\ u_y^7 \end{Bmatrix} = zN_b^7 M_{sc} \begin{Bmatrix} n \\ yM_{sc} \end{Bmatrix} (t_{sc}-t)^{-\frac{1}{2}} + O(1) \tag{3.1-30}$$

as $t \to t_{sc}$ for $t < t_{sc}$, $n > 0$, $z > 0$, $\frac{x}{\rho} \geq \frac{c_s}{c}$, $\frac{z}{n} < \frac{M_{sdc}}{M_{sc}}$, and $c > c_s$, where N_b^7 is given by (3.1-20).

$$\begin{Bmatrix} u_x^7 \\ u_y^7 \end{Bmatrix} = N_f^7 \gamma (\ell^2-1)^{\frac{1}{2}} \begin{Bmatrix} 1 \\ \operatorname{sgn}(y) M_{dc} \end{Bmatrix} (t-t_{sdc})^{\frac{1}{2}} + O\left((t-t_{sdc})^{\frac{3}{2}}\right) \tag{3.1-31}$$

as $t \to t_{sdc}$ for $t > t_{sdc}$, $n > 0$, $\frac{z}{|y|} < \frac{M_{sdc}}{M_{dc}}$, $\frac{x}{r} \geq \frac{c_d}{c}$, and $c > c_d$, where N_f^7 is given by (3.1-22)..

The behavior of u_x and u_y near the wave fronts is analogous to u_z. For a discussion of the details associated with the expansions in (3.1-23) - (3.1-31), the reader is referred to the corresponding expansions for u_z.

Stationary Point Load (c = 0):

The wave front expansions for the interior displacements due to a stationary point load with time dependence H(t) can be obtained as a special case of the results given thus far in this subsection. As expected, for $c = 0$ the wave fronts trailing behind the load and the corresponding wave front expansions do not exist. Furthermore, the expansions for the wave fronts emanating from the origin of the coordinates, which now is also the position of the load, are most efficiently written in their cylindrical components. In particular, by setting $c = 0$ in the expansions for u_x^j, u_y^j, and u_z^j, $(j = 1,\ldots,4)$, above and expressing the results in terms of the cylindrical geometry in Fig. 2 (which each wave contributing to a displacement satisfies as well as the total displacement), one finds that $u_\theta^j = 0$ at all wave fronts and

1) Hemispherical, Dilatational Waves, u_r^1 and u_z^1,

$$\begin{Bmatrix} u_r^1 \\ u_z^1 \end{Bmatrix} = N^1 \begin{Bmatrix} r \\ z \end{Bmatrix} + O(t-t_d) \tag{3.1-32}$$

as $t \to t_d$ for $t > t_d$ and $z > 0$, where N^1 is given by (3.1-2);

2) Hemispherical, Equivoluminal Waves, u_r^2 and u_z^2,

$$\begin{Bmatrix} u_r^2 \\ u_z^2 \end{Bmatrix} = \begin{cases} N_\ell^2 r \begin{Bmatrix} -z \\ r \end{Bmatrix} + O(t-t_s) & \text{for } \frac{r}{\rho} < \frac{c_s}{c_d} \\ N_g^2 r \begin{Bmatrix} -z \\ r \end{Bmatrix} + O\left((t-t_s)^{\frac{1}{2}}\right) & \text{for } \frac{r}{\rho} > \frac{c_s}{c_d} \end{cases} \tag{3.1-33}$$

as $t \to t_s$ for $t > t_s$ and $z > 0$, where N_ℓ^2 and N_g^2 are given by (3.1-5);

3) Hemispherical, Equivoluminal Waves, u_r^3 and u_z^3,

$$\begin{Bmatrix} u_r^3 \\ u_z^3 \end{Bmatrix} = N^3 r \begin{Bmatrix} -z \\ r \end{Bmatrix} \log\left(\frac{t}{t_s} - 1\right) + O(1) \tag{3.1-34}$$

as $t \to t_s$ for $t > t_s$, $z > 0$, and $\frac{r}{\rho} > \frac{c_s}{c_d}$, where N^3 is given by (3.1-8a);

4) Conical Head Waves, u_r^4 and u_z^4,

$$\begin{Bmatrix} u_r^4 \\ u_z^4 \end{Bmatrix} = N^3 r \begin{Bmatrix} -z \\ r \end{Bmatrix} \log\left(1 - \frac{t}{t_s}\right) + O(1) \tag{3.1-35}$$

as $t \to t_s$ for $t < t_s$, $z > 0$, and $\frac{r}{\rho} > \frac{c_s}{c_d}$, where N^3 is given by (3.1-8a);

$$\begin{Bmatrix} u_r^4 \\ u_z^4 \end{Bmatrix} = N^4 r \begin{Bmatrix} (\ell^2-1)^{\frac{1}{2}} \\ -1 \end{Bmatrix} (t - t_{sd}) + O\left((t-t_{sd})^2\right) \tag{3.1-36}$$

as $t \to t_{sd}$ for $t > t_{sd}$ and $\frac{z}{r} < (\ell^2-1)^{\frac{1}{2}}$, where N^4 is given by (3.1-14).

The expansions behind the dilatational wave front, the equivoluminal wave front for $\frac{r}{\rho} < \frac{c_s}{c_d}$, and the head wave front as given in (3.1-32), (3.1-33), and (3.1-36) respectively compare exactly with the corresponding results published by Knopoff and Gilbert [13]. However, the logarithmic singularity at the two-sided, equivoluminal wave front, as displayed by (3.1-34) and (3.1-35), was not detected by

these authors. This discrepancy was first pointed out by Aggarwal and Ablow [14], but by a different technique than the one employed here. The wave front expansions in (3.1-32) - (3.1-36) can also be computed from the exact displacements for $c = 0$ and $z > 0$ in section 2.7.

3.1.2. Surface of the Half-Space.

The wave front expansions for $z = 0$, not being a special case of the $z > 0$ results in subsection 3.1.1, are computed in this subsection from the surface displacements in section 2.6.

Vertical Displacement, u_z:

1) Circular, Dilational Wave, U_z^1.

The application of the transformation $k^2 = 1 + \left(\frac{t^2}{t_d^2} - 1\right)\sin^2\alpha$ to U_z^1 in (2.6-6a) gives

$$U_z^1 = \frac{\ell^2\gamma^2}{\pi^2\mu r} H(t-t_d)\left(\frac{t}{t_L} - 1\right)\left(\frac{t^2}{t_d^2} - 1\right) P\int_0^{\frac{\pi}{2}} \hat{U}{}_z^1 \, d\alpha , \qquad (3.1\text{-}37)$$

where

$$\hat{U}{}_z^1 = \left[\frac{(\ell^2 - 2k^2)^2}{\left[\gamma^2\left(\frac{t}{t_L} - 1\right)^2 + \frac{\gamma^2}{r^2}\left(\frac{t^2}{t_d^2} - k^2\right)\right] G(k^2)}\right]\Bigg|_{k^2 = 1 + \left(\frac{t^2}{t_d^2} - 1\right)\sin^2\alpha} \sin^2\alpha \, . \qquad (3.1\text{-}38)$$

Now a wave front expansion of U_z^1 can be computed by the technique used on u_z^1 in the preceding subsection. That is, by expanding $\hat{U}{}_z^1$ as $t \to t_d$ and integrating this expansion, one finds

$$U_z^1 = \frac{-\ell^2 c_d}{2\pi\mu r^2(\ell^2-2)^2}\left(1-\frac{cx}{c_d r}\right)^{-1}(t-t_d) + O\left((t-t_d)^2\right) \qquad (3.1\text{-}39)$$

as $t \to t_d$ for $t > t_d$, $\left|\frac{c_d}{c} - \frac{x}{r}\right| > 0$, and $0 \le c < \infty$. The condition $\left|\frac{c_d}{c} - \frac{x}{r}\right| > 0$ arises because $\hat{U}_z^1$ contains a singularity when $t = t_L$ and $x > 0$, which with $t = t_d$ implies that $\frac{x}{r} = \frac{c_d}{c}$. As shown in Figs. 7 and 22, this restriction is only applicable for $c > c_d$.

2) Circular, Equivoluminal Wave, U_z^2.

With the transformation $k^2 = \ell^2 + \left(\frac{t^2}{t_d^2} - \ell^2\right)\sin^2\alpha$, the wave front expansion of U_z^2 as given in (2.6-6b) is analogous to U_z^1 and the result is

$$U_z^2 = \frac{-2(\ell^2-1)c_s}{\pi\mu r^2 \ell^2}\left(1-\frac{cx}{c_s r}\right)^{-1}(t-t_s) + O\left((t-t_s)^2\right) \qquad (3.1\text{-}40)$$

as $t \to t_s$ for $t > t_s$, $\left|\frac{c_s}{c} - \frac{x}{r}\right| > 0$, and $0 \le c < \infty$. As shown in Figs. 15, 25, and 30, the restriction $\left|\frac{c_s}{c} - \frac{x}{r}\right| > 0$ is only applicable for $c > c_s$.

3) Triangular, Dilatational Wave, U_z^3.

The wave front expansion of U_z^3 as given in (2.6-8a) is just an algebraic expansion as $t \to t_{dc}$ with the result

$$U_z^3 = \frac{-(2c)^{\frac{1}{2}}\ell^2\gamma^2 M_{dc}^{\frac{1}{2}}}{\pi\mu(\ell^2-2)^2|y|^{\frac{3}{2}}}(t-t_{dc})^{\frac{1}{2}} + O\left((t-t_{dc})^{\frac{3}{2}}\right) \qquad (3.1\text{-}41)$$

as $t \to t_{dc}$ for $t > t_{dc}$, $|y| > 0$, $\frac{x}{r} \ge \frac{c_d}{c}$, and $c > c_d$. The restrictions associated with this expansion have the same physical interpretation as the corresponding ones with u_z^5 in (3.1-15).

4) Triangular, Equivoluminal Wave, U_z^4.

By expanding U_z^4 in (2.6-8b) as $t \to t_{sc}$, one finds

$$U_z^4 = \frac{-4(2c)^{\frac{1}{2}}\gamma^2(\ell^2-1)M_{sc}^{\frac{1}{2}}}{\pi\mu\ell^4|y|^{\frac{3}{2}}}(t-t_{sc})^{\frac{1}{2}} + O\left((t-t_{sc})^{\frac{3}{2}}\right) \qquad (3.1\text{-}42)$$

as $t \to t_{sc}$ for $t > t_{sc}$, $|y| > 0$, $\frac{x}{r} \geq \frac{c_s}{c}$, and $c > c_s$.

Horizontal Displacements, u_x and u_y:

Unlike the vertical displacement, on the surface of the half-space the horizontal displacements do not separate into terms which can be identified as dilatational and equivoluminal waves (even though the dilatational and equivoluminal wave fronts are still distinguishable). This is typical of two-and three-dimensional half-space problems in dynamic elasticity where the disturbance is caused by normal surface loading (see, for example, DeHoop [22] and Pekeris [3]). In addition, from (2.6-16), (2.6-18), (2.6-24), and (2.6-26) one sees that the forms of u_x and u_y do not lend themselves to asymptotic expansions near the circular, equivoluminal wave front. However, they can be expanded behind the dilatational wave fronts and ahead of the triangular, equivoluminal wave front. These expansions can be computed by the same techniques used for u_z and the results are just stated here.

1) Circular, Dilatational Wave Front.

$$\begin{Bmatrix} U_x^1 \\ U_y^1 \end{Bmatrix} = \frac{\ell^2(\ell^2-1)^{\frac{1}{2}}c_d}{\pi\mu r^3(\ell^2-2)^3}\left(1-\frac{cx}{c_d r}\right)^{-1}\begin{Bmatrix} x \\ y \end{Bmatrix}(t-t_d) + O\left((t-t_d)^2\right) \qquad (3.1\text{-}43)$$

as $t \to t_d$ for $t > t_d$, $\left|\frac{c_d}{c} - \frac{x}{r}\right| > 0$, and $0 \leq c < \infty$.

2) Triangular, Dilatational Wave Front.

$$\begin{Bmatrix} U_x^4 \\ U_y^4 \end{Bmatrix} = \frac{2(2c)^{\frac{1}{2}}\ell^2\gamma^3(\ell^2-1)^{\frac{1}{2}}M_{dc}^{\frac{1}{2}}}{\pi\mu(\ell^2-2)^3|y|^{\frac{3}{2}}} \begin{Bmatrix} 1 \\ \operatorname{sgn}(y)\, M_{dc} \end{Bmatrix} (t-t_{dc})^{\frac{1}{2}} + O\left((t-t_{dc})^{\frac{3}{2}}\right) \tag{3.1-44}$$

as $t \to t_{dc}$ for $t > t_{dc}$, $|y| > 0$, $\frac{x}{r} \geq \frac{c_d}{c}$, and $c > c_d$.

3) Triangular, Equivoluminal Wave Front.

$$\begin{Bmatrix} U_x^4 \\ U_y^4 \end{Bmatrix} = \frac{-2(2c)^{\frac{1}{2}}\gamma^3(\ell^2-1)^{\frac{1}{2}}M_{sc}^{\frac{1}{2}}}{\pi\mu\ell^4|y|^{\frac{3}{2}}} \begin{Bmatrix} 1 \\ \operatorname{sgn}(y)\, M_{sc} \end{Bmatrix} (t_{sc}-t)^{\frac{1}{2}} + O\left((t_{sc}-t)^{\frac{3}{2}}\right) \tag{3.1-45}$$

as $t \to t_{sc}$ for $t < t_{sc}$, $|y| > 0$, $\frac{x}{r} \geq \frac{c_s}{c}$, and $c > c_s$.

As expected for normal surface loading, the displacements are continuous through all the wave fronts on the surface of the half-space.

Stationary Point Load ($c = 0$):

The wave front expansions for the surface displacements due to a stationary point load with time dependence $H(t)$ are a special case of the results given thus far in this subsection. As expected for $c = 0$, the triangular wave front expansions do not exist and the circular ones are most efficiently written in their cylindrical components. By assessing (3.1-39) - (3.1-45) for $c = 0$ and using the cylindrical geometry in Fig. 2, one finds that $U_\theta^j = 0$ at all of the wave fronts and

1) Circular, Dilatational Wave, U_z^1,

$$U_z^1 = \frac{-\ell^2 c_d}{2\pi\mu r^2(\ell^2-2)^2}(t-t_d) + O\left((t-t_d)^2\right) \tag{3.1-46}$$

as $t \to t_d$ for $t > t_d$;

2) Circular, Equivoluminal Wave, U_z^2,

$$U_z^2 = \frac{-2(\ell^2-1)c_s}{\pi\mu r^2\ell^2}(t-t_s) + O\left((t-t_s)^2\right) \tag{3.1-47}$$

as $t \to t_s$ for $t > t_s$;

3) Circular, Dilatational Wave Front,

$$U_r^1 = \frac{\ell^2(\ell^2-1)^{\frac{1}{2}}c_d}{\pi\mu r^2(\ell^2-2)^3}(t-t_d) + O\left((t-t_d)^2\right) \tag{3.1-48}$$

as $t \to t_d$ for $t > t_d$.

The wave front expansions in (3.1-46) - (3.1-48) could also have been computed from the exact displacements for $c = 0$ and $z = 0$ in section 2.7.

3.2. RAYLEIGH WAVES

In section 2.6 the surface displacements were computed for $0 \leq c < \infty$, displaying singularities at the arrival time of the triangular and circular Rayleigh waves. For the horizontal displacements these waves were separate contributions to the exact solution and they do not require further investigation. However, for the vertical displace-

ment the Rayleigh singularities are embedded in the circular waves as Cauchy principal values and in the triangular waves as algebraic singularities. In this section the behavior of $u_z(\underline{X},t)$ near these singularities is determined.

The most convenient form of the circular waves for assessing the circular Rayleigh wave is obtained from U_z^1 and U_z^2 in (2.6-6) by expressing their sum as

$$U_z^1 + U_z^2 = I_z^1 + I_z^2 + I_z^3 \,. \tag{3.2-1}$$

The functions I_z^1, I_z^2, and I_z^3 take the form

$$I_z^1 = \left[H(t-t_d) - H(t-t_s)\right]\left(\frac{t}{t_L} - 1\right)\int_1^{t/t_d} \hat{I}_z \, dk \,, \tag{3.2-2a}$$

$$I_z^2 = H(t-t_s)\left(\frac{t}{t_L} - 1\right)\int_1^{\ell} \hat{I}_z \, dk \,, \tag{3.2-2b}$$

$$I_z^3 = H(t-t_s)\left(\frac{t}{t_L} - 1\right) P\int_{\ell}^{t/t_d} \hat{I}_z^3 \, dk \,, \tag{3.2-2c}$$

where

$$\hat{I}_z = \frac{\ell^2\gamma^2(k^2-1)^{\frac{1}{2}}(\ell^2-2k^2)^2 k}{\pi^2\mu r\left[\gamma^2\left(\frac{t}{t_L}-1\right)^2 + \frac{\gamma^2}{r^2}\left(\frac{t^2}{t_d^2}-k^2\right)\right]\left(\frac{t^2}{t_d^2}-k^2\right)^{\frac{1}{2}} G(k^2)} \,, \tag{3.2-3a}$$

$$\hat{I}_z^3 = \frac{\ell^2\gamma^2(k^2-1)^{\frac{1}{2}} k}{\pi^2\mu r\left[\gamma^2\left(\frac{t}{t_L}-1\right)^2 + \frac{\gamma^2}{r^2}\left(\frac{t^2}{t_d^2}-k^2\right)\right]\left(\frac{t^2}{t_d^2}-k^2\right)^{\frac{1}{2}} R(k^2)} \,, \tag{3.2-3b}$$

with $G(k^2)$ given in (2.6-7) and

$$R(k^2) = (\ell^2-2k^2)^2 - 4(k^2-1)^{\frac{1}{2}}(k^2-\ell^2)^{\frac{1}{2}}k^2 \quad . \qquad (3.2\text{-}4)$$

In this form the Rayleigh singularity only appears in I_z^3. In particular, $\hat{I}_z^3$ contains a simple pole at $k = \gamma_R$ for $t \geq t_R$. However, all three integrands in (3.2-2) contain a non-integrable singularity at $k = t/t_d$ for $t = t_L$ if $x > 0$.

To assess I_z^3 near $t = t_R$, the arrival time of the circular Rayleigh wave, equation (3.2-2c) is written with $t = t_R + \Delta t_d = t_d(\gamma_R + \Delta)$ as

$$I_z^3 = \left(\frac{cx}{c_R r} + \frac{\Delta cx}{c_d r} - 1\right) P \int_{\ell}^{\gamma_R+\Delta} \hat{I}_z^3 \Big|_{t = t_R+\Delta t_d} dk \quad . \qquad (3.2\text{-}5)$$

If one assumes that $|\Delta| \ll 1$, where Δ is either positive or negative, then the Rayleigh pole, which is the zero of $R(k^2)$ at $k = \gamma_R$, always lies near the upper limit of the integral in (3.2-5). When assessing the contribution of this pole one must also consider the singularity at $k = t/t_d$ for $t = t_L$ if $x > 0$. In particular, for $c > c_R$ the contours $t = t_L$ and $t = t_R$ coincide along the rays $\frac{x}{r} = \frac{c_R}{c}$ at the intersection of the triangular and circular Rayleigh waves. These rays are shown in Fig. 34 as dashed lines and they are excluded in the following computation. However, for $c < c_R$, $t = t_L$ and $t = t_R$ do not coincide, as shown in Fig. 34, and the singularity at $k = t/t_d$ for $t = t_L$ does not enter into the Rayleigh wave expansion.

Then, by "piecing off" the upper limit of the integral in (3.2-5),

one finds

$$I_z^3 = \left(\frac{cx}{c_R r} + \frac{\Delta cx}{c_d r} - 1\right)\left[\int_{\ell}^{\beta} + P\int_{\beta}^{\gamma_R+\Delta}\right] \hat{I}_z^3 \Big|_{t = t_R + \Delta t_d} dk\,, \qquad (3.2\text{-}6)$$

where $\gamma_R+\Delta-\beta$ is an arbitrarily small, positive number. The first integral in (3.2-6) is $O(1)$ as $|\Delta| \to 0$. By expanding the integrand of the second integral about $k = \gamma_R$ and using the Taylor series expansion

$$R(k^2) = -2\gamma_R^2 \Psi (k^2-\gamma_R^2)[1 + O(k^2-\gamma_R^2)], \qquad (3.2\text{-}7)$$

where

$$\Psi = 2\left(\frac{c_R^2}{c_s^2} - 2\right) + \left(1 - \frac{c_R^2}{c_s^2}\right)^{\frac{1}{2}}\left(1 - \frac{c_R^2}{c_d^2}\right)^{-\frac{1}{2}} + \left(1 - \frac{c_R^2}{c_d^2}\right)^{\frac{1}{2}}\left(1 - \frac{c_R^2}{c_s^2}\right)^{-\frac{1}{2}} + 2\left(1 - \frac{c_R^2}{c_s^2}\right)^{\frac{1}{2}}\left(1 - \frac{c_R^2}{c_d^2}\right)^{\frac{1}{2}}, \qquad (3.2\text{-}8)$$

one finds

$$I_z^3 = \frac{\ell^2(\gamma_R^2-1)^{\frac{1}{2}}}{2\pi^2 \mu r \gamma_R \Psi}\left(1 - \frac{cx}{c_R r}\right)^{-1}[1+O(\Delta)]\, P\int_{\beta}^{\gamma_R+\Delta} \frac{dk}{(k^2-\gamma_R^2)[(\gamma_R+\Delta)^2-k^2]^{\frac{1}{2}}} + O(1) \qquad (3.2\text{-}9)$$

as $|\Delta| \to 0$. The transformation $k = (\gamma_R+\Delta)\alpha$ reduces the integral in (3.2-9) to

$$P\int_{\beta(\gamma_R+\Delta)^{-1}}^{1} \frac{d\alpha}{[(\gamma_R+\Delta)^2\alpha^2 - \gamma_R^2](1-\alpha^2)^{\frac{1}{2}}} = P\int_0^1 \frac{d\alpha}{[(\gamma_R+\Delta)^2\alpha^2 - \gamma_R^2](1-\alpha^2)^{\frac{1}{2}}} + O(1) \qquad (3.2\text{-}10)$$

as $|\Delta| \to 0$. The definite integral in (3.2-10) is a special case of

$$P\int_0^1 \frac{d\alpha}{(A^2-\alpha^2)(1-\alpha^2)^{\frac{1}{2}}} = \begin{cases} 0 & \text{for } A^2 < 1 \\ \dfrac{\pi}{2(A^2-1)^{\frac{1}{2}}} & \text{for } A^2 > 1 \end{cases}, \qquad (3.2\text{-}11)$$

which is tabulated in reference [26] (table 12, formula (1)). Then, by combining (3.2-10) and (3.2-11) with $A^2 = \gamma_R^2(\gamma_R+\Delta)^{-2}$ and substituting the result into (3.2-9) with $\Delta = (t-t_R)/t_d$, one finds

$$I_z^3 = \begin{cases} O(1) & \text{for } t > t_R \\ \dfrac{-\ell^2(\gamma_R^2-1)^{\frac{1}{2}}}{4\sqrt{2}\,\pi\mu r\gamma_R^3\Psi}\left(1-\dfrac{cx}{c_R r}\right)^{-1}\left(1-\dfrac{t}{t_R}\right)^{-\frac{1}{2}}+O(1) & \text{for } t < t_R \end{cases} \tag{3.2-12}$$

as $t \to t_R$ for $\left|\dfrac{c_R}{c}-\dfrac{x}{r}\right| > 0$ and $0 \le c < \infty$. I_z^3 dominates the behavior of $u_z(\underline{X},t)$ as $t \to t_R$ and it displays the one-sided, $(t_R-t)^{-\frac{1}{2}}$ singularity which is typical of the surface displacements in three-dimensional problems (see, for example, Pekeris [3] where the surface displacements produced by a stationary point load are computed).

To assess the triangular Rayleigh wave it is convenient to write U_z^3 and U_z^4 in (2.6-8) as

$$U_z^3 + U_z^4 = I_z^4 + I_z^5 , \tag{3.2-13}$$

where

$$I_z^4 = \frac{-(c^2y^2/\pi c_s^2\mu)\alpha_d[(M_{sc}^2-1)y^2-2\xi^2]^2}{[(M_{sc}^2-1)y^2-2\xi^2]^4-16\alpha_d^2\alpha_s^2(\xi^2+y^2)^2}\left[H(t-t_{dc})-H(t-t_{sc})\right]H(t-t_L)H(x) , \tag{3.2-14a}$$

$$I_z^5 = \frac{-(c^2y^2/\pi c_s^2\mu)\alpha_d}{[(M_{sc}^2-1)y^2-2\xi^2]^2-4\alpha_d\alpha_s(\xi^2+y^2)}H(t-t_{sc})H(t-t_L)H(x) , \tag{3.2-14b}$$

and M_{sc} is given in (3.1-16a). In this form only I_z^5 is singular at the arrival time of the triangular Rayleigh wave. The expansion of

I_z^5 as $t \to t_{Rc}$ is an algebraic computation which depends primarily on the auxiliary result

$$[(M_{sc}^2 - 1)y^2 - 2\xi^2]^2 - 4\alpha_d\alpha_s(\xi^2 + y^2)$$

$$= -4\left(\frac{c^2}{c_R^2} - 1\right)^{\frac{1}{2}} |y|^3 \frac{c^2}{c_R^2}\Psi\, c(t-t_{Rc})[1 + O(t-t_{Rc})] \qquad (3.2\text{-}15)$$

as $t \to t_{Rc}$ for $|y| > 0$ and $c > c_R$, and it is

$$I_z^5 = \frac{\ell(\gamma_R^2 - 1)^{\frac{1}{2}}}{4\pi c_s \mu \gamma_R^2 \Psi}\left(\frac{c^2}{c_R^2} - 1\right)^{-\frac{1}{2}}(t-t_{Rc})^{-1} + O(1) \qquad (3.2\text{-}16)$$

as $t \to t_{Rc}$ for $\frac{x}{r} \geq \frac{c_R}{c}$, $|y| > 0$, and $c > c_R$. The constant Ψ is given in (3.2-8). The restrictions following this expansion are similar to those following the wave front expansion of u_z^5 in subsection 3.1.1 and they are discussed there. I_z^5 dominates the behavior of $u_z(\underline{X},t)$ as $t \to t_{Rc}$ and it has the two-sided, $(t-t_{Rc})^{-1}$ singularity which is typical of the vertical displacement in two-dimensional problems (see, for example, DeHoop [22] where the surface displacements produced by a line load are computed). Furthermore, the strength of the singularity in I_z^5 increases as c approaches c_R. However, as $c \to c_R$ the domain of the surface of the half-space where I_z^5 is pertinent shrinks to the position of the load and the circular Rayleigh wave. Therefore $u_z(\underline{X},t)$ remains bounded for $c = c_R$, except in the neighborhood of the load and the circular Rayleigh wave where the solution is unbounded for all c. This type of behavior was also observed for $u_x(\underline{X},t)$ in section 2.6.

The Rayleigh wave evaluation appropriate to the vertical displacement for a stationary point load with time dependence H(t) can be obtained as a special case of the results given above. That is, by evaluating (3.2-12) and (3.2-16) for $c = 0$, one finds that only the circular Rayleigh wave remains and it becomes

$$I_z^3 = \begin{cases} O(1) & \text{for } t > t_R \\ \dfrac{-\ell^2(\gamma_R^2-1)^{\frac{1}{2}}}{4\sqrt{2}\,\pi\mu r\gamma_R^3\Psi}\left(1-\dfrac{t}{t_R}\right)^{-\frac{1}{2}} + O(1) & \text{for } t < t_R \end{cases} \tag{3.2-17}$$

as $t \to t_R$. For $\lambda = \mu$ the result in (3.2-17) compares exactly with the corresponding one given by Pekeris [3] (see equation (47) of this reference). Also, the Rayleigh wave expansion in (3.2-17) can be computed from the exact vertical displacement for $c = 0$ and $z = 0$ in section 2.7.

3.3. CONTINUITY OF THE DISPLACEMENTS

In constructing the solution in Chapter 2, $t = t_L$ and $t = t_E$ arose as surfaces, for fixed time and $x > 0$, on which different contributions of the displacements have singularities. In particular, the waves emanating from the initial position of the load contain improper integrals and the disturbances trailing behind the load have algebraic discontinuities on these surfaces. Although each displacement is expected to be continuous over them, a general verification

of this continuity property is a very tedious computation and it is not undertaken in this investigation. However, this computation is much simpler for the surface of the half-space and it is outlined in subsection 3.3.1. It should be noted that the technique used there is applicable to the more general case.

In addition, in the plane under the path of the load a region arises for transonic and subsonic load motion where the continuity of the solution must also be investigated. The region in question is portrayed in Figs. 27 and 32 as the thatched area and a detailed analysis of the displacements for this region is given in subsection 3.3.2.

3.3.1. On the Surface of the Half-Space.

To verify that $u_z(\underline{X},t)$ as given in section 2.6 is continuous over $t = t_L$, it is necessary to show that the discontinuities generated by the improper integrals in U_z^1 and U_z^2 for $t = t_L$ properly coincide with the algebraic discontinuities in U_z^3 and U_z^4 for the same time. In particular, considering first the dilatational contributions to $u_z(\underline{X},t)$, U_z^1 will be evaluated for $t \to t_L$ and the result combined with U_z^3 assessed for $t \to t_L$, showing that $U_z^1 + U_z^3$ is continuous over $t = t_L$. Then, in a similar way, the equivoluminal contributions to $u_z(\underline{X},t)$ will be shown to be continuous over $t = t_L$.

By inspection of (2.6-2a) one sees that for t near t_L the major contribution of the integral in U_z^1 comes from the lower limit and it can be assessed by the technique used in subsection 3.1.1 for

the improper integral in u_z^3 and in section 3.2 for the one in I_z^3. That is, by piecing off the lower limit of the integral in (2.6-2a) and expanding the integrand for small w and t near t_L, one finds

$$U_z^1 = \frac{2}{\pi} N_d \int_0^{\epsilon} \frac{a\, dw}{w^2 + a^2} + O(t-t_L) \qquad (3.3\text{-}1)$$

as $t \to t_L$ for $\frac{c_d}{c} > \frac{x}{r}$, $\left|\frac{x}{r} - \frac{c_R}{c}\right| > 0$, $x > 0$, $|y| > 0$, and $0 < c < \infty$, where $a = \frac{r\gamma}{|y|}\left(\frac{t}{t_L} - 1\right)$ and

$$N_d = \frac{(\ell^2 \gamma x^3 / 2\pi\mu |y|)(\gamma^2 r^2 - x^2)^{\frac{1}{2}} (\ell^2 x^2 - 2\gamma^2 r^2)^2}{(\ell^2 x^2 - 2\gamma^2 r^2)^4 - 16\gamma^4 r^4 (\gamma^2 r^2 - x^2)(\gamma^2 r^2 - \ell^2 x^2)} \,. \qquad (3.3\text{-}2)$$

The integral in (3.3-1) takes the form

$$\int_0^{\epsilon} \frac{a\, dw}{w^2 + a^2} = \int_0^{\infty} \frac{a\, dw}{w^2 + a^2} + O(a) = \frac{\pi}{2} \operatorname{sgn}(a) + O(a) \,, \qquad (3.3\text{-}3)$$

where the definite integral is tabulated in reference [25] (p. 281, formula 404) and sgn (~) is defined in (2.5-8). Then the substitution of (3.3-3) into (3.3-1) with $a = \frac{r\gamma}{|y|}\left(\frac{t}{t_L} - 1\right)$ gives

$$U_z^1 = N_d \operatorname{sgn}(t-t_L) + O(t-t_L) \qquad (3.3\text{-}4)$$

as $t \to t_L$ for $\frac{c_d}{c} > \frac{x}{r}$, $\left|\frac{x}{r} - \frac{c_R}{c}\right| > 0$, $x > 0$, $|y| > 0$, and $0 < c < \infty$. The restrictions following (3.3-4) arise naturally in the computation. The condition $\frac{c_d}{c} > \frac{x}{r}$ is vacuous if $c < c_d$ and, if $c > c_d$, it implies that (3.3-4) is not valid across the intersection of the triangular and circular, dilatational wave fronts. Similarly, the condition $\left|\frac{x}{r} - \frac{c_R}{c}\right| > 0$, which is vacuous if $c < c_R$, implies that this expansion

is not valid through the intersection of the triangular and circular Rayleigh waves. The rays defined by $\frac{x}{r} = \frac{c_d}{c}$ and $\frac{x}{r} = \frac{c_R}{c}$ are shown in Fig. 34. Furthermore, the condition $|y| > 0$, which is only applicable if $c < c_d$, implies that this expansion is not valid at the position of the load which lies on $t = t_L$ for $c < c_d$. Finally, this expansion is valid for all values of the load speed which are greater than zero, even though the relative position of the contour $t = t_L$ varies with different intervals of c as shown in Fig. 34.

The expansion of U_z^3 as $t \to t_L$ is an algebraic computation from equation (2.6-8a) and it is

$$U_z^3 = -2N_d + O(t-t_L) \tag{3.3-5}$$

as $t \to t_L$ for $t > t_L$, $\frac{c_d}{c} > \frac{x}{r}$, $\left|\frac{x}{r} - \frac{c_R}{c}\right| > 0$, $x > 0$, $|y| > 0$, and $0 < c < \infty$, where N_d is given in (3.3-2). Then the summation of U_z^1 and U_z^3 as given in (3.3-4) and (3.3-5) yields

$$U_z^1 + U_z^3 = -N_d + O(t-t_L) \tag{3.3-6}$$

as $t \to t_L$ for $t > t_L$ and $t < t_L$; $\frac{c_d}{c} > \frac{x}{r}$, $\left|\frac{x}{r} - \frac{c_R}{c}\right| > 0$, $x > 0$, $|y| > 0$, and $0 < c < \infty$. As this equation shows, $U_z^1 + U_z^3$ approaches the same limit as $t \to t_L$ for $t > t_L$ and $t < t_L$. Therefore the sum of the dilatational contributions to $u_z(\underline{X},t)$ is continuous over $t = t_L$.

By an analogous computation from (2.6-2b) and (2.6-8b), one can show that

$$U_z^2 + U_z^4 = -N_s + O(t-t_L) \qquad (3.3\text{-}7)$$

as $t \to t_L$ for $t > t_L$ and $t < t_L$; $\frac{c_s}{c} > \frac{x}{r}$, $\left|\frac{x}{r} - \frac{c_R}{c}\right| > 0$, $x > 0$, $|y| > 0$, and $0 < c < \infty$, where

$$N_s = \frac{(2\ell^2\gamma^3x^3r^2/\pi\mu|y|)(\gamma^2r^2-\ell^2x^2)^{\frac{1}{2}}(\gamma^2r^2-x^2)}{(\ell^2x^2-2\gamma^2r^2)^4 - 16\gamma^4r^4(\gamma^2r^2-x^2)(\gamma^2r^2-\ell^2x^2)} . \qquad (3.3\text{-}8)$$

Equation (3.3-7) shows that the sum of the equivoluminal contributions to $u_z(\underline{X},t)$ is continuous over $t = t_L$. Consequently, since both the dilatational and equivoluminal contributions to $u_z(\underline{X},t)$ are continuous over $t = t_L$, so is $u_z(\underline{X}, t)$ itself.

In a similar way, $u_x(\underline{X},t)$ and $u_y(\underline{X},t)$ can be shown to be continuous over $t = t_L$, but no supporting computations will be given.

3.3.2. Through the Plane Under the Path of the Load.

As was shown in subsections 2.4.3 and 2.4.4 for transonic and subsonic load motion, singularities arise in different contributions to the displacements as $|\theta| \to 0$ which are peculiar to the plane under the path of the load. Although physically the solution is expected to vary continuously as $|\theta| \to 0$, it remains to verify this property. As an example, u_y for subsonic load motion is assessed in this subsection for $|\theta| \to 0$, showing that $u_y \to 0$ and therefore that u_y varies continuously through the $\theta = 0$ plane.

The waves emanating from the initial position of the load that contribute to u_y are given in (2.5-2) for $\sigma = y$. When expanding these waves as $|\theta| \to 0$, one must investigate the integrands in

(2.5-2) noting, in particular, the singularities that arise for $\theta = 0$ (see (2.4-82) and the text following (2.5-2) for details concerning these singularities). Then it follows easily that u_y^1, u_y^2, and u_y^4 are $O(\theta)$ as $|\theta| \to 0$. However, the integrand in u_y^3 has an indeterminant form $(\frac{0}{0})$ for $\theta = 0$ if $t_L < t < t_{sdc}^o$ and $w = \frac{\gamma}{z}\alpha_s$. To evaluate u_y^3 as $|\theta| \to 0$ for $t_L < t < t_{sdc}^o$, the integral in u_y^3 must first be assessed for small θ, but with $|\theta| > 0$. Then the limit as $|\theta| \to 0$ is taken. The critical region of the $\theta = 0$ plane where u_y^3 requires this special consideration is shown in Fig. 32 as the thatched area. Outside the thatched area, u_y^3 is $O(\theta)$ as $|\theta| \to 0$.

Then, to actually assess u_y^3 as $|\theta| \to 0$ for $t_L < t < t_{sdc}^o$, equation (2.5-2c) is written as

$$u_y^3 = \left[\int_{T_s}^{\frac{\gamma}{z}\alpha_s - \epsilon} + \int_{\frac{\gamma}{z}\alpha_s - \epsilon}^{\frac{\gamma}{z}\alpha_s + \epsilon} + \int_{\frac{\gamma}{z}\alpha_s + \epsilon}^{T_{sd}} \right] \mathrm{Re}\left[K_{ys}(q_{sd}, w, \theta) \frac{dq_{sd}}{dt} \right] dw, \qquad (3.3\text{-}9)$$

where ϵ is an arbitrarily small positive number. The first and third integrals in (3.3-9) are $O(\theta)$ as $|\theta| \to 0$. When the integrand of the second term is expanded about $w = \frac{\gamma}{z}\alpha_s$ by using the transformation $w = \frac{\gamma}{z}\alpha_s + \beta$, one finds

$$u_y^3 = \frac{1}{\pi} N_o \int_{-\epsilon}^{\epsilon} \frac{a\, d\beta}{\beta^2 + a^2} + O(\theta) \qquad (3.3\text{-}10)$$

as $|\theta| \to 0$ for $t_L < t < t_{sdc}^o$ and $z > 0$, where $a = \gamma c z^{-2} x (t - t_L) \sin\theta$ and

$$N_o = \frac{(2\xi^2/\pi\mu)(z^2M_{sdc}^2 - \xi^2)^{\frac{1}{2}}[(M_{sc}^2-1)z^2 + 2\alpha_s^2]^2}{[(M_{sc}^2-1)z^2 + 2\alpha_s^2]^4 + 16(z^2M_{sdc}^2 - \xi^2)\xi^2(\alpha_s^2 - z^2)^2} \quad . \qquad (3.3\text{-}11)$$

Then the substitution of the auxiliary result

$$\int_{-\epsilon}^{\epsilon} \frac{a\, d\beta}{\beta^2 + a^2} = 2\int_{0}^{\epsilon} \frac{a\, d\beta}{\beta^2 + a^2} = \pi\, \mathrm{sgn}\,(a) + O(a)\,, \qquad (3.3\text{-}12)$$

which follows from (3.3-3), into (3.3-10) with $a = \gamma c z^{-2} x(t-t_L)\sin\theta$ yields

$$u_y^3 = N_o\, \mathrm{sgn}\,(\theta) + O(\theta) \qquad (3.3\text{-}13)$$

as $|\theta| \to 0$ for $t_L < t < t_{sdc}^o$ and $z > 0$.

The disturbances trailing behind the load that contribute to u_y are given in (2.5-5) for $\sigma = y$ with (2.5-7). When they are expanded for small y one finds

$$\left.\begin{aligned} u_y^5 &= O(y) \\ u_y^6 &= -N_o\, \mathrm{sgn}\,(y)\left[H(t-t_L) - H(t-t_{sdc}^o)\right] + O(y) \end{aligned}\right\} \qquad (3.3\text{-}14)$$

as $|y| \to 0$ for $x > 0$ and $z > 0$, where N_o is given in (3.3-11). The contribution u_y^7 is identically zero for $c < c_s$, regardless of the value of y. As (3.3-14) shows, u_y^6 does not vanish as $|y| \to 0$ for $x > 0$ and $t_L < t < t_{sdc}^o$, which is the thatched region in Fig. 32.

By comparing (3.3-13) and (3.3-14) one sees that the non-vanishing terms in u_y^3 and u_y^6 are of opposite sign and they exist

in the same region of the $\theta = 0$ plane. Therefore, by using (2.5-1) for $\sigma = y$ and the results given above for u_y^j, in particular (3.3-13) and (3.3-14), one concludes that $u_y = O(\theta)$ as $|\theta| \to 0$ for $z > 0$. Consequently, u_y varies continuously through the $\theta = 0$ plane and vanishes in the plane.

In a similar way, u_y for transonic load motion and u_x and u_z for transonic and subsonic load motion can be shown to vary continuously through the $\theta = 0$ plane. However, no supporting computations will be given.

3.4. STEADY-STATE DISPLACEMENTS FOR SUPERSONIC LOAD MOTION

As noted in Chapter 2 for the interior and surface solutions, the disturbances trailing behind the load represent steady-state contributions to the displacements. For $c > c_d$ the load "runs away" from the waves emanating from the initial position of the load. That is, for long time these waves do not contribute to the displacements at points which are a finite distance from the position of the load. Therefore the disturbances trailing behind the load represent the entire steady-state solution for $c > c_d$. By the same type of reasoning one concludes that for $c < c_d$ these disturbances do not represent the entire steady-state solution (assuming that the magnitude of the waves emanating from the initial position of the load does not go to zero for long time).

Mathematically, to go from a transient expression which is a function of (x,y,z,t) to the corresponding steady-state term, one

substitutes $x = ct - \xi$ (where ξ is the distance from the position of the load along the x-axis as shown in Fig. 2) into the transient expression and then lets t tend to infinity. In the limit as $t \to \infty$ one assumes that $\frac{\xi}{ct}$, $\frac{y}{ct}$, and $\frac{z}{ct}$ go to zero. This leaves the resulting expression as a function of coordinate points (ξ,y,z) which are a finite distance from the position of the load.

By applying either this mathematical technique or the intuitive argument above to the displacements as given in subsection 2.4.5 and section 2.5, one finds the steady-state displacements for $z > 0$ and $c > c_d$ to be

$$u_m(\xi,y,z) = \hat{u}_m^5 H(\xi - nM_{dc}) + \hat{u}_m^6 H(\xi - nM_{sc})$$

$$+ \hat{u}_m^7 H\left(\frac{|y|}{n} - \phi_c\right)\left[H(\xi - zM_{sdc} - |y|M_{sc}) - H(\xi - nM_{sc})\right], \quad (3.4\text{-}1)$$

where M_{dc}, M_{sc}, and M_{sdc} are given in (3.1-16a). In this equation ($m = x,y,z$) and the hat functions, which have an algebraic form, are given for $m = x$ in (2.5-6), $m = y$ in (2.5-7), and $m = z$ in (2.4-97). The first term in (3.4-1) represents the conical, dilatational wave; the second the conical, equivoluminal wave; and the last the plane head wave. These waves are shown in Fig. 36. The steady-state displacements for $z > 0$ and $c > c_d$ were also computed by Lansing [2] by a technique which assumed steady-stateness at the outset, but he only reduced them to single integrals. As a special case, in the plane under the path of the load (the $y = 0$ plane) and for $\lambda = \mu$ Lansing integrated his results, leaving the displacements in an algebraic form which agrees in detail with (3.4-1) assessed for $y = 0$

and $\lambda = \mu$ (see equations (59) and (60) of reference [2]). It should be noted that the remaining references mentioned in Chapter 1 with regard to steady-state solutions of the moving load problem do not contain exact results for the case of supersonic load motion. Instead, they include special cases which are not considered here.

To obtain the steady-state, surface displacements for $c > c_d$, one applies either the mathematical technique or the intuitive argument given above to the surface results in section 2.6. Again, only the disturbances trailing behind the load, which for $z = 0$ are the triangular waves, remain and the displacements become

$$\begin{Bmatrix} u_x(\xi,y,0) \\ u_y(\xi,y,0) \end{Bmatrix} = \frac{(2c^2y^2/\pi c_s^2\mu)[(M_{sc}^2-1)y^2-2\xi^2]\alpha_d\alpha_{sd}}{[(M_{sc}^2-1)y^2-2\xi^2]^4-16\alpha_d^2\alpha_s^2(\xi^2+y^2)^2} \begin{Bmatrix} |y| \\ \xi\,\mathrm{sgn}(y) \end{Bmatrix}$$

$$\cdot\left[H(\xi-|y|M_{dc})-H(\xi-|y|M_{sc})\right]+\frac{\Phi}{4c\mu}\begin{Bmatrix} M_{Rc}^{-1} \\ \mathrm{sgn}(y) \end{Bmatrix}\delta(\xi-|y|M_{Rc}) \tag{3.4-2a}$$

$$u_z(\xi,y,0) = \frac{-(c^2y^2/\pi c_s^2\mu)\alpha_d}{[(M_{sc}^2-1)y^2-2\xi^2]^4-16\alpha_d^2\alpha_s^2(\xi^2+y^2)^2}$$

$$\cdot\left\{[(M_{sc}^2-1)y^2-2\xi^2]^2H(\xi-|y|M_{dc})+4\alpha_d\alpha_s(\xi^2+y^2)H(\xi-|y|M_{sc})\right\}, \tag{3.4-2b}$$

where $M_{Rc} = \left(\frac{c^2}{c_R^2}-1\right)^{\frac{1}{2}}$ and the remaining notation is defined in section 2.6 and (3.1-16a). Both terms in (3.4-2b) are singular at $\xi = |y|M_{Rc}$, which corresponds to the arrival time of the triangular

Rayleigh wave. The behavior of $u_z(\xi,y,0)$ near $\xi = |y|M_{Rc}$ follows from (3.2-16) and it is

$$u_z(\xi,y,0) = \frac{\ell c(\gamma_R^2-1)^{\frac{1}{2}}}{4\pi\mu c_s \gamma_R^2 \Psi M_{Rc}} (\xi - |y|M_{Rc})^{-1} + O(1) \qquad (3.4\text{-}3)$$

as $\xi \to |y|M_{Rc}$ for $|y| > 0$.

When the horizontal displacements in (3.4-2a) are expressed in the polar geometry shown at the bottom of Fig. 36, they simplify to

$$u_{\bar{r}}(\bar{r},\phi,0) = 0 \qquad (3.4\text{-}4a)$$

$$u_\phi(\bar{r},\phi,0) = \frac{\frac{-2c^2\sin^2\phi}{\pi c_s^2 \mu \bar{r}} \left(\frac{c^2}{c_s^2}\sin^2\phi - 1\right)^{\frac{1}{2}} \left(1 - \frac{c^2}{c_d^2}\sin^2\phi\right)^{\frac{1}{2}} \left(\frac{c^2}{c_s^2}\sin^2\phi - 2\right)}{\left(\frac{c^2}{c_s^2}\sin^2\phi - 2\right)^4 - 16\left(1 - \frac{c^2}{c_d^2}\sin^2\phi\right)\left(1 - \frac{c^2}{c_s^2}\sin^2\phi\right)}$$

$$\cdot \operatorname{sgn}(\phi) H(-\cos\phi)\left[H\left(\frac{c_d}{c} - |\sin\phi|\right) - H\left(\frac{c_s}{c} - |\sin\phi|\right)\right]$$

$$- \frac{\Phi}{4c_R \mu M_{Rc}} \operatorname{sgn}(\phi) H(-\cos\phi)\delta\left(\frac{c_R}{c} - |\sin\phi|\right) . \qquad (3.4\text{-}4b)$$

In this form $u_{\bar{r}} = 0$, which implies that all the "in surface plane" particle motion is normal to the triangular wave fronts. For $\lambda = \mu$ the displacements in (3.4-2b) (expressed in terms of the polar coordinates in Fig. 36) and those in (3.4-4) compare exactly with the ones given by Lansing [2] (see equations (57) and (58) of this reference), except that he omitted the Rayleigh wave contribution to u_ϕ.

The wave front expansions appropriate to the steady-state

displacements given in this section can be obtained from the results in section 3.1 by using the techniques mentioned at the outset of this section. However, these expansions will not be displayed here.

BIBLIOGRAPHY

1. Payton, R. G., "An Application of the Dynamic Betti-Rayleigh Reciprocal Theorem to Moving-Point Loads in Elastic Media," Quart. Appl. Math., Vol. 21, 1964, pp. 299-313.

2. Lansing, D. L., "The Displacements in an Elastic Half-Space Due to a Moving Concentrated Normal Load," NASA Technical Report, NASA TR R-238, 1966.

3. Pekeris, C. L., "The Seismic Surface Pulse," Proc. Nat. Acad. Sci., Vol. 14, 1955, pp. 469-480.

4. Mandel, J. and Avramesco, A., "Déplacements Produits par une Charge Mobile à la Surface d'un Semi-Espace Elastique," Compt. Rend. Acad. Sci., Paris, Vol. 252, pt. 3, 1961, pp. 3730-3735.

5. Papadopoulos, M., "The Elastodynamics of Moving Loads," J. Austral. Math. Soc., Vol. 3, 1963, pp. 79-92.

6. Grimes, C. K., "Studies on the Propagation of Elastic Waves in Solid Media," Doctoral Dissertation, California Institute of Technology, Pasadena, California, 1964.

7. Eason, G., "The Stresses Produced in a Semi-Infinite Solid by a Moving Surface Force," Int. J. Engng. Sci., Vol. 2, 1965, pp. 581-609.

8. Chao, C. C., "Dynamic Response of an Elastic Half-Space to Tangential Surface Loadings," J. Appl. Mech., Vol. 27, 1960, pp. 559-567.

9. Cagniard, L., Reflection and Refraction of Progressive Seismic Waves, Translated by E. A. Flinn and C. H. Dix, McGraw-Hill Book Co., New York, 1962.

10. DeHoop, A. T., "A Modification of Cagniard's Method for Solving Seismic Pulse Problems," Appl. Sci. Res., Section B, Vol. 8, 1959, pp. 349-356.

11. Mitra, M., "Disturbance Produced in an Elastic Half-Space by Impulsive Normal Pressure," Proc. Camb. Phil. Soc., Vol. 60, 1964, pp. 683-696.

12. Eason, G., "The Displacements Produced in an Elastic Half-Space by a Suddenly Applied Surface Force," J. Inst. Maths. Applics., Vol. 2, 1966, pp. 299-326.

13. Knopoff, L. and Gilbert, F., "First Motion Methods in Theoretical Seismology," J. Acoust. Soc. Amer. Vol. 31, 1959, pp. 1161-1168.

14. Aggarwal, H. R. and Ablow, C. M., "Solution to a Class of Three-Dimensional Pulse Propagation Problems in an Elastic Half-Space," Int. J. Engng Sci., Vol. 5, 1967, pp. 663-679.

15. Lamb, H., "On the Propagation of Tremors Over the Surface on an Elastic Solid," Phil. Trans. Roy. Soc. Lond. (A), Vol. 203, 1904, pp. 1-42.

16. Lang, H. A., "The Complete Solution for an Elastic Half-Space Under a Point Step Load," Rep. No. P-1141, Rand Corp., Santa Monica, California, 1957.

17. Lang, H. A., "Surface Displacements in an Elastic Half-Space," ZAMM, Vol. 41, 1961, pp. 141-153.

18. Craggs, J. W., "On Axially Symmetric Waves, III. Elastic Waves in a Half-Space," Proc. Cambridge Philos. Soc., Vol. 59, 1963, pp. 803-809.

19. Sternberg, E., "On the Integration of the Equations of Motion in the Classical Theory of Elasticity," Arch. Rat. Mech. Anal., Vol. 6, 1960, pp. 34-60.

20. Sneddon, I. N., Fourier Transforms, Mc Graw-Hill Book Co., New York, 1951.

21. Carslaw, H. S. and Jaeger, J. C., Operational Methods in Applied Mathematics, Oxford University Press, 1941.

22. DeHoop, A. T., "The Surface Line Source Problem," Second Annual Report, Seismic Scattering Project, Inst. Geophysics, Univ. of Calif., Los Angeles, California, 1957.

23. Copson, E. T., An Introduction to the Theory of Functions of a Complex Variable, Oxford at the Clarendon Press, 1962.

24. Jeffreys, H. and Jeffreys, B. S., Methods of Mathematical Physics, Cambridge at the University Press, 1956.

25. Hodgman, C. D., editor, Mathematical Tables from Handbook of Chemistry and Physics, Eleventh Edition, Chemical Rubber Publishing Co., Ohio, 1960.

26. DeHaan, D. B., Nouvelles Tables D'Intégrales Définies, Hafner Publishing Co., New York, 1957.

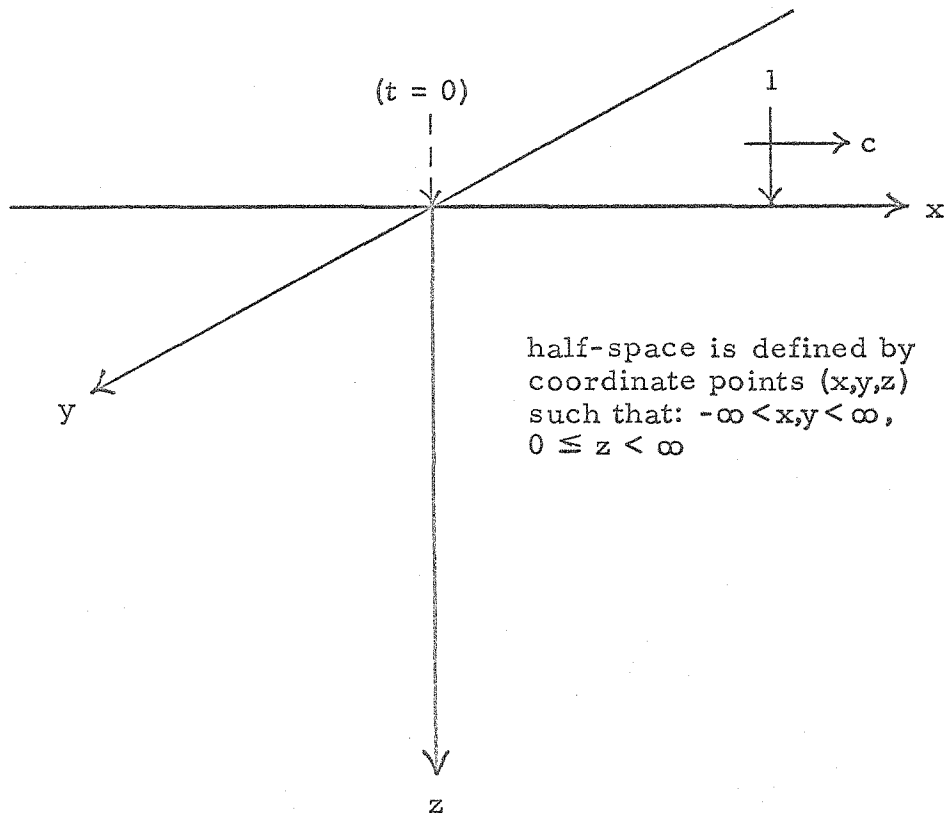

FIGURE 1

Traveling Point Load Problem

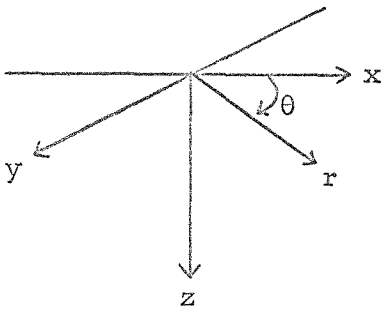

$$x = r\cos\theta \qquad r = (x^2+y^2)^{\frac{1}{2}}$$

$$y = r\sin\theta \qquad \theta = \tan^{-1}(y/x)$$

$$z = z$$

$$0 \le r < \infty\,,\quad -\pi \le \theta < \pi\,,\quad 0 \le z < \infty$$

$$u_r = u_x\cos\theta + u_y\sin\theta$$

$$u_\theta = -u_x\sin\theta + u_y\cos\theta$$

$$u_z = u_z$$

Cylindrical Geometry

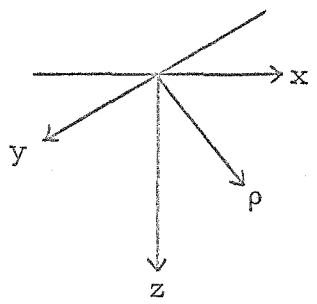

$$\rho = (x^2+y^2+z^2)^{\frac{1}{2}}$$

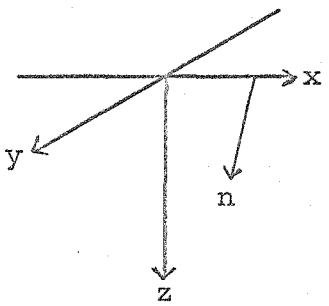

$$n = (y^2+z^2)^{\frac{1}{2}}$$

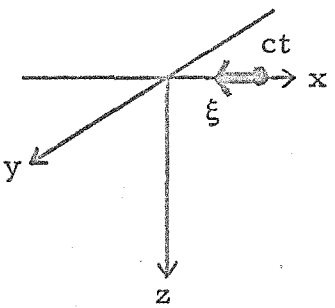

$$\xi = ct - x$$

FIGURE 2

Half-Space Coordinates

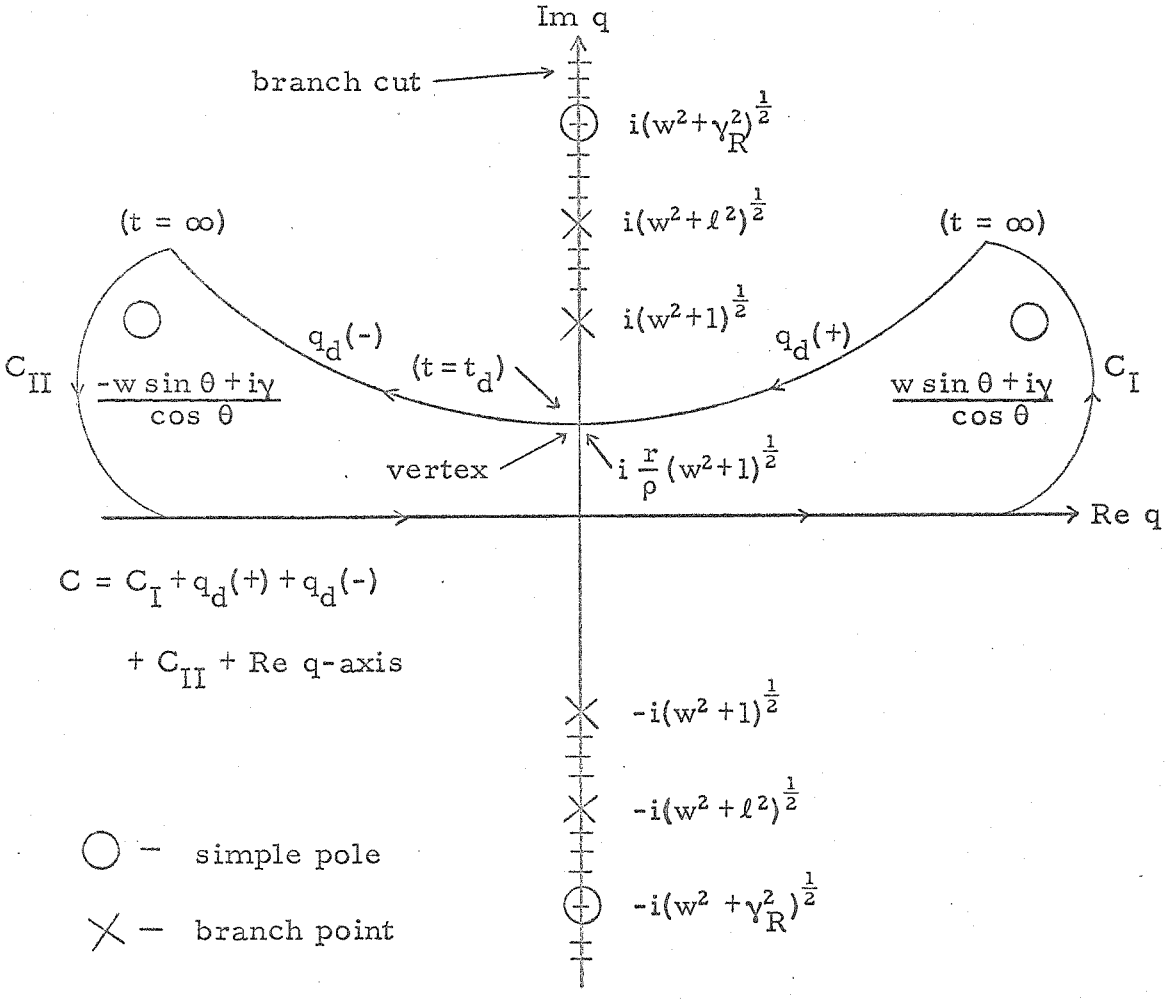

Remarks

(1) $w \in [0, M)$

(2) $\theta \geq 0$, $z > 0$

(3) $\mathrm{Re}\,(m_d z - iqr) > 0$ for $\mathrm{Im}\, q \geq 0$

FIGURE 3

Contour Integration in the q-Plane for the Dilatational Contribution, Case I

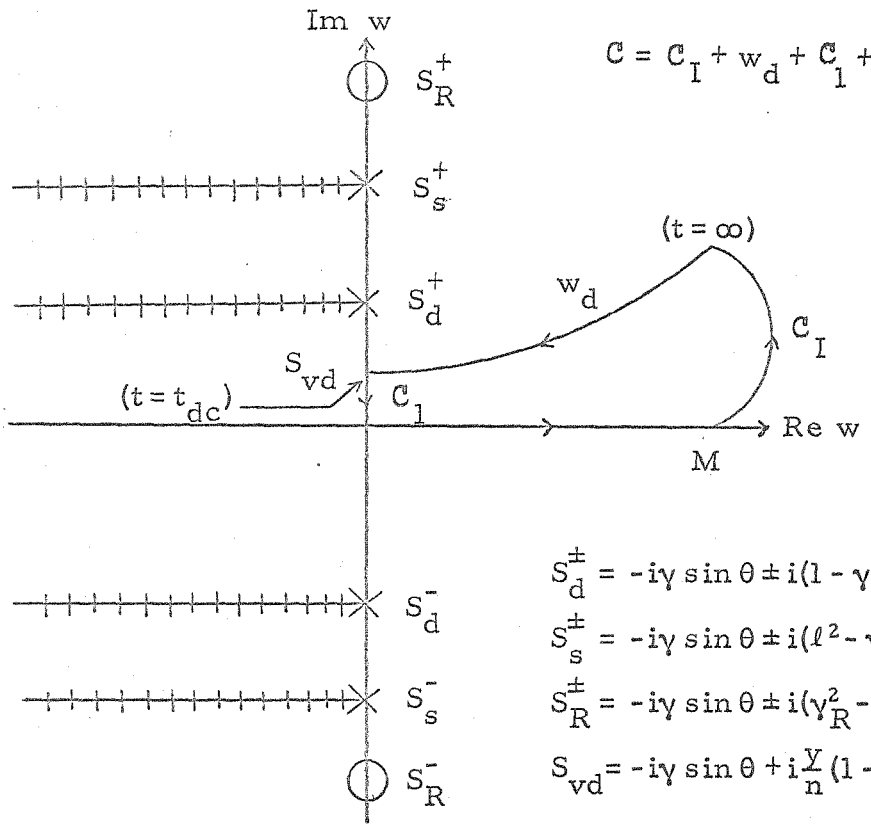

$\mathcal{C} = \mathcal{C}_I + w_d + \mathcal{C}_1 + \text{Re w-axis}$

$$S_d^{\pm} = -i\gamma \sin\theta \pm i(1-\gamma^2)^{\frac{1}{2}} \cos\theta$$

$$S_s^{\pm} = -i\gamma \sin\theta \pm i(\ell^2-\gamma^2)^{\frac{1}{2}} \cos\theta$$

$$S_R^{\pm} = -i\gamma \sin\theta \pm i(\gamma_R^2-\gamma^2)^{\frac{1}{2}} \cos\theta$$

$$S_{vd} = -i\gamma \sin\theta + i\frac{\gamma}{n}(1-\gamma^2)^{\frac{1}{2}} \cos\theta$$

Remarks

(1) $\theta \geq 0$, $z > 0$

(2) The conditions in remark (1) and (2.4-7) - case I determine the relative position of the singularities, the vertex, and the Re w-axis as shown.

(3) $\text{Re}\left[(m_d z - iqr)\Big|_{q = \frac{w\sin\theta + i\gamma}{\cos\theta}}\right] > 0$ for $\text{Im } w \geq 0$

FIGURE 4

Contour Integration in the w-Plane for the Dilatational Contribution, Supersonic Load Motion, Case I

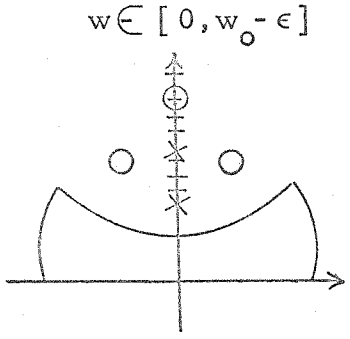

$C = C_I + C_{II} + q_d(+) + q_d(-)$
$+ \text{Re q-axis}$

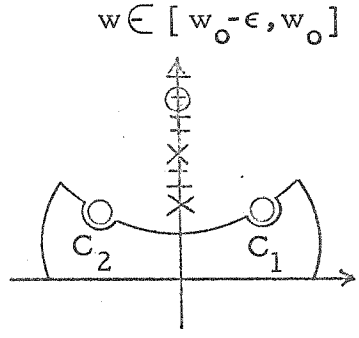

$C = C_I + C_{II} + q_d(+) + q_d(-)$
$+ C_1 + C_2 + \text{Re q-axis}$

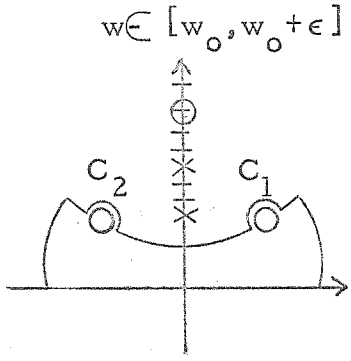

$C = C_I + C_{II} + q_d(+) - q_d(-)$
$+ C_1 + C_2 + \text{Re q-axis}$

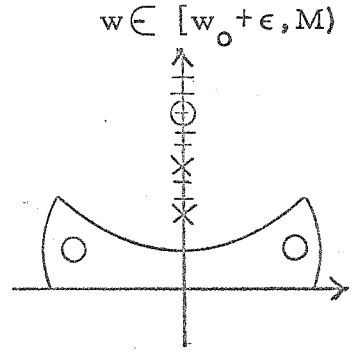

$C = C_I + C_{II} + q_d(+) + q_d(-)$
$+ \text{Re q-axis}$

(see Fig. 3 for the deleted notation)

FIGURE 5

Contour Integrations in the q-Plane for
the Dilatational Contribution, Case II

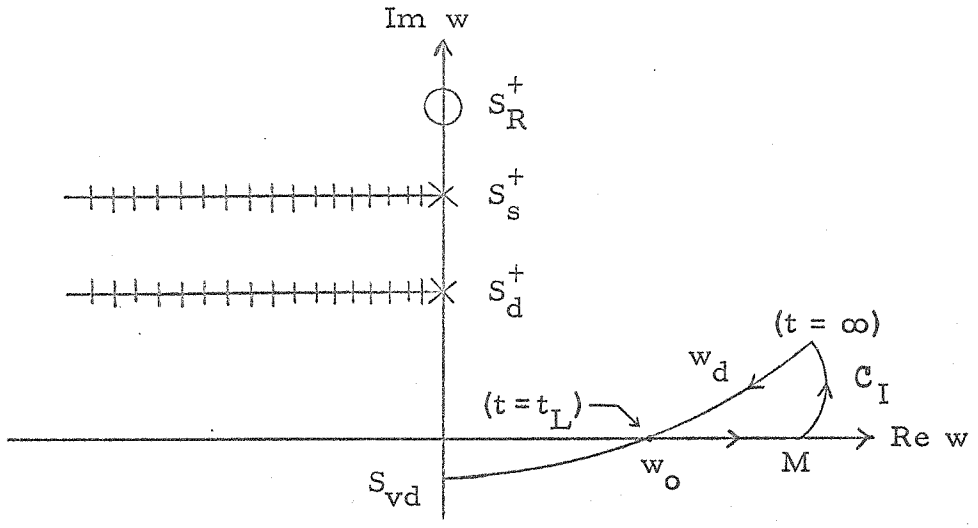

$C = C_I + w_d$ + Re w-axis

S_d^+, S_s^+, S_R^+, S_{vd} are given in Fig. 4

Remarks

(1) $\theta \geq 0$, $z > 0$

(2) The relative position of the singularities and the Re w-axis can be different than shown, but the differences have no effect on the contour integration. The conditions in remark (1) and (2.4-7) - case II imply that the vertex lies below the Re w-axis and that w_d intersects the Re w-axis at $w = w_o$ for $t = t_L$.

(3) Same as Fig. 4.

FIGURE 6

Contour Integration in the w-Plane for the Dilatational Contribution, Supersonic Load Motion, Case II

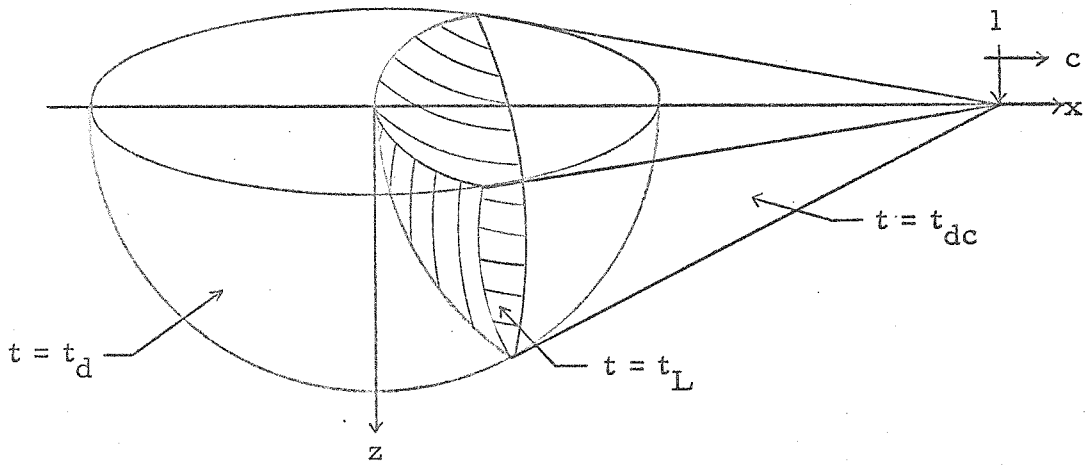

Three-Dimensional Perspective

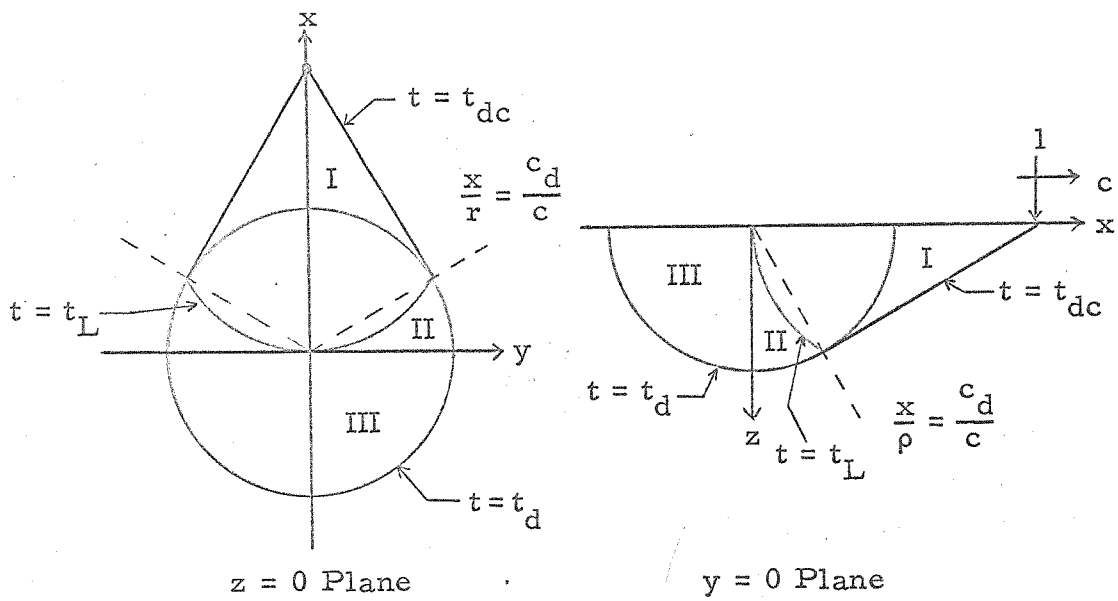

FIGURE 7

Dilatational Wave Pattern for Supersonic Load Motion

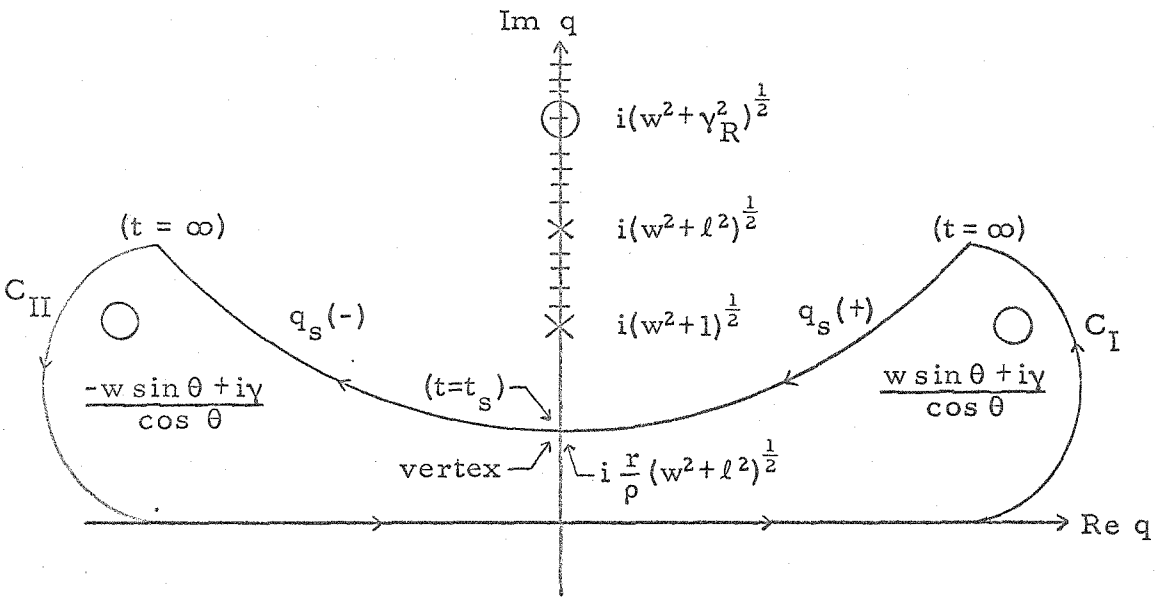

$$C = C_I + q_s(+) + q_s(-) + C_{II} + \text{Re q-axis}$$

Remarks

(1) Case I: $\frac{r}{\rho} < \frac{c_s}{c_d}$, $w \in [0, \infty)$

Case II: $\frac{r}{\rho} > \frac{c_s}{c_d}$, $w \in (w_1, \infty)$

(2) $\theta \geq 0$, $z > 0$

(3) $\text{Re}\,(m_s z - iqr) > 0$ for $\text{Im}\, q \geq 0$

FIGURE 8

Contour Integration in the q-Plane for the Equivoluminal Contribution, Cases I and II

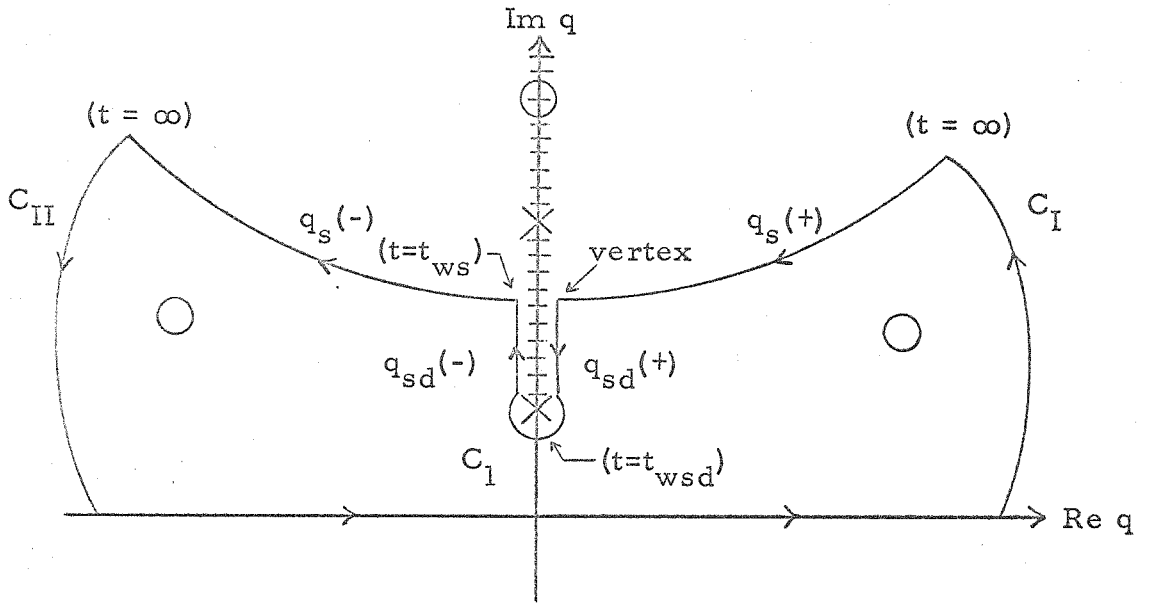

$$C = C_I + q_s(+) + q_{sd}(+) + C_1 + q_{sd}(-) + q_s(-) + C_{II} + \text{Re q-axis}$$

(see Fig. 8 for the deleted notation)

Remarks

(1) $\frac{r}{\rho} > \frac{c_s}{c_d}$, $w \in [0, w_1)$

(2), (3) same as Fig. 8

FIGURE 9

Contour Integration in the q-Plane for the Equivoluminal Contribution, Case II

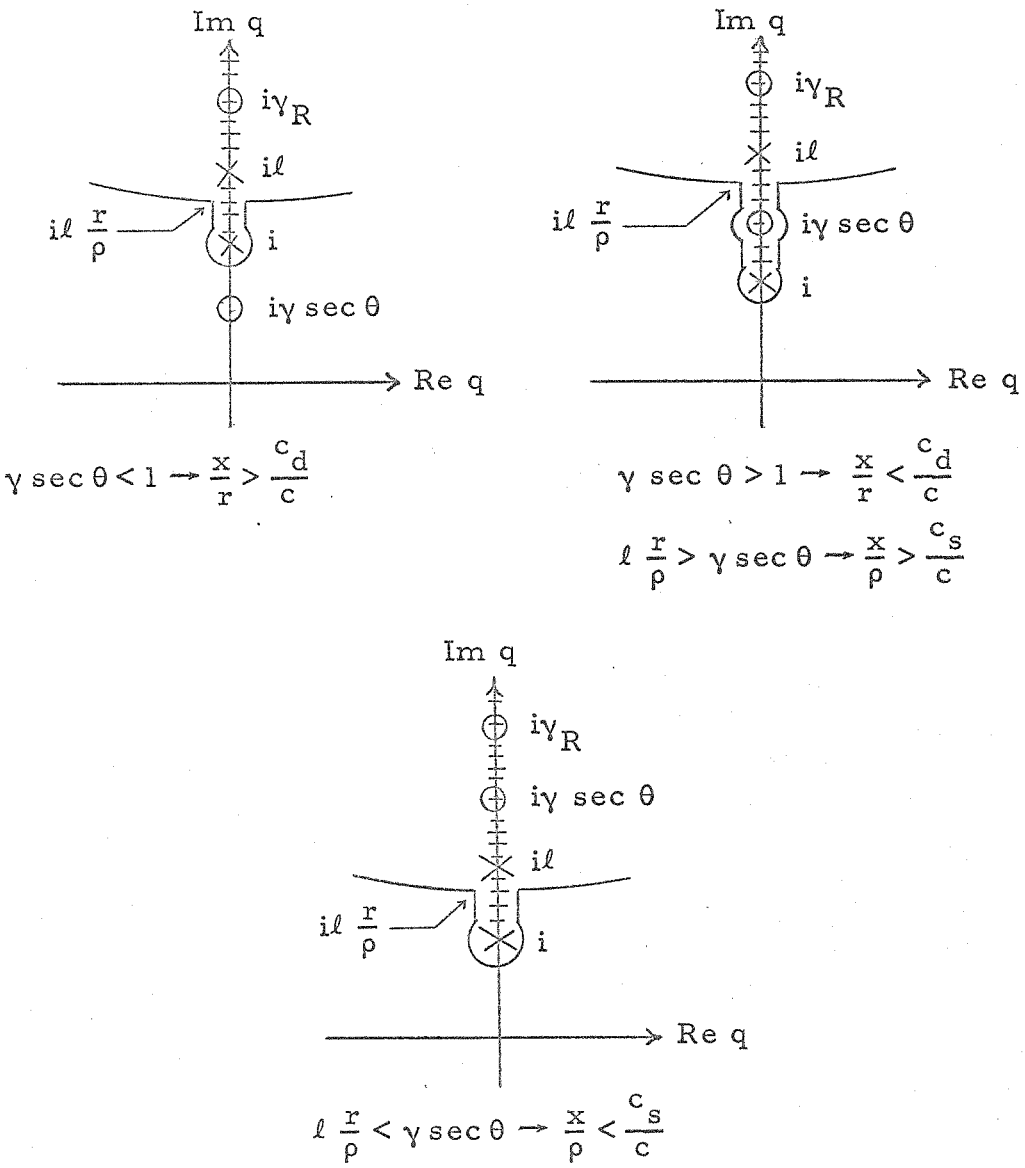

(This figure is special cases of Fig. 9 for w = 0)

FIGURE 10

Relative Position of the Singularities in the q-Plane

for the Equivoluminal Contribution, w = 0

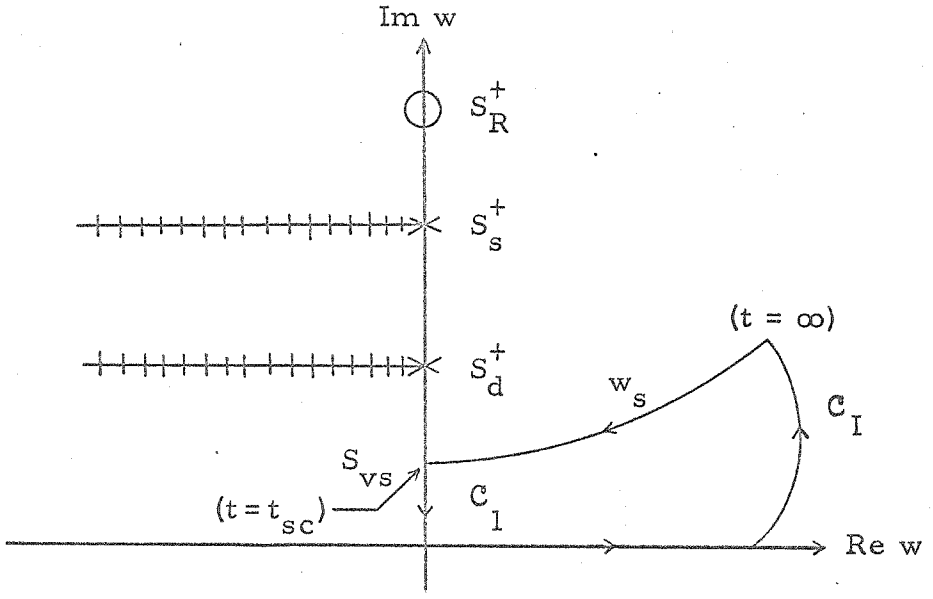

$C = C_I + w_s + C_1 + \text{Re w-axis}$

$S_{vs} = -i\gamma \sin\theta + i\frac{\gamma}{n}(\ell^2 - \gamma^2)^{\frac{1}{2}} \cos\theta$ (S_{vs} is the vertex of w_s)

S_d^+, S_s^+, S_R^+ are given in Fig. 4

Remarks

(1) $\theta \geq 0$, $z > 0$, $\frac{\gamma}{n} < \phi_c$

(2) The conditions in remark (1) and (2.4-40) - Cases I and II determine the relative position of the singularities, the vertex, and the Re w-axis as shown.

(3) $\text{Re}\left[(m_s z - iqr) \Big|_{q = \frac{w \sin\theta + i\gamma}{\cos\theta}}\right] > 0$ for $\text{Im } w \geq 0$

FIGURE 11

Contour Integration in the w-Plane for the Equivoluminal Contribution, Supersonic Load Motion, Cases I and II

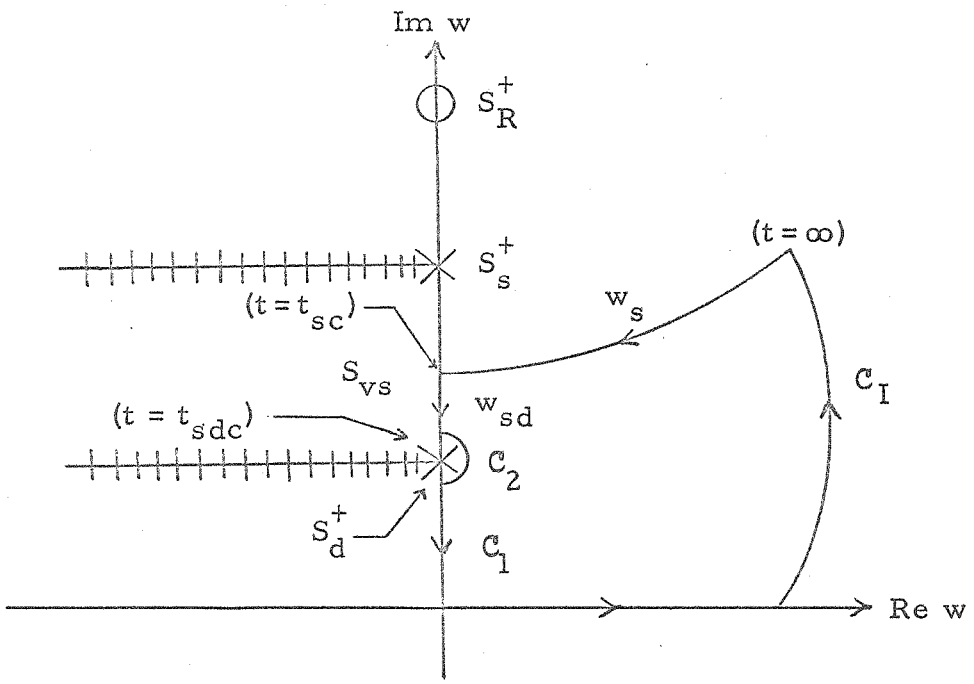

$C = C_I + w_s + w_{sd} + C_2 + C_1$ + Re w-axis

S_d^+, S_s^+, S_R^+ are given in Fig. 4; S_{vs} in Fig. 11

Remarks

(1) $\theta \geq 0$, $z > 0$, $\frac{y}{n} > \phi_c$

(2) The conditions in remark (1) and (2.4-40) - Case II determine the relative position of the singularities, the vertex, and the Re w-axis as shown.

(3) same as Fig. 11

FIGURE 12

Contour Integration in the w-Plane for the Equivoluminal Contribution, Supersonic Load Motion, Case II

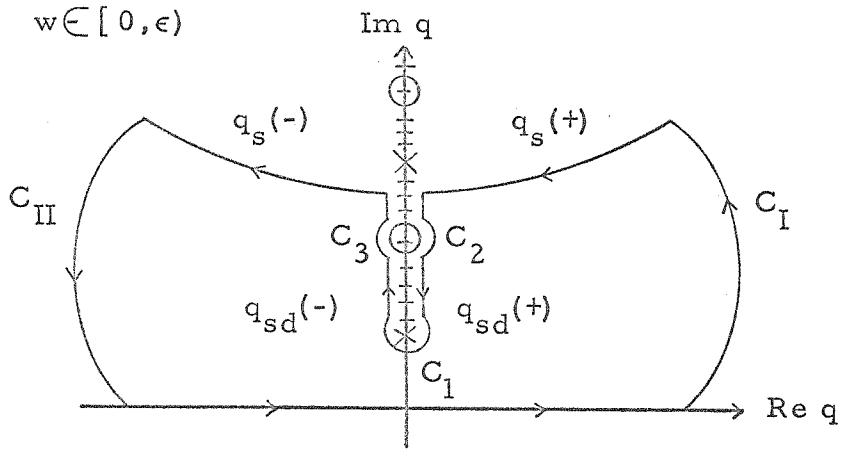

$$C = C_I + q_s(+) + C_2 + q_{sd}(+) + C_1 + q_{sd}(-) + C_3 + q_s(-) + C_{II} + \text{Re q-axis}$$

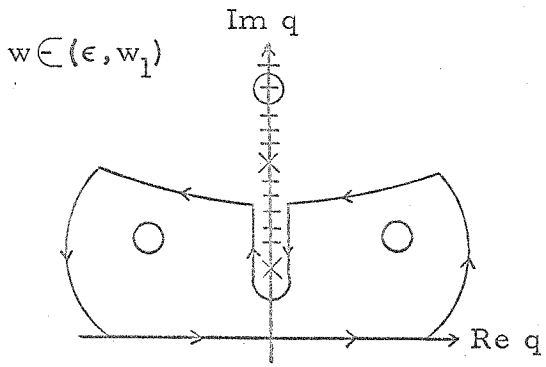

$$C = C_I + q_s(+) + q_{sd}(+) + C_1 + q_{sd}(-) + q_s(-) + C_{II} + \text{Re q-axis}$$

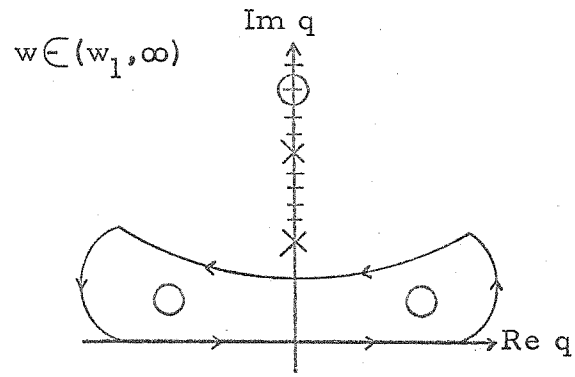

$$C = C_I + q_s(+) + q_s(-) + C_{II} + \text{Re q-axis}$$

(see Figs. 8 and 9 for the deleted notation)

FIGURE 13

Contour Integration in the q-Plane for
the Equivoluminal Contribution, Case III

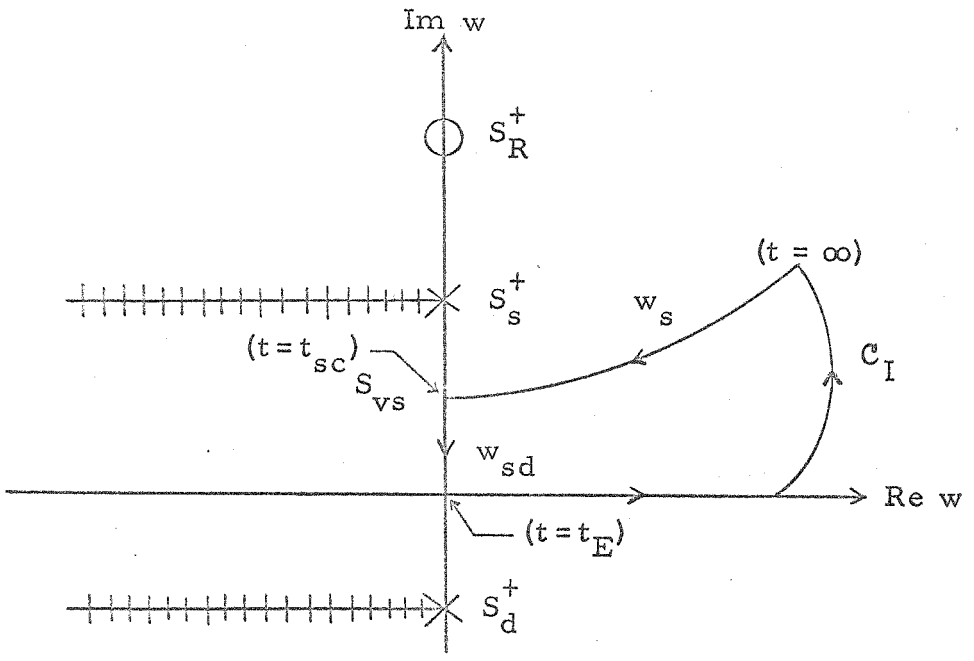

$C = C_I + w_s + w_{sd}$ + Re w-axis

S_d^+, S_s^+, S_R^+ are given in Fig. 4; S_{vs} in Fig. 11

Remarks

(1) $\theta \geq 0$, $z > 0$, $\frac{Y}{n} > \phi_c$

(2) The conditions in remark (1) and (2.4-40) - Case III determine the relative poisition of the singularities, the vertex, and the Re w-axis as shown.

(3) same as Fig. 11

FIGURE 14

Contour Integration in the w-Plane for the Equivoluminal Contribution, Supersonic Load Motion, Case III

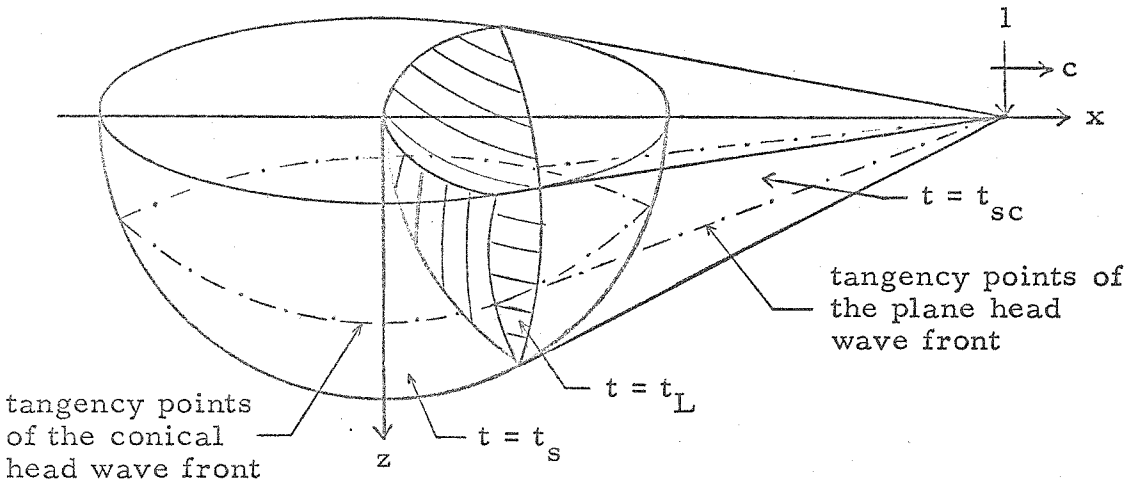

Three-Dimensional Perspective

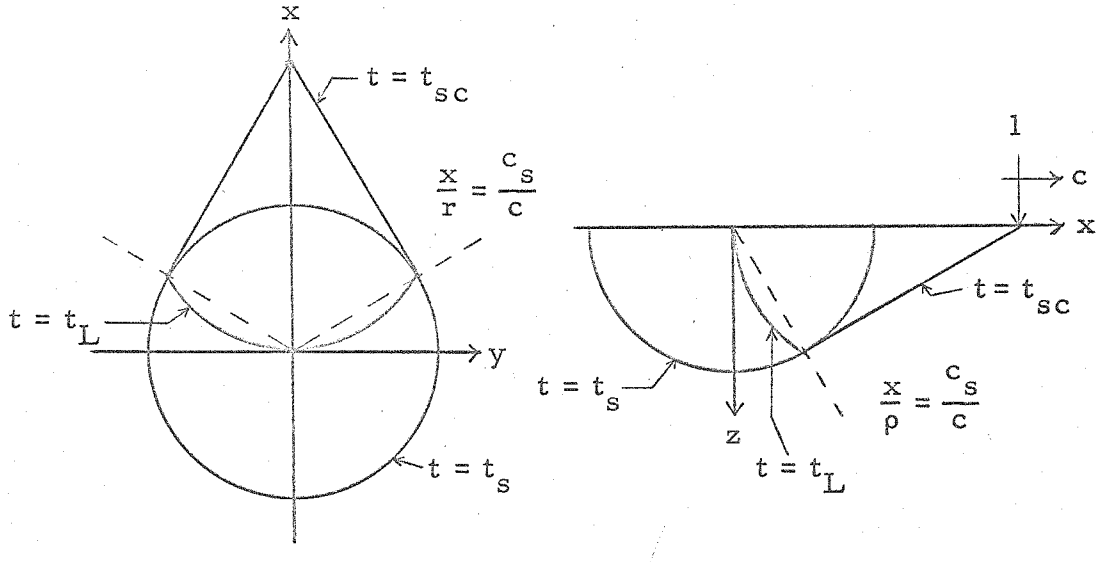

FIGURE 15

Equivoluminal Wave Pattern for

Supersonic Load Motion (Head Waves Not Shown)

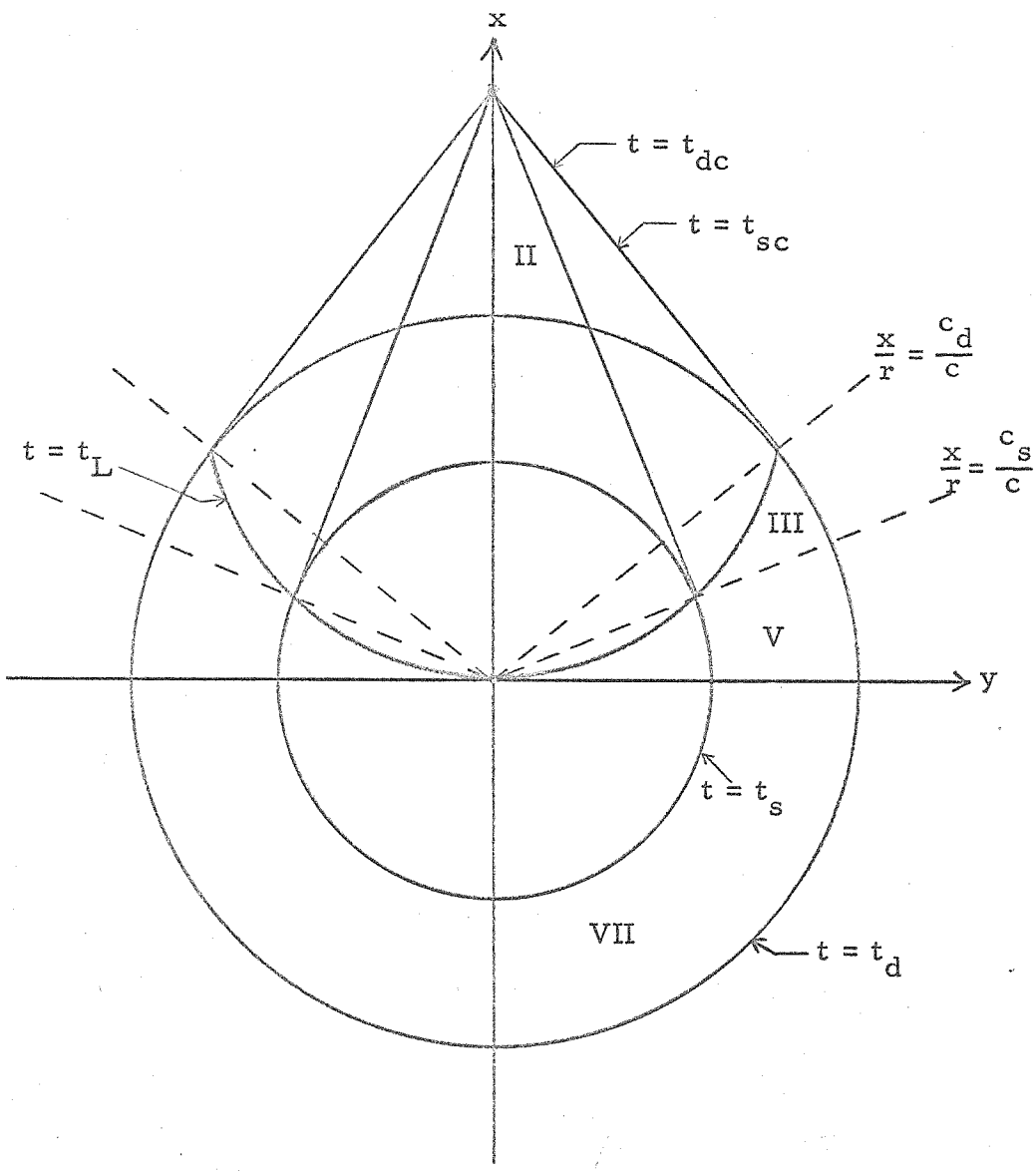

FIGURE 16

Wave Pattern in the Surface Plane
for Supersonic Load Motion

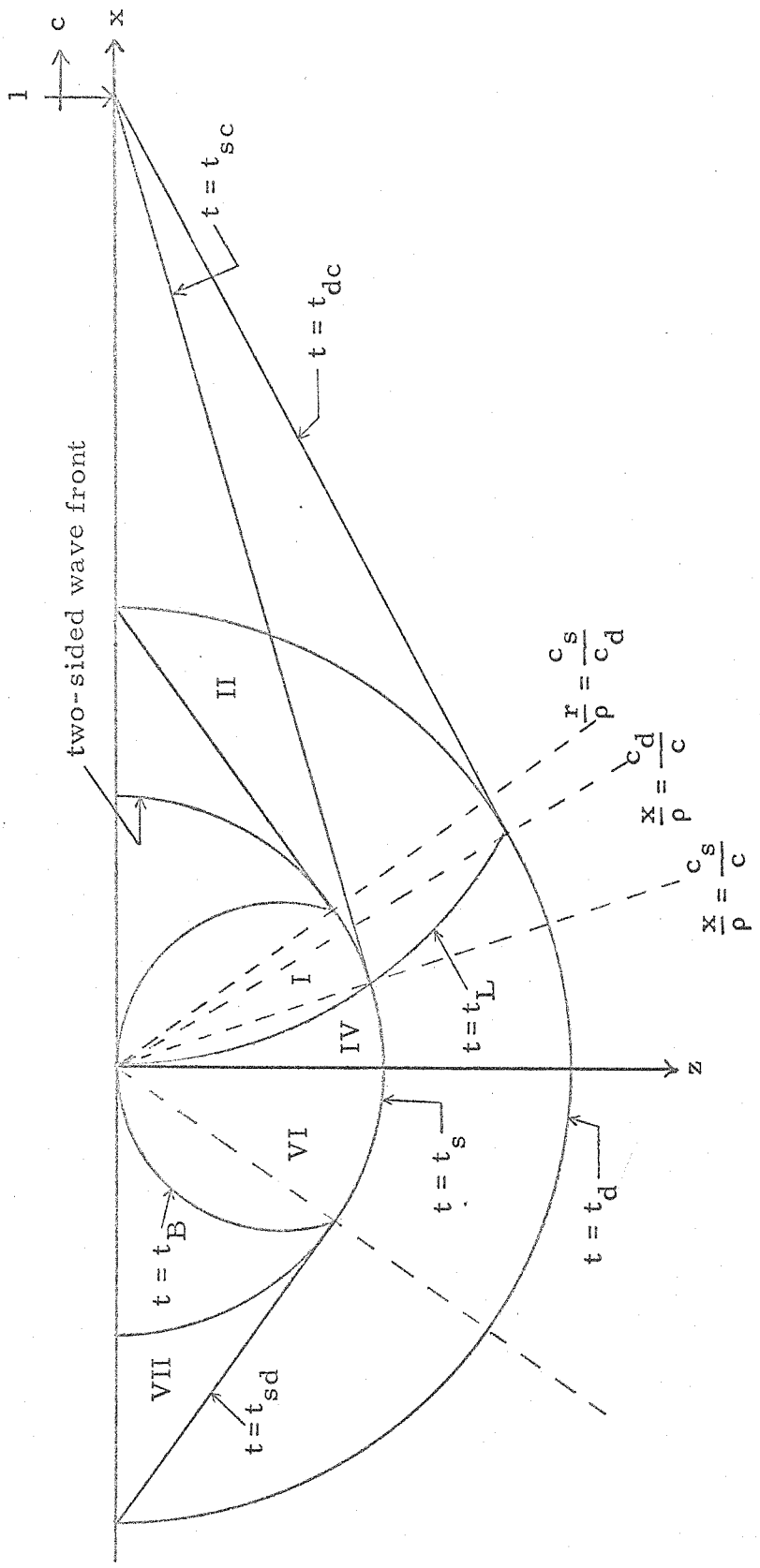

FIGURE 17

Wave Pattern in the Plane Under the Path of the Load for Supersonic Load Motion

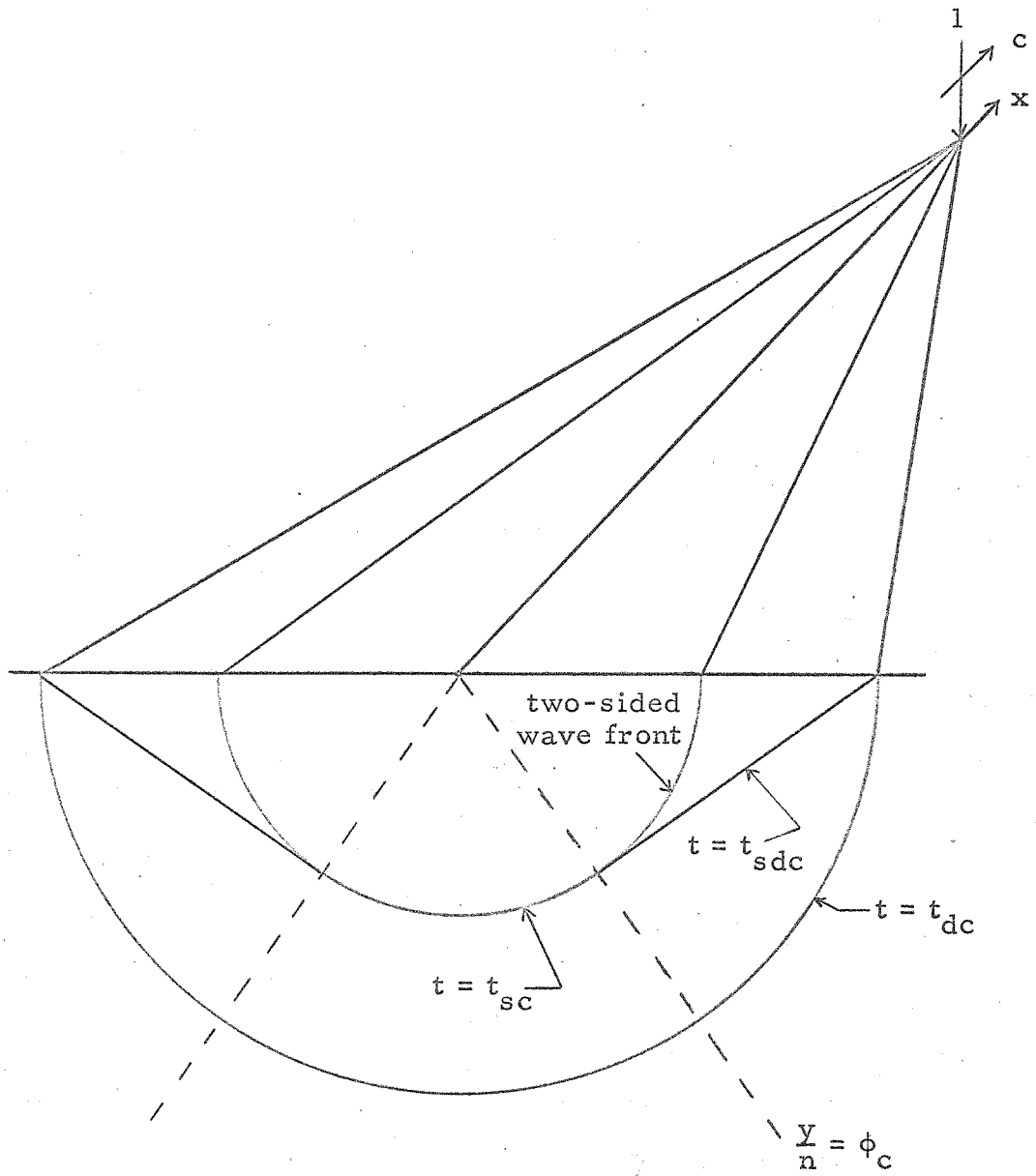

FIGURE 18

Waves Trailing Behind the Load for
Supersonic Load Motion

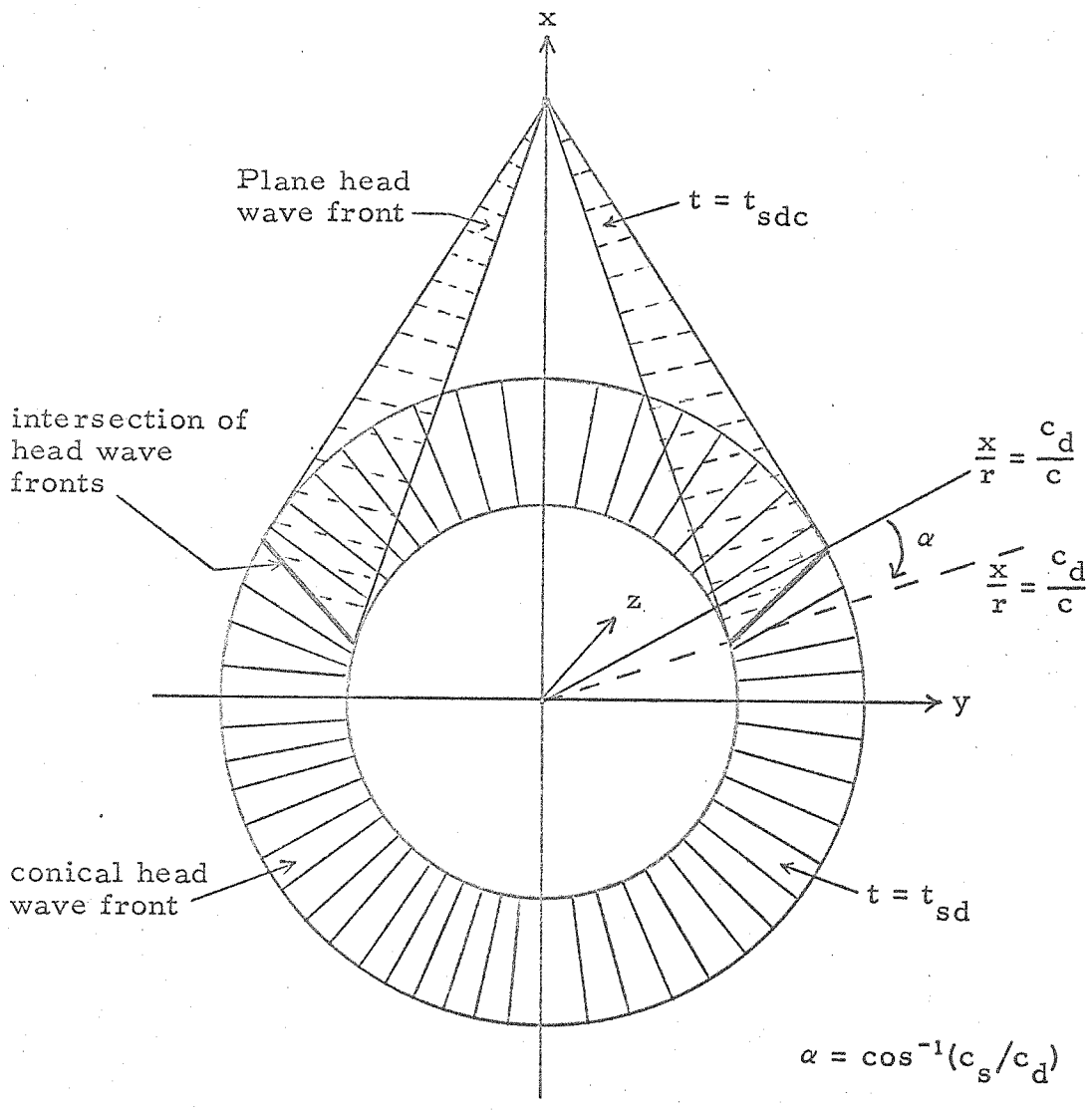

FIGURE 19

Head Wave Fronts for Supersonic Load Motion

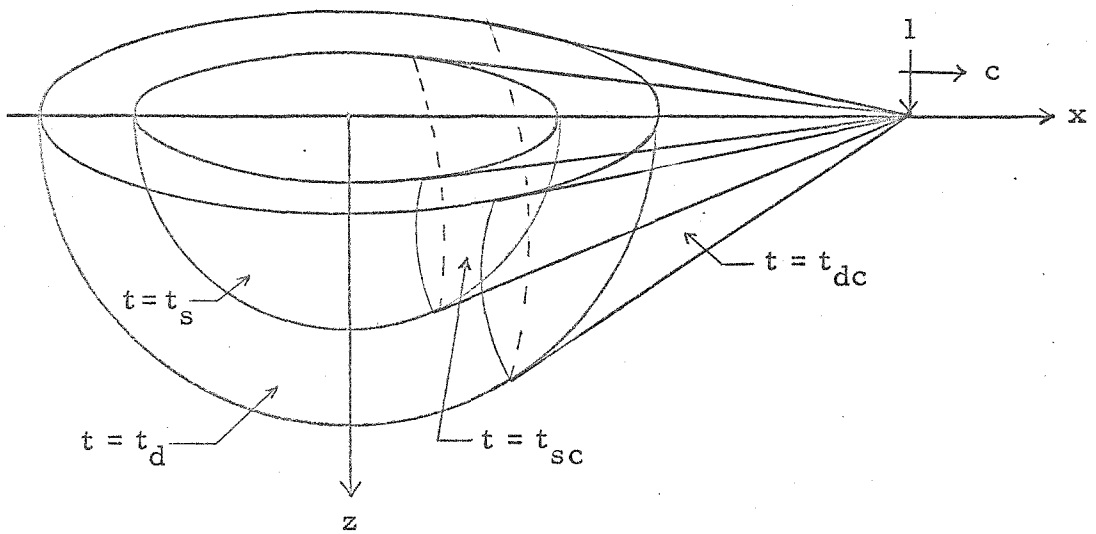

FIGURE 20

Body Waves for Supersonic Load Motion

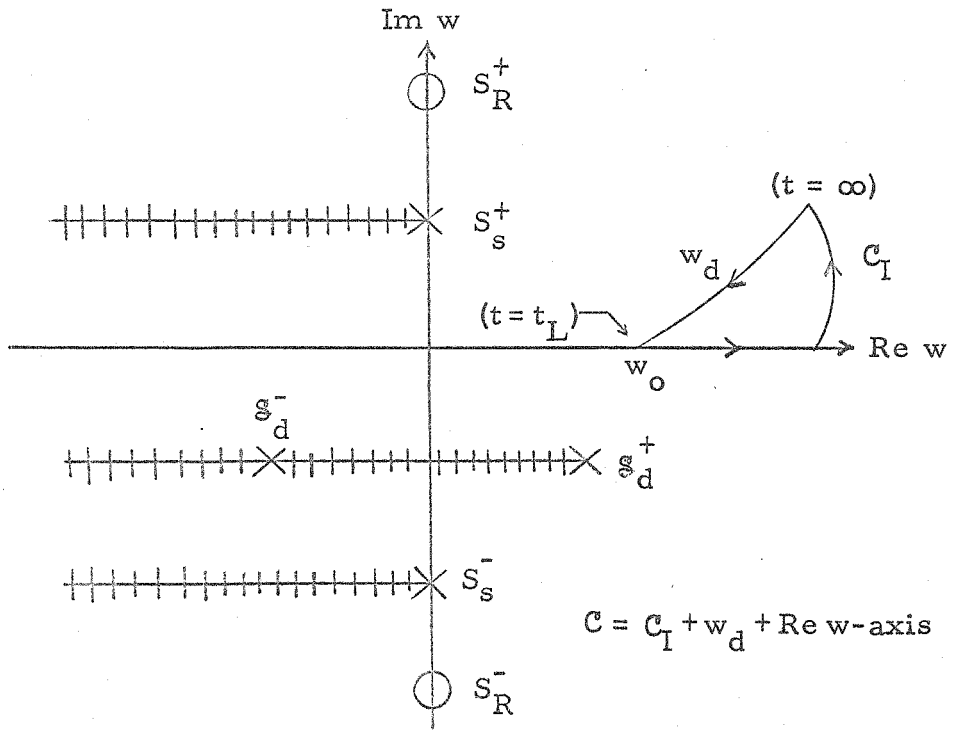

$S_s^{\pm}$, $S_R^{\pm}$ are given in Fig. 4; $s_d^{\pm} = -i\gamma \sin\theta \pm (\gamma^2-1)^{\frac{1}{2}} \cos\theta$

Remarks

(1) $\theta \geq 0$, $z > 0$

(2) The relative position of the singularities and the Re w-axis can be different than shown, but the differences have no effect on the contour integration. The contour w_d intersects the Re w-axis at $w = w_o$ for $t = t_L$.

(3) same as Fig. 4

FIGURE 21

Contour Integration in the w-Plane for the Dilatational Contribution, Transonic Load Motion, Case II

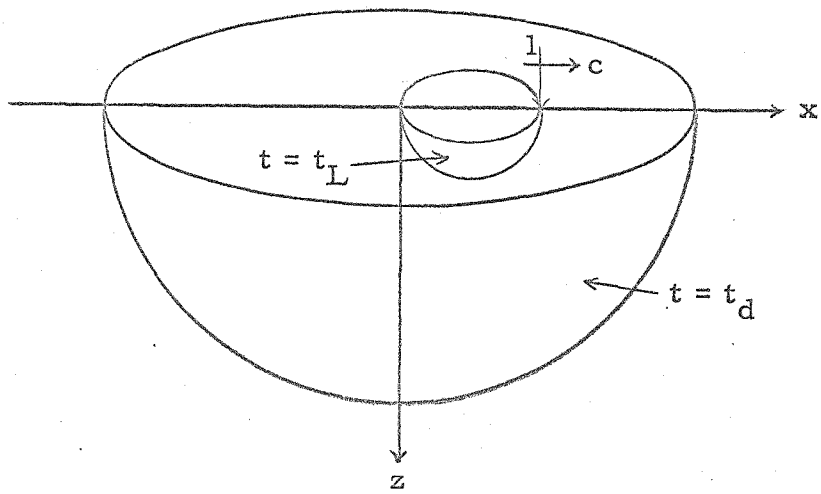

Three-Dimensional Perspective

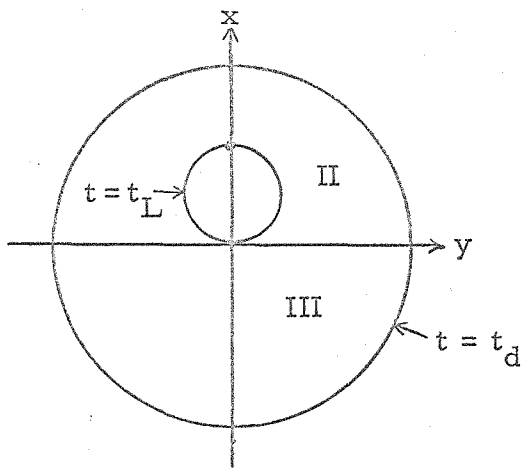

z = 0 Plane

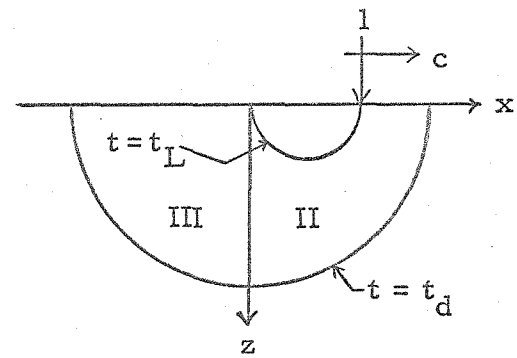

y = 0 Plane

FIGURE 22

Dilatational Wave Pattern for Transonic and Subsonic Load Motion

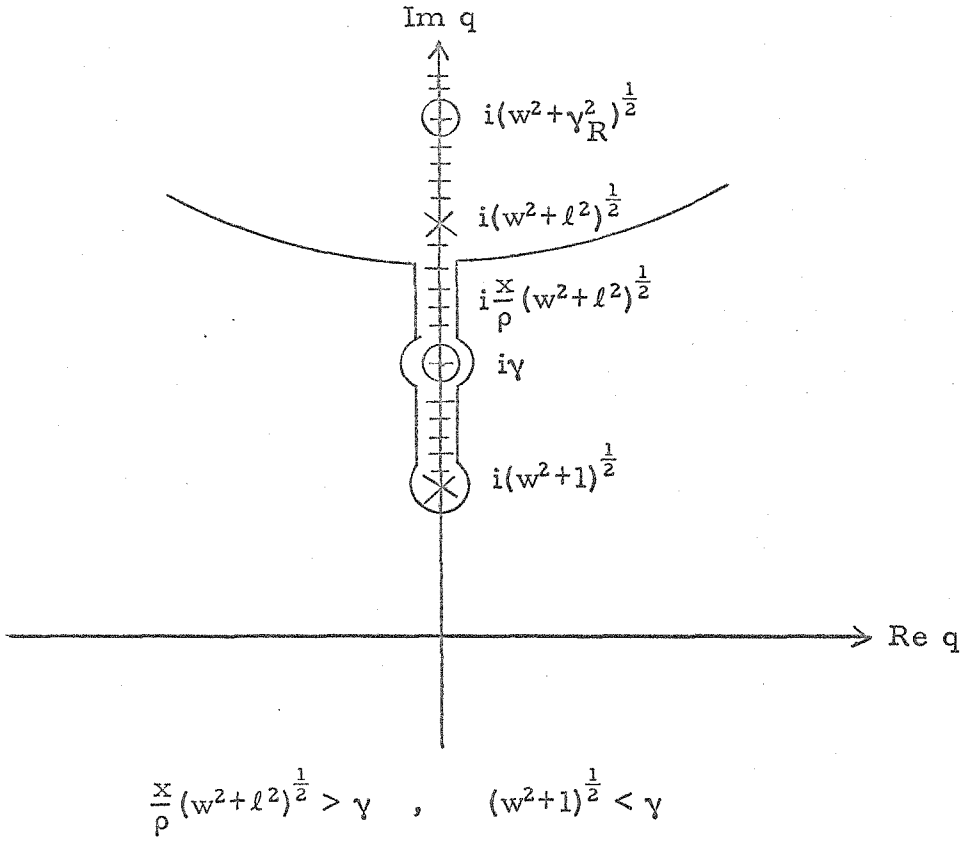

(This figure is a special case of Fig. 9, namely $\theta = 0$)

FIGURE 23

Relative Position of the Singularities in the q-Plane for the Equivoluminal Contribution, Transonic and Subsonic Load Motion, and the Plane Under the Path of the Load

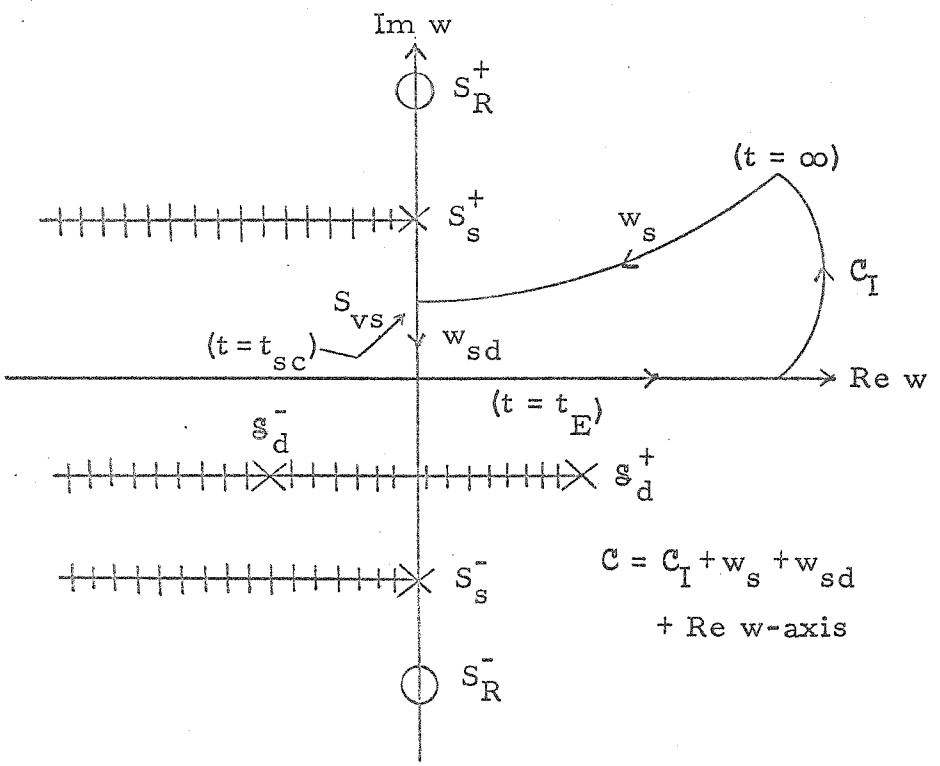

$S_s^{\pm}$, $S_R^{\pm}$ are given in Fig. 4; S_{vs} in Fig. 11; and $s_d^{\pm}$ in Fig. 21

Remarks

(1) $\theta > 0$, $z > 0$

(2) The conditions in remark (1) and (2.4-40) - Case III determine the relative position of the singularities, the vertex, and the Re w-axis as shown.

(3) same as in Fig. 11

FIGURE 24

Contour Integration in the w-Plane for the Equivoluminal Contribution, Transonic Load Motion, Case III

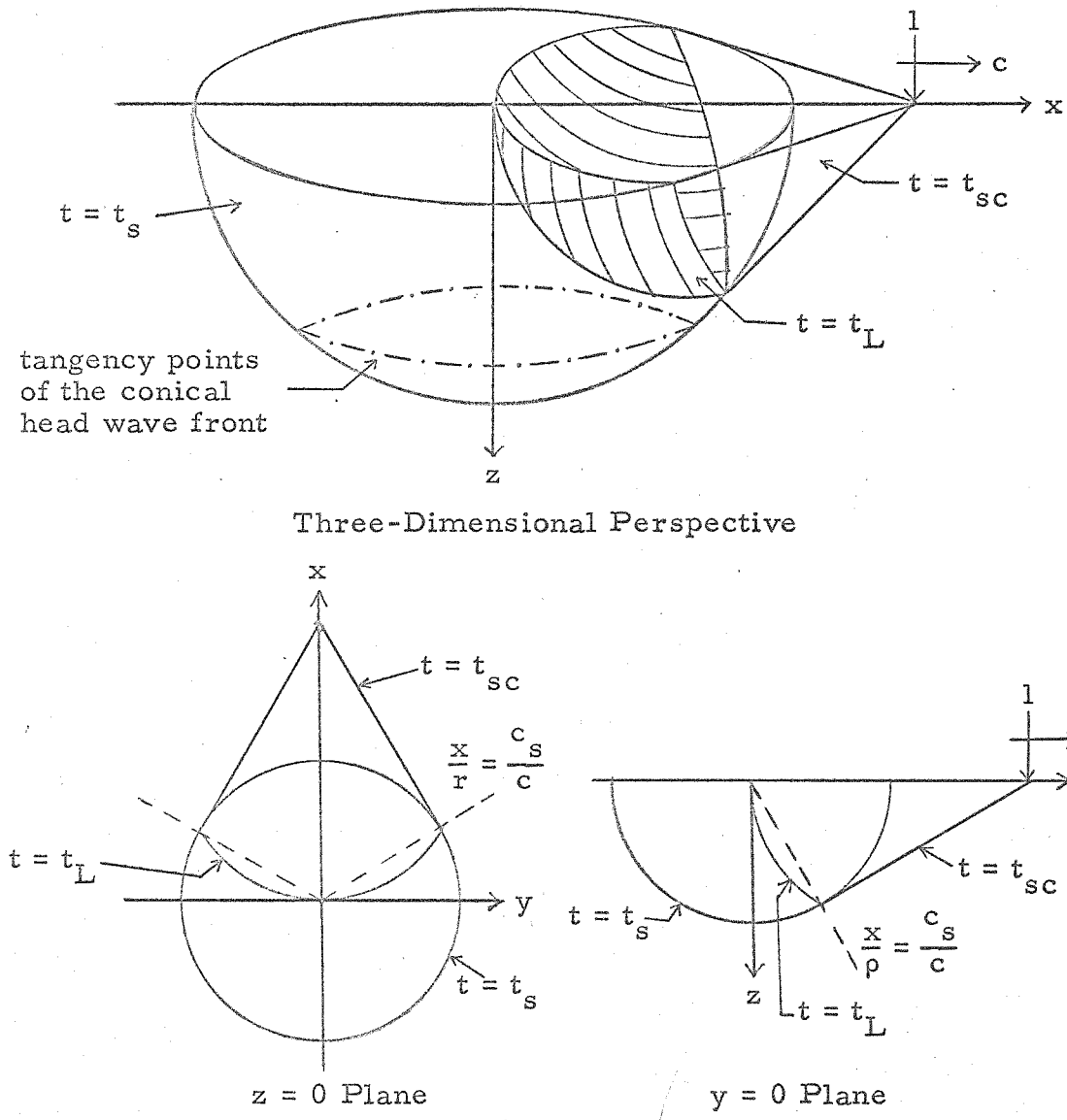

FIGURE 25

Equivoluminal Wave Pattern for
Transonic Load Motion (Head Wave Not Shown)

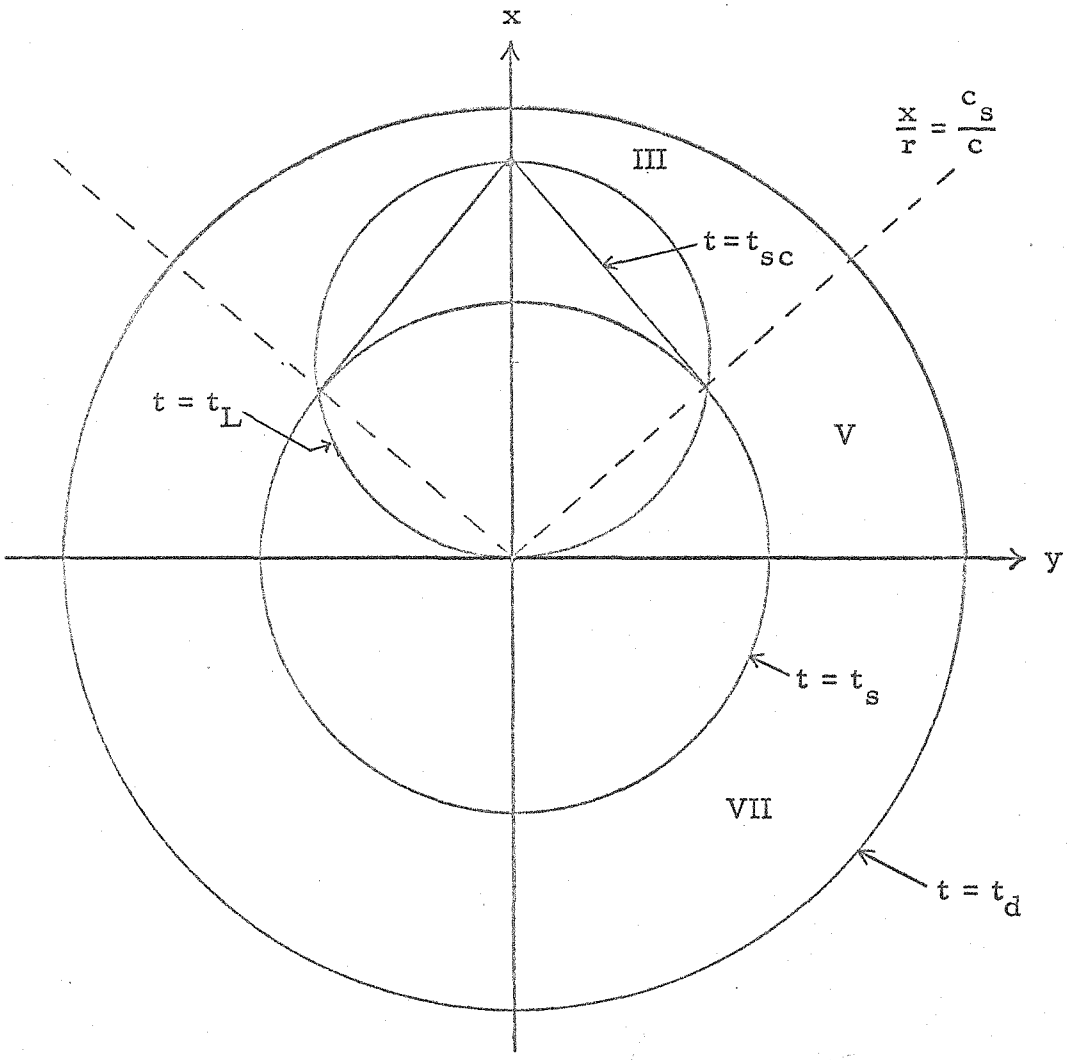

FIGURE 26

Wave Pattern in the Surface Plane for
Transonic Load Motion

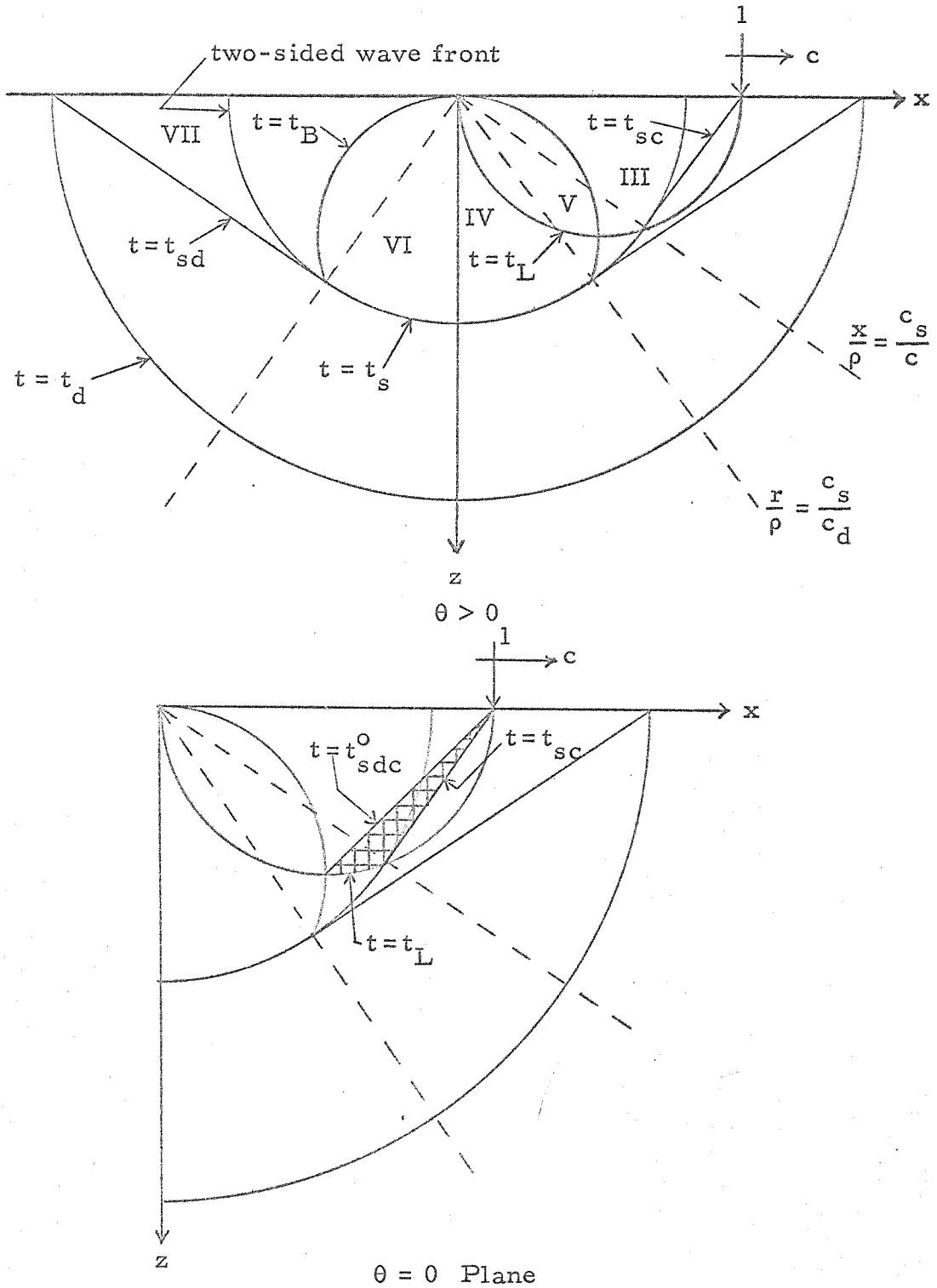

θ = 0 Plane

FIGURE 27

Wave Pattern in the Plane Under the Path of the Load for Transonic Load Motion

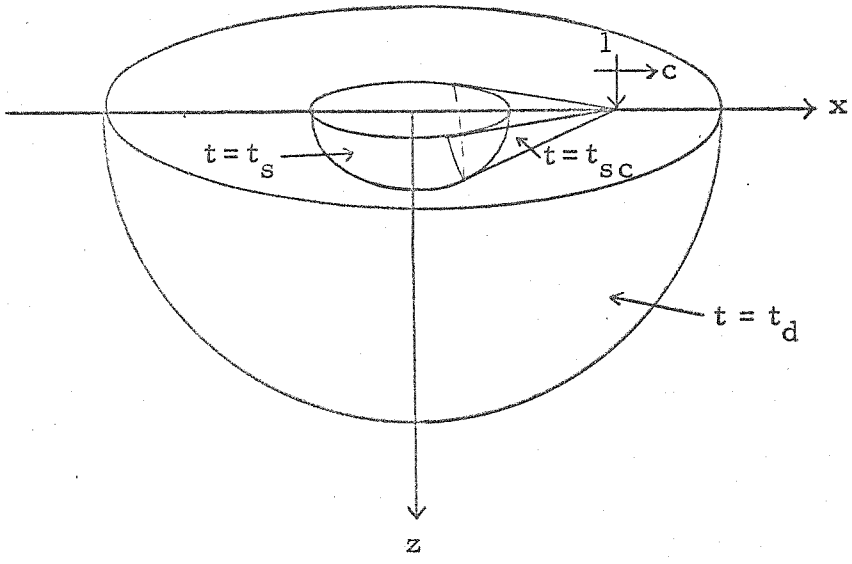

FIGURE 28

Body Waves for Transonic Load Motion

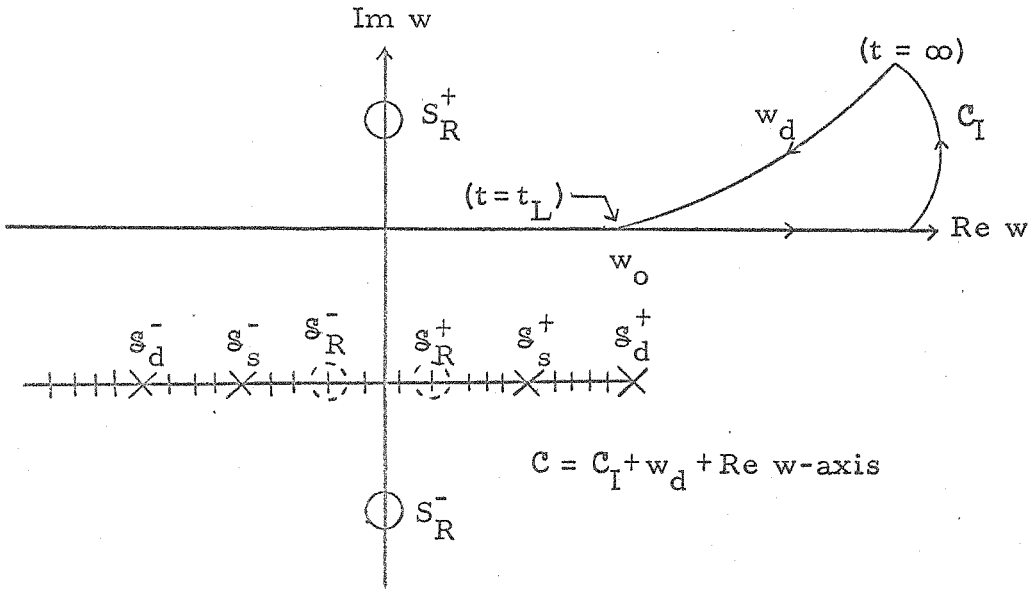

$S_R^{\pm}$ are given in Fig. 4, $s_d^{\pm}$ in Fig. 21

$s_s^{\pm} = -i\gamma \sin\theta \pm (\gamma^2 - \ell^2)^{\frac{1}{2}} \cos\theta$

$s_R^{\pm} = -i\gamma \sin\theta \pm (\gamma^2 - \gamma_R^2)^{\frac{1}{2}} \cos\theta$

Remarks

(1) $\theta \geq 0$, $z > 0$

(2) The Rayleigh poles are shown assuming that $c > c_R$. If $c < c_R$ these poles are located at $w = s_R^{\pm}$, indicated by dashed circles. Remark (2) of Fig. 21 holds here.

(3) same as Fig. 4

FIGURE 29

Contour Integration in the w-Plane for the Dilatational Contribution, Subsonic Load Motion, Case II

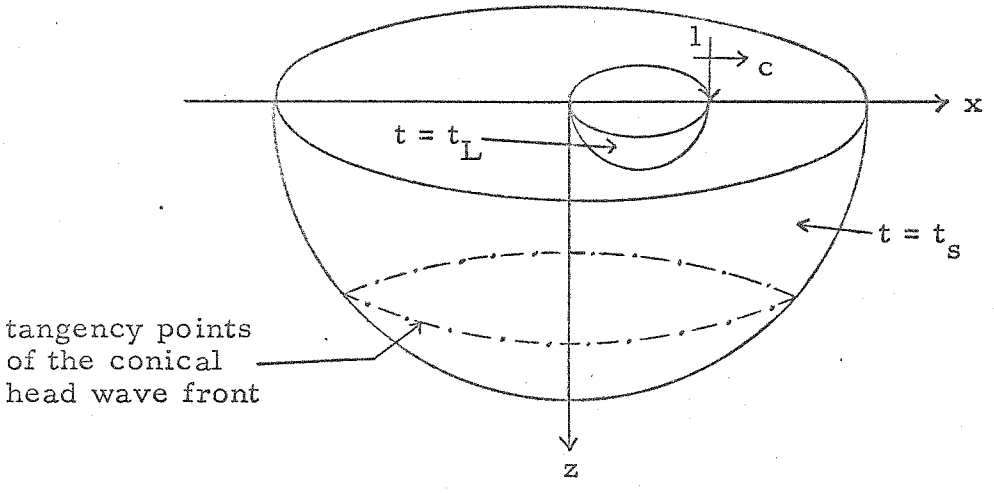

Three-Dimensional Perspective

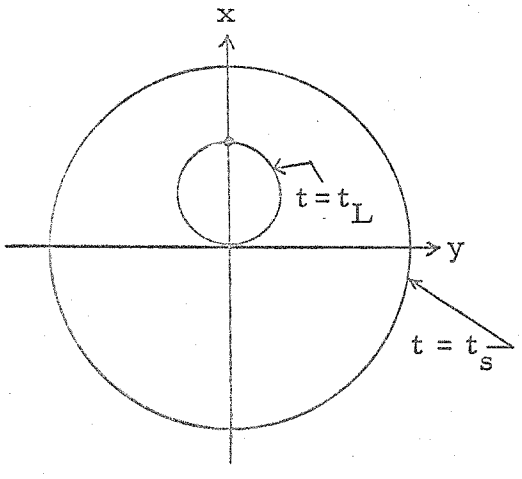

z = 0 Plane

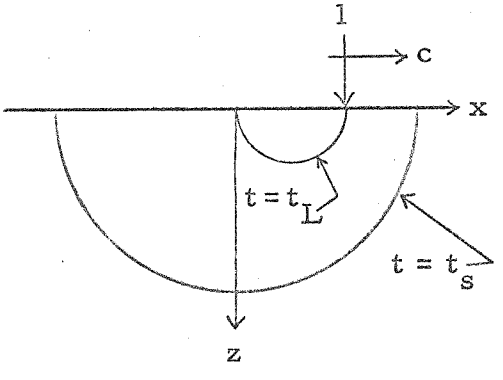

y = 0 Plane

FIGURE 30

Equivoluminal Wave Pattern for Subsonic Load Motion (Head Wave Not Shown)

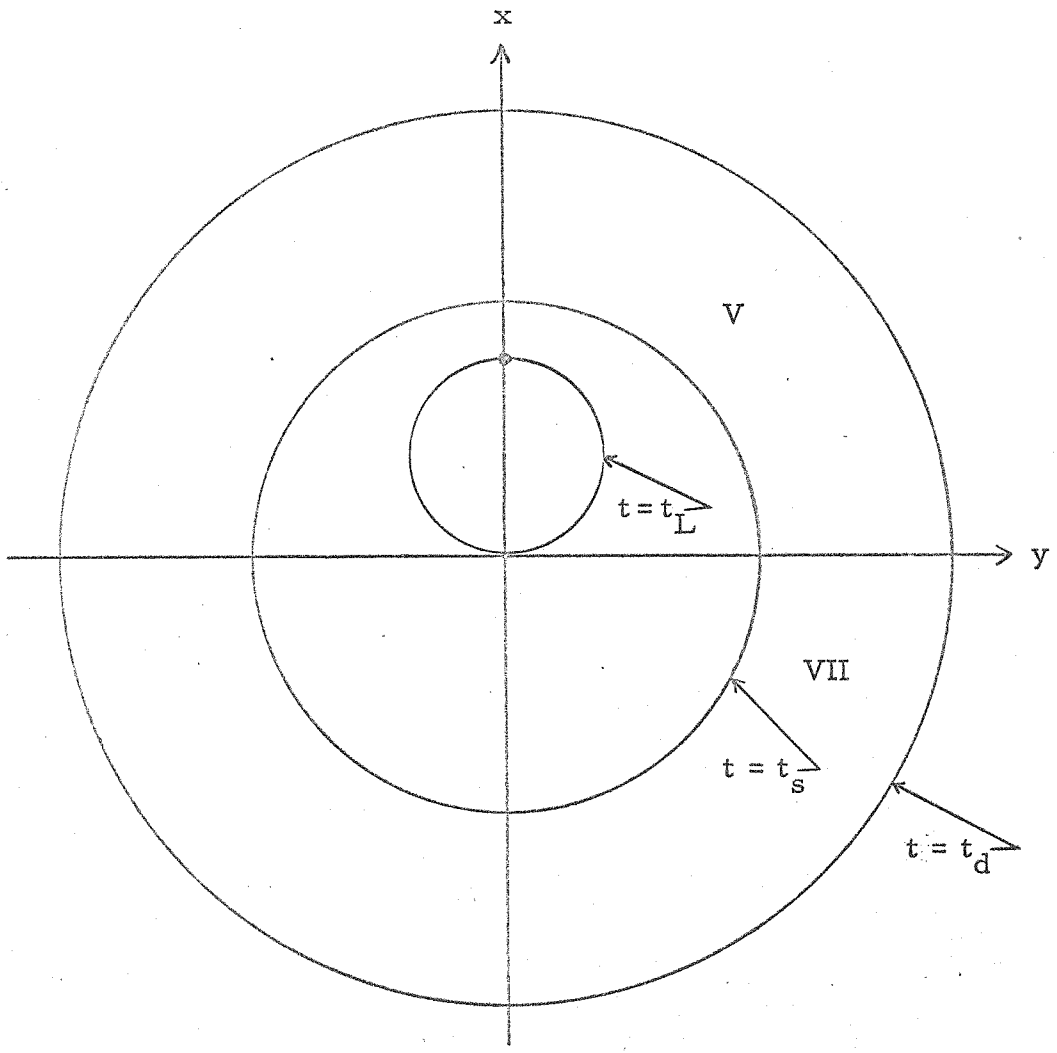

FIGURE 31

Wave Pattern in the Surface Plane
for Subsonic Load Motion

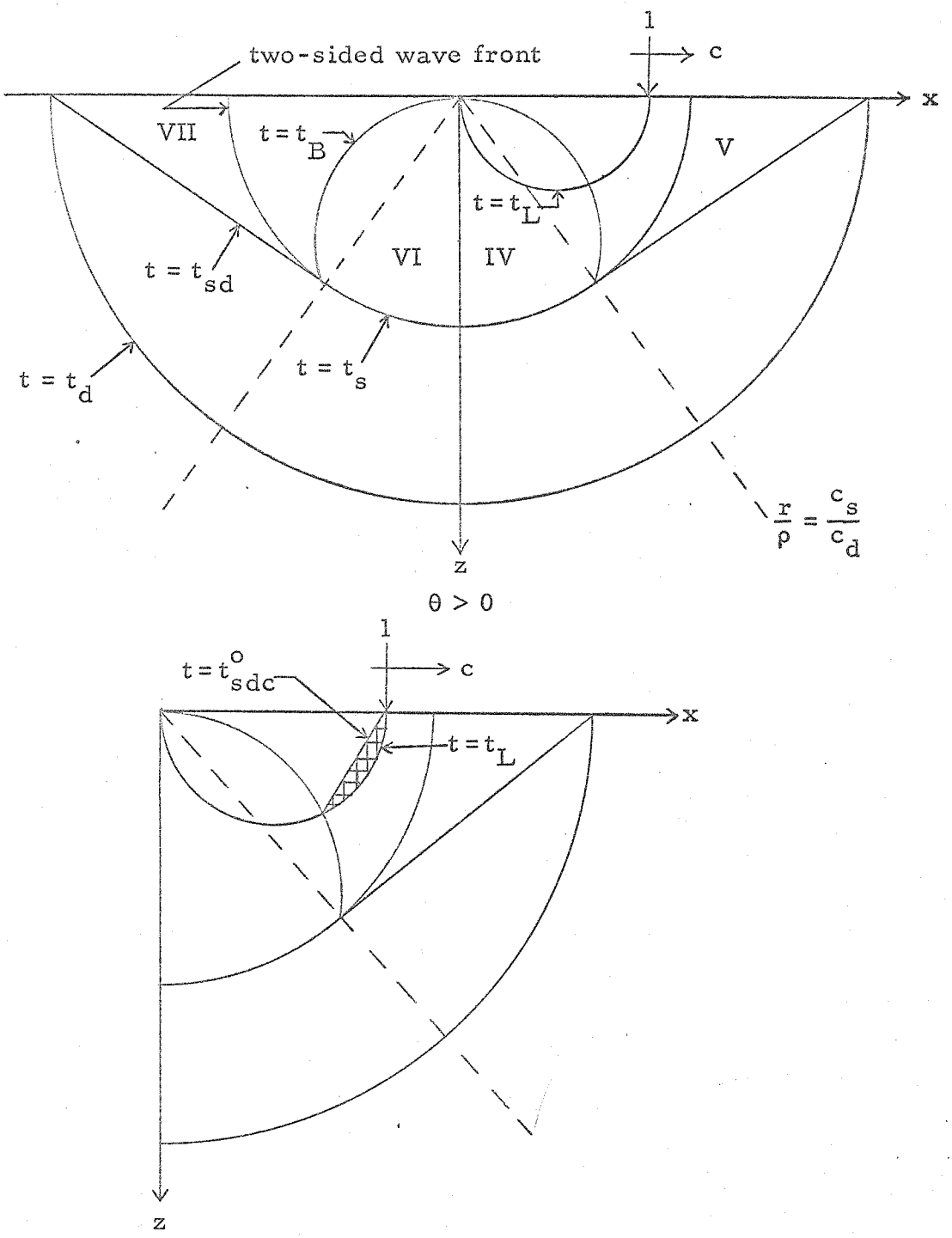

FIGURE 32

Wave Pattern in the Plane Under the Path of the Load for Subsonic Load Motion

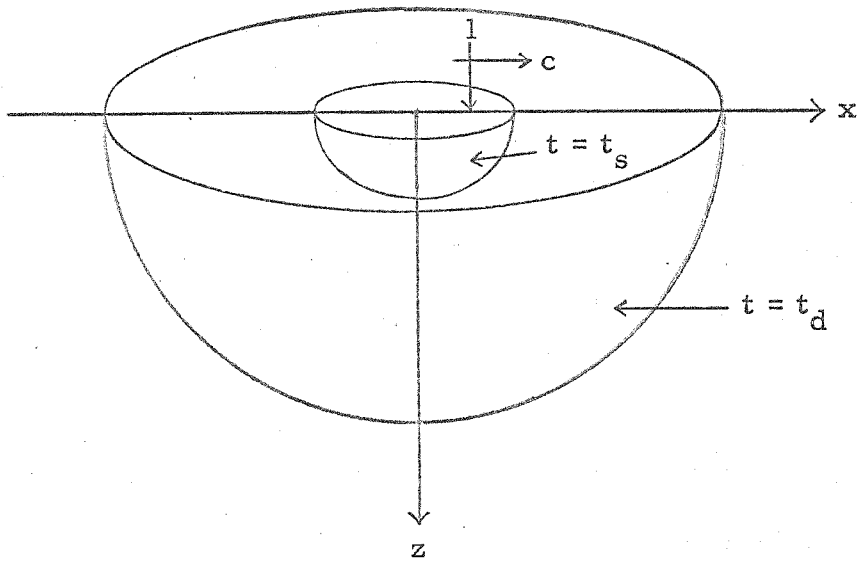

FIGURE 33

Body Waves for Subsonic Load Motion

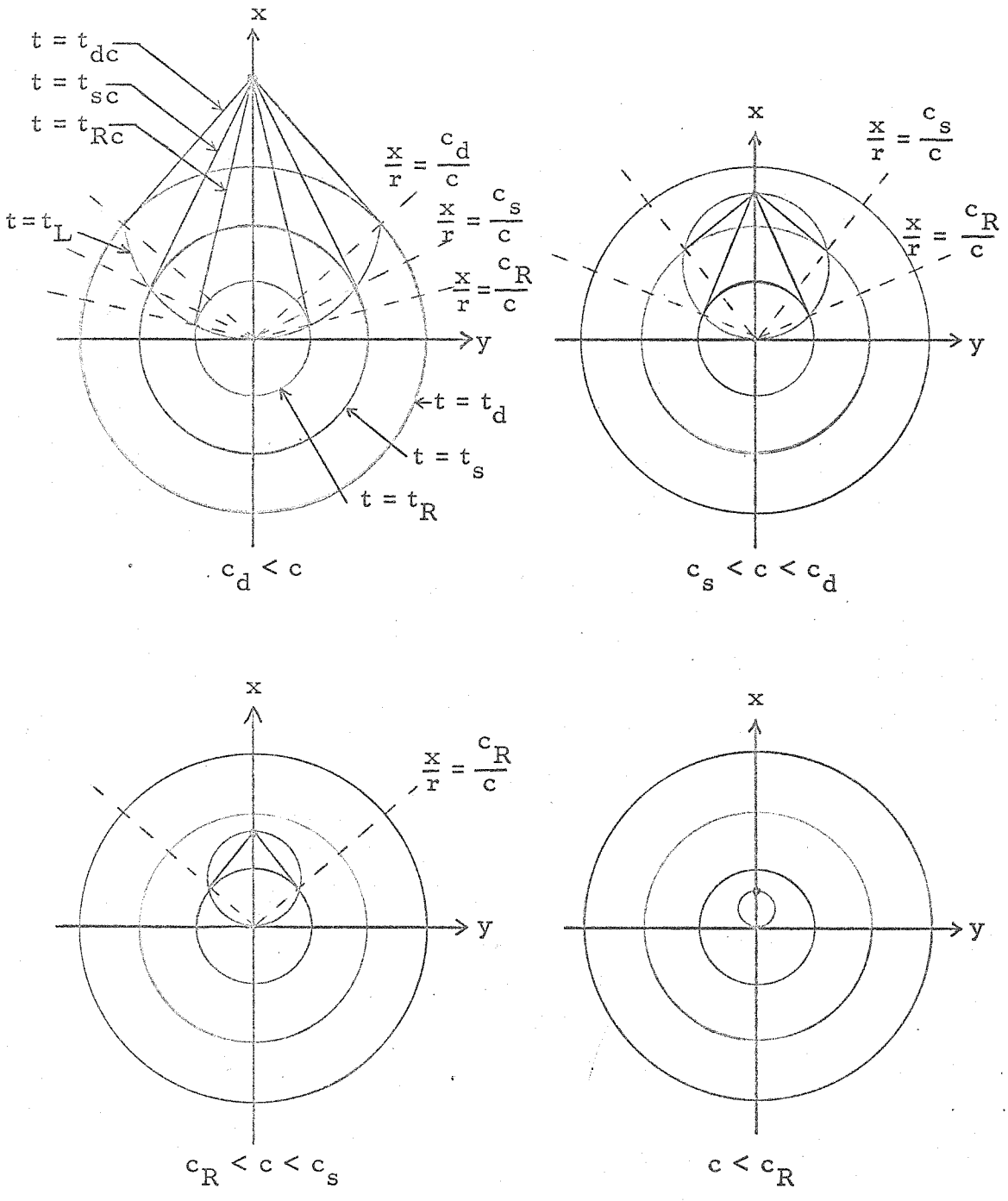

FIGURE 34

Wave Pattern in the Surface Plane
Including Rayleigh Waves

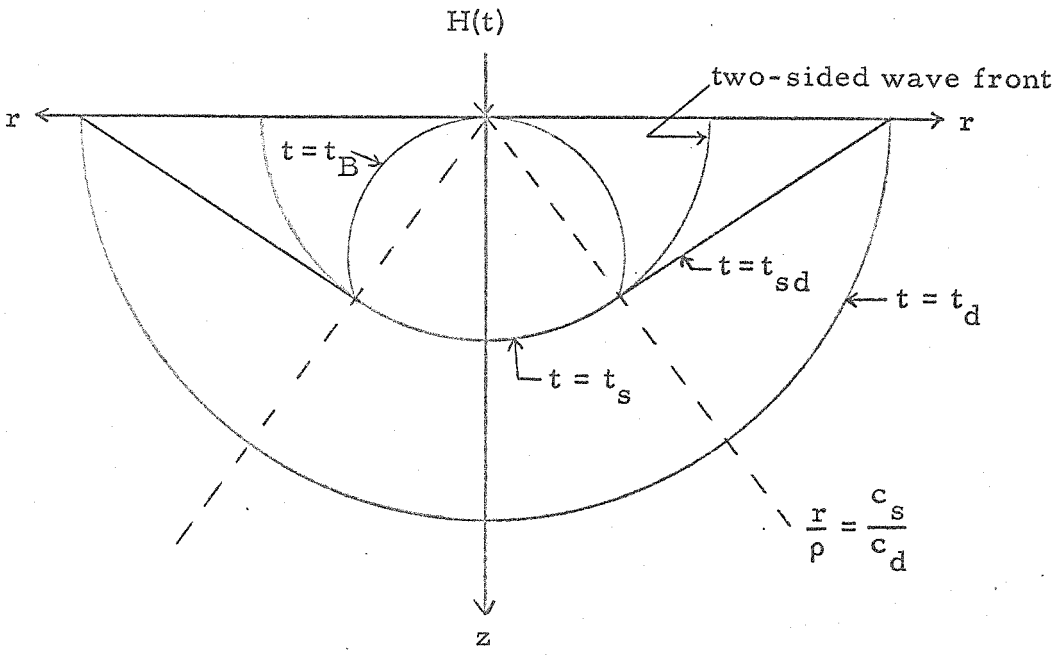

rz-Plane

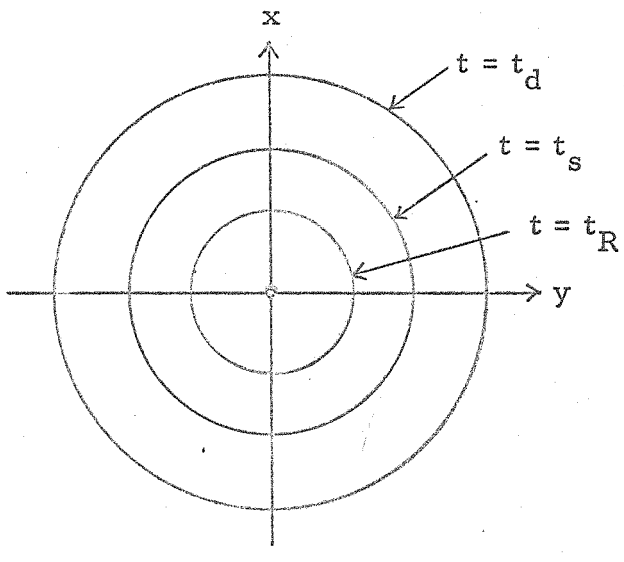

z = 0 Plane

FIGURE 35

Wave Pattern for the Stationary Point Load

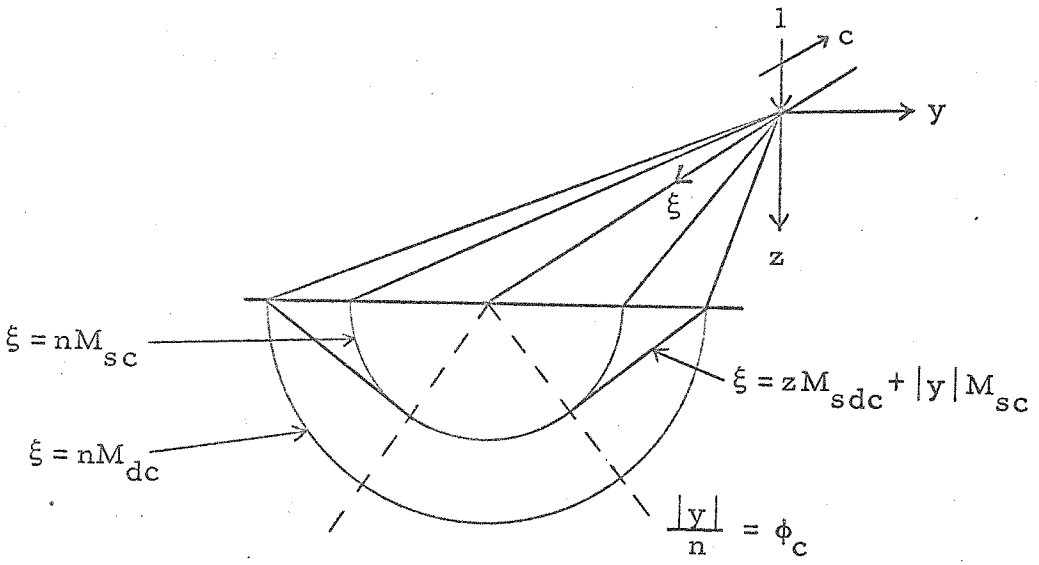

Three-Dimensional Perspective

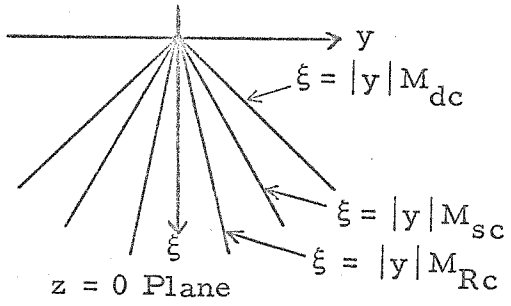

z = 0 Plane

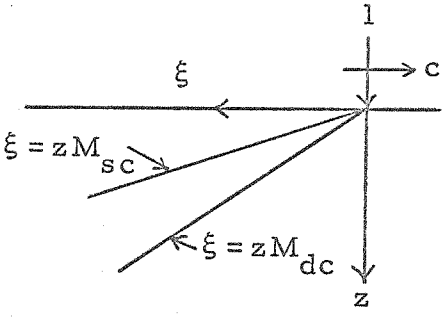

y = 0 Plane

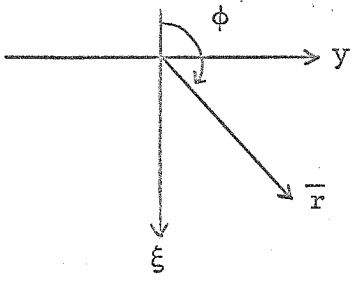

$$\xi = -\bar{r}\cos\phi \qquad \bar{r} = (\xi^2+y^2)^{\frac{1}{2}}$$

$$y = \bar{r}\sin\phi \qquad \phi = -\tan^{-1}\left(\frac{y}{\xi}\right)$$

$$u_{\bar{r}} = u_x\cos\phi + u_y\sin\phi$$

$$u_\phi = -u_x\sin\phi + u_y\cos\phi$$

Polar Geometry

FIGURE 36

Steady-State Wave Pattern for Supersonic Load Motion